

Hiep Vo Tran

Particle Size Control for Functionalization of Iron Oxide Nanoparticles with Potential Applications in Diagnostics

Master's thesis in Chemical Engineering

Supervisor: Sulalit Bandyopadhyay

Co-supervisor: Zeeshan Ali

June 2022

Hiep Vo Tran

Particle Size Control for Functionalization of Iron Oxide Nanoparticles with Potential Applications in Diagnostics

Master's thesis in Chemical Engineering
Supervisor: Sulalit Bandyopadhyay
Co-supervisor: Zeeshan Ali
June 2022

Norwegian University of Science and Technology
Faculty of Natural Sciences
Department of Chemical Engineering

Preface

This report has been written by a Chemical Engineering student at Norwegian University of Science and Technology (NTNU) at the Faculty of Natural Sciences and the Department of Chemical Engineering. The Master's Thesis with the course code TKP4900 was written in the Spring 2022. The project has been performed under the supervision team of Associate Professor Sulalit Bandyopadhyay and PhD Candidate Zeeshan Ali.

The project has been performed with a great team effort. It has challenged me to dive into the research of surface modification of iron oxide nanoparticles. It has taught me to master the theory from supervisors to relevant literatures and research articles, which has been a quite rewarding learning experience. The project has also taught me to explore the field nanotechnology thoroughly, and I am grateful that this project has been given to me.

I would like to express my gratitude towards Sulalit Bandyopadhyay and Zeeshan Ali for their commitment and professional guidance throughout this project. The topic that my supervisors' study is very important for today's research area. I am thankful that they provided me this topic allowing me to grasp the captivating research theme particle size control for functionalization of iron oxide nanoparticles with potential applications in diagnostics.

Declaration of Compliance

I, Hiep Vo Tran, hereby declare that this is an independent work according to the exam regulations of the Norwegian University of Science and Technology (NTNU).

Signature:

Hiep Vo Tran

Place and Date:

Trondheim – Gløshaugen, Date: 12.06.2022

Abstract

Small average diameter along with narrow particle size distribution is required to provide a satisfactory magnetic saturation performance of iron oxide nanoparticles (IONPs) for diagnostic applications. The use of polyvinylpyrrolidone (PVP) as a coating agent has previously been reported by other studies to control the particle size, to obtain highly monodisperse particles, and to reduce agglomerations of IONPs synthesized by the co-precipitation method. To this extent, however, there are no reports examining the interplay between factors such as mass, molecular weight, concentration, pH, and zeta potential of PVP on the surface of IONPs with the intention of controlling the size. Thereby, this thesis reports the optimization of colloidal stability using various masses of IONPs and various molecular weights and concentrations of PVP for efficient coating, followed by silanization. The size of PVP coating of IONPs appears to be significantly dependent on the interaction between the experimental factors with hydrodynamic sizes ranging from 177 to 1915 nm, whereas the zeta potential values vary from 6 to 20 mV. The surface charge of the zeta potential appears to be positive and structural identification analysis indicates that there are no PVP molecule chains present in the dispersion. However, the pH study reveals that PVP is either partially or weakly adsorbed, or alternatively no PVP adsorbed on the surface of IONPs. The presence of PVP also does not appear to affect the silanization process significantly. The results show that the presence of PVP does not improve the colloidal stability and is potentially not an excellent candidate for biomedical applications.

Keywords: Iron oxide nanoparticles, diagnostics, polyvinylpyrrolidone, silanization, colloidal stability

Sammendrag

Liten gjennomsnittlig diameter sammen med smal partikkelstørrelsesfordeling er nødvendig for å gi en tilfredsstillende magnetisk metningsytelse av jernoksid nanopartikler for diagnostiske anvendelser. Bruken av polyvinylpyrrolidon (PVP) som et beleggmiddel har tidligere blitt rapportert av andre studier for å kontrollere partikkelstørrelsen, for å oppnå svært monodisperse partikler og for å redusere agglomerasjoner av jernoksid nanopartikler syntetisert ved samutfellingsmetoden. For så vidt er det imidlertid ingen rapporter som undersøker samspillet mellom faktorer som masse, molekylvekt, konsentrasjon, pH og zeta-potensial til PVP på overflaten av jernoksid nanopartikler med den hensikt å kontrollere størrelsen. Derfor rapporterer denne oppgaven optimalisering av kolloidal stabilitet ved bruk av ulike masser av jernoksid nanopartikler og ulike molekylvekter og konsentrasjoner av PVP for effektivt belegg, etterfulgt av silanisering. Størrelsen på PVP-belegget av jernoksid nanopartikler ser ut til å være betydelig avhengig av interaksjonen mellom de eksperimentelle faktorene med hydrodynamiske størrelser fra 177 til 1915 nm, mens zeta-potensialverdiene varierer fra 6 til 20 mV. Overflateladningen til zeta-potensialet ser ut til å være positiv og strukturell identifiseringsanalyse indikerer at det ikke er noen PVP-molekykjeder tilstede i dispersjonen. Imidlertid avslører pH-studien at PVP er enten delvis eller svakt adsorbent, eller alternativt ingen PVP adsorbent på overflaten av jernoksid nanopartikler. Tilstedeværelsen av PVP ser heller ikke ut til å påvirke silaniseringsprosessen i betydelig grad. Resultatene viser at tilstedeværelsen av PVP ikke forbedrer den kolloidale stabiliteten og er potensielt ikke en utmerket kandidat for biomedisinske applikasjoner.

Nøkkelord: Jernoksid nanopartikler, diagnostikk, polyvinylpyrrolidon, silanisering, kolloidal stabilitet

Table of Contents

Preface	i
Abstract	iii
Sammendrag	v
Table of Contents	vii
List of Tables	xii
List of Figures	xiv
Nomenclature	xix
1 Introduction	1
1.1 Why Applications of Iron Oxide Nanoparticles for Diagnosis?	2
1.2 Key Problems with Iron Oxide Nanoparticles	3
1.3 Importance of Surface Modification of Iron Oxide Nanoparticles	4
1.4 Aim and Objectives	5
1.5 Centre of the Work	6
1.6 Continuation of the Specialization Project.....	7
1.7 Structure of the Thesis	8
2 Introduction to Iron Oxide Nanoparticles	10
2.1 The Rise of Nanotechnology and Magnetic Nanoparticles.....	10
2.2 Superparamagnetic Behaviour of Iron Oxide Nanoparticles	11
2.2.1 Types of Iron Oxides with Different Magnetic Fields.....	11
2.2.2 Superparamagnetic State	12
2.3 The Nucleation Mechanism	12
2.4 Synthesis of Iron Oxide Nanoparticles by Co-Precipitation	15
3 Introduction to Surface and Colloid Chemistry	17
3.1 Why are Surfaces and Colloids Important?	17
3.2 Colloidal Systems	18
3.2.1 Classification of Colloids	19
3.2.2 Types and Applications of Colloidal Systems.....	19
3.2.3 Terminology in Colloidal Systems	22

3.3 Colloidal Stability	23
3.3.1 The van der Waals Forces	24
3.3.2 The Electrostatic Forces	25
3.3.3 Key Parameters of Electrical Forces	28
3.3.4 The DLVO Theory	31
3.3.5 The Steric Forces	33
3.3.6 Steric Stabilization	34
4 Introduction to Polymers at Interface	38
4.1 Adsorption of Polymers in Colloidal Systems	38
4.2 Adsorbed Polymers with Various Interactions	38
4.3 Polymer Adsorption and the Control of Steric Stabilization.....	40
4.3.1 Various Surface Configurations of Polymer Adsorption.....	40
4.4 Positive and Negative Adsorption	42
5 Introduction to Polyvinylpyrrolidone.....	45
5.1 Features of Polyvinylpyrrolidone	45
5.2 Physicochemical Properties of Polyvinylpyrrolidone	46
6 Introduction to <i>Post-Situ</i> Surface Modification.....	49
6.1 <i>Post-Situ</i> Surface Modification Strategy and Mechanisms.....	49
6.2 Coating with Silica	51
6.2.1 The Stöber Method.....	52
7 Literature Review	54
7.1 Surface Modification of Iron Oxide Nanoparticles with Polyvinylpyrrolidone.....	54
7.2 <i>Post-Situ</i> Functionalization with Silica.....	63
7.2.1 Previously Studied Thesis at NTNU	66
7.3 Iron Oxide Nanoparticles with Silica and Polyvinylpyrrolidone	68
7.4 Gaps in Literature	72
8 Materials and Methods	74
8.1 Formulas	74
8.2 Instruments	75
8.3 Equipment.....	77
8.4 Chemicals and Solutions.....	79

8.5 Procedure	80
8.5.1 Synthesis of Iron Oxide Nanoparticles by the Co-Precipitation Method.....	80
8.5.2 <i>Post-Situ</i> Functionalization of Iron Oxide Nanoparticles with Polyvinylpyrrolidone	82
8.5.3 Batch Silanization of Iron Oxide Nanoparticles	83
8.5.4 Batch Silanization of Iron Oxide Nanoparticles with Polyvinylpyrrolidone	84
8.6 Sample Preparation for Characterization Techniques	85
8.6.1 Sample Preparation for Dynamic Light Scattering	85
8.6.2 Sample Preparation for Fourier-Transform Infrared Spectroscopy	85
8.6.3 Sample Preparation for Scanning Electron Microscope	86
8.6.4 Sample Preparation for LumiSizer	86
8.7 pH Measurement.....	87
8.7.1 Direct pH Measurement	87
8.7.2 pH Change.....	88
8.8 Experimental Design	89
8.8.1 Design for Polyvinylpyrrolidone Coating of Iron Oxide Nanoparticles.....	89
8.8.2 Design for Silica Coating of Iron Oxide Nanoparticles.....	91
9 Results and Discussion.....	93
9.1 Iron Oxide Nanoparticles by the Co-Precipitation Method	93
9.1.1 Concentration Test Analysis.....	93
9.1.2 Particle Size Distribution Analysis.....	94
9.1.3 Surface Charge and Stability Analysis	96
9.2 Polyvinylpyrrolidone Coating of Iron Oxide Nanoparticles	97
9.2.1 Control of Particle Size and Stability Analysis	97
9.2.2 Structural Identification Analysis.....	106
9.2.3 pH Analysis	111
9.3 Silica Coating of Iron Oxide Nanoparticles with Polyvinylpyrrolidone	117
9.3.1 Morphology Analysis	117
9.3.2 Particle Size Distribution Analysis.....	126
9.3.3 Particle Size Analysis	128
10 Conclusion.....	131
10.1 Recommendations.....	132

Bibliography 134

List of Tables

Table 3. 1: Various types of colloidal systems (34, p. 6).	20
Table 3. 2: Various applications of surface and colloid chemistry (33, p. 4).	21
Table 3. 3: Various types of forces between the colloidal particles (33, p. 212).	23
Table 5. 1: Physicochemical properties of PVP (49).....	47
Table 8. 1: List of equipment.	78
Table 8. 2: List of chemicals and solutions.	79
Table 8. 3: Experimental design for IONPs@PVP.	90
Table 8. 4: Experimental design for IONPs@SiO ₂ in the presence of with and without PVP.	91
Table 9. 1: Particle size of IONPs.	95
Table 9. 2: Particle size distribution of IONPs.	95
Table 9. 3: pH results based on the original samples.	112
Table 9. 4: pH results on 100-IONPs@PVP for 10 000 g/mol and 0.1 g/L PVP based on original sample in comparison to various dilutions. The ZP value for the dilution at 1:20 is from Figure 9.4-C , while the ZP value for the dilution at 1:100 is from Figure 9.9 . No ZP is measured for the original sample.	116

List of Figures

Figure 1. 1: Schematic illustration of work for the thesis.	6
Figure 2. 1: A schematic illustration of the Gibbs free energy as a function of the radius of the nuclei.....	14
Figure 3. 1: The electrical double layer (35, p. 54).	26
Figure 3. 2: The electrical double layer on the surface of a nanoparticle based on the Gouy-Chapman-Stern model with the various energy potentials represented (36).....	27
Figure 3. 3: Schematic illustration of (a) the electrical double layer forces and (b) the steric stabilization adsorbed by polymers (33, p. 214).	28
Figure 3. 4: Schematic illustration of the total interaction energy as a function of the distance (H) between the particles (32, p. 213).	32
Figure 3. 5: Representation of the potential energy diagram for a steric stabilized colloidal system with and without electrical double layer repulsion (33, p. 275).	35
Figure 3. 6: Schematic illustration of steric destabilization of colloidal systems of (a) depletion flocculation and (b) bridging flocculation (33, p. 277).	36
Figure 4. 1: Schematic overview of various interactions between colloidal particles with and without polymer (43).....	39
Figure 4. 2: Surface configurations of polymer adsorption with (a) only tails or (b) with loops, tails, and trains (33, p. 177).	41
Figure 4. 3: Schematic illustration of various framework when adding polymers to the interface of the particles in terms of (a-c) negative adsorption (depletion) of polymers or (d-f) positive adsorption (accumulation) of polymers (44).	43
Figure 5. 1: The molecular structure of N-vinylpyrrolidone (46).	46
Figure 5. 2: The chemical structure of PVP (47).	46
Figure 6. 1: Surface Modification of IONPs by ligand addition (17).....	50
Figure 6. 2: Surface modification of IONPs by ligand exchange (17).	50
Figure 6. 3: Surface modification of IONPs by encapsulation method (17).	50
Figure 6. 4: Post-Synthesis scheme of silica functionalized IONPs by J.R Sosa-Acosta (Modified) (10).....	51

Figure 7. 1: TEM images and histogram of PVP coated IONPs (53).	54
Figure 7. 2: TEM images of IONPs@PVP (54).....	55
Figure 7. 3: SEM images of (a) uncoated IONPs and (b) PVP coated IONPs (modified) (55).....	57
Figure 7. 4: TEM images of (a) un-coated IONPs and (b) PVP coated IONPs, and particle size distribution of (c) un-coated IONPs and (d) PVP coated IONPs (55).	57
Figure 7. 5: Schematic illustration of IONPs@PVP nanospherical shapes and the chemical formula of PVP (56).	58
Figure 7. 6: FE-SEM images of three various contents of PVP coated on the surface of IONPs (56).....	58
Figure 7. 7: SEM images of IONPs@PVP (a) 1 g PVP, (b) 2 g PVP, and (c) 3 g PVP (57).....	60
Figure 7. 8: The changes in zeta potential of IONPs in water system with various amounts of PVP added to the dispersions (58).....	62
Figure 7. 9: Experimental procedure of silica NPs preparation by two-stage mixed method (a) and schematic diagram of semi-batch and batch process system (b) (60).	64
Figure 7. 10: Illustration of the experimental set-up used for the preparation of the controlled particle growth at a constant addition rate by Nozawa et al (61).	65
Figure 7. 11: Results of (A) TEM image, (B) FE-SEM image, and (C) particle size distribution of IONPs@SiO ₂ @PVP nanocomposite (modified) (64).	69
Figure 7. 12: A schematic illustration of surface modification of IONPs@SiO ₂ . (b) TEM images of IONPs@SiO ₂ with various TEOS amount added to the coating process, where the number on the top to left identifies the average silica shell thickness for each image. (c) TEM images of NPs@SiO ₂ with and without the presence of PVP (modified) (65).....	71
Figure 8. 1: Photo of magnetic separation from experimental work.	84

Figure 9. 1: Concentration test of IONPs. The synthesized method for IONPs by the co-precipitation gives 4 batches. The mixed IONPs are a result of these corresponding batches. The error bars represent the standard deviation calculated from the triplicate measurement of the specific sample. 93

Figure 9. 2: Hydrodynamic size of IONPs. The synthesized method for IONPs by the co-precipitation gives 4 batches. The mixed IONPs are a result of these corresponding batches. The error bars represent the standard deviation calculated from the triplicate measurement of the specific sample. 95

Figure 9. 3: Zeta Potential of IONPs. The synthesized method for IONPs by the co-precipitation gives 4 batches. The mixed IONPs are a result of these corresponding batches. The error bars represent the standard deviation calculated from the triplicate measurement of the specific sample. 96

Figure 9. 4: Hydrodynamic size of x-IONPs@PVP: (A) 0.1 g/L and (B) 0.5 g/L PVP in water dispersion with various molecular weights of PVP. Zeta potential of x-IONPs@PVP: (C) 0.1 g/L and (D) 0.5 g/L PVP in water dispersion with various molecular weights of PVP. The letter x represents the mass of IONPs used for the characterization (x = 25, 50, or 100 mg). The sample for non-functionalized IONPs is from the mixed IONPs batch. The error bars indicate the standard deviation calculated from the triplicate measurement of the specific sample. 100

Figure 9. 5: (A) Hydrodynamic size and (B) Zeta potential of x-IONPs@PVP for 10 000 g/mol PVP with various concentrations. (C) Hydrodynamic size and (D) zeta potential of 25-IONPs@PVP for 40 000 and 360 000 g/mol PVP with various concentrations. The letter x represents the mass of IONPs used for characterization (25, 50, or 100 mg). The error bars indicate the standard deviation from the triplicate measurement of the specific sample. 103

Figure 9. 6: (A) Hydrodynamic size and (B) zeta potential of 25-IONPs@PVP with various washing steps for 10 000 g/mol and 0.5 g/L PVP in water dispersion. The sample for non-functionalized IONPs is from the mixed IONPs batch. The error bars indicate the standard deviation from the calculated triplicate measurement of the specific sample. 105

Figure 9. 7: FT-IR spectra of (A) various molecular weights of PVP, (B) x-IONPs@PVP for 10 000 g/mol and 0.5 g/L PVP, (C) x-IONPs@PVP for 40 000 g/mol and 0.1 g/L PVP, and (D) x-IONPs@PVP for 360 000 g/mol and 0.1 g/L PVP. The letter x represents the mass of IONPs used for characterization (x = 25, 50 or 100 mg). The spectra of pure PVP and non-functionalized IONPs are used to compare with IONPs@PVP. 108

Figure 9. 8: FT-IR spectra of 25-IONPs@PVP for 10 000 g/mol and 0.5 g/L PVP: (A) Supernatant, (B) 0 wash, (C) 1st wash, (D) 2nd wash, and (E) 3rd wash. The FT-IR spectra of pure PVP and non-functionalized IONPs are used to compare with IONPs@PVP. 110

Figure 9. 9: Zeta potential as a function of pH for IONPs and IONPs@PVP. The sample for non-functionalized IONPs is from the mixed IONPs batch, whereas the sample for PVP coating of IONPs is from the sample 100-IONPs@PVP for 10 000 and 0.1 g/L PVP. The error bars represent the standard deviation from the calculated triplicate measurements of the specific sample. 115

Figure 9. 10: SEM images of (A) 25-IONPs@SiO₂, (B) 25-IONPs@PVP@SiO₂ for 10 000 g/mol and 0.5 g/L PVP, and (C) 25-IONPs@PVP@SiO₂ for 360 000 g/mol and 0.1 g/L PVP. 121

Figure 9. 11: SEM images of (B-1, B-2) 25-IONPs@PVP@SiO₂ for 10 000 g/mol and 0.5 g/L PVP, and (C-1) 25-IONPs@PVP@SiO₂ for 360 000 g/mol and 0.1 g/L PVP in terms of aggregation. 122

Figure 9. 12: SEM images of (A) 50-IONPs@SiO ₂ , (B) 50-IONPs@PVP@SiO ₂ for 10 000 g/mol and 0.5 g/L PVP, and (C) 50-IONPs@PVP@SiO ₂ for 360 000 g/mol and 0.1 g/L PVP.....	123
Figure 9. 13: SEM images of (A-1) 50-IONPs@SiO ₂ , (B-1) 50-IONPs@PVP@SiO ₂ for 10 000 g/mol and 0.5 g/L PVP, and (C-1) 50-IONPs@PVP@SiO ₂ for 360 000 g/mol and 0.1 g/L PVP in terms of aggregation.	124
Figure 9. 14: SEM images of (A) 100-IONPs@SiO ₂ , (B) 100-IONPs@PVP@SiO ₂ for 10 000 g/mol and 0.5 g/L PVP, and (C) 100-IONPs@PVP@SiO ₂ for 360 000 g/mol and 0.1 g/L PVP.....	125
Figure 9. 15: Particle size distribution of 25-IONPs@SiO ₂ (A) without PVP, (B) 10 000 g/mol and 0.5 g/L PVP, and (C) 360 000 g/mol and 0.1 g/L PVP. Particle size distribution of 50-IONPs@SiO ₂ (D) without PVP, (E) 10 000 g/mol and 0.5 g/L PVP, and (F) 360 000 g/mol and 0.1 g/L PVP. Particle size distribution characterized by SEM and particles counted using the ImageJ software program.....	127
Figure 9. 16: Particle Size (average diameter) of IONPs@SiO ₂ in the presence of with and without PVP characterized by SEM, where the error bars represent a measurement of the polydispersity of the particle size distribution. The letter x represents the mass of IONPs used for the characterization (x = 25, 50, or 100 mg). The abbreviation of SiO ₂ stands for Si.	129

Nomenclature

Acronyms

World Health Organization	WHO
Polymerase Chain Reaction	PCR
Magnetic Nanoparticles	MNPs
Iron Oxide Nanoparticles	IONPs
Nanoparticles	NPs
Magnetic Resonance Imaging	MRI
van der Waals	vdW
Electrical Double Layer	EDL
Deryaguin-Landau-Verwey-Overbeek	DLVO
Badische Anilin-und Soda-Fabrik	BASF
Transmission Electron Microscope	TEM
Field-Emission Scanning Electron Microscope	FE-SEM
Dynamic Light Scattering	DLS
Scanning Electron Microscope	SEM
Fourier-Transform Infrared	FT-IR
Zeta Potential	ZP

Abbreviations

Ribonucleic Acid	RNA
Deoxyribonucleic Acid	DNA
Polyvinylpyrrolidone	PVP
Ethanol	EtOH
Isopropanol	IPA
Tetra orthosilicate	TEOS
Polyethylene Glycol	PEG
Trimethyl Silane	TMS

Coating Acronyms

Silica Coating of Iron Oxide Nanoparticles

IONPs@SiO₂

Polyvinylpyrrolidone Coating of Iron Oxide Nanoparticles

IONPs@PVP

Silica Coating of Iron Oxide Nanoparticles with Polyvinylpyrrolidone

IONPs@PVP@SiO₂

Pure Silica Coating of Nanoparticles

NPs@SiO₂

1 Introduction

What has been like for us during these strange, challenging, and tough moments to combat this pandemic? The whole world has been suffering under the shadow of coronavirus (COVID-19), which is known as the pandemic disease caused by SARS-CoV-2 respiratory virus (1). The disease was declared a global public health threat by the World Health Organization (WHO) on March, 2020 (2). The SARS-CoV-2 has caused critical health problems around the world, as well as unparalleled socio-economic burden. The disease could spread among humans to humans from those infected, with no, mild or serious symptoms. In early January 2020, following the announcement of the genetic code of coronavirus, the polymerase chain reaction (PCR) based technique was utilized for the diagnosis of patients suffering from SARS-CoV-2 infection (3). A project on this particular application has also been employed at Norwegian University of Science and Technology (NTNU) for the diagnosis of those who potentially carried the virus (4).

On 12 March 2020, Norway shut down due to the pandemic. The uncertainty concerning the infection circumstances somehow forced extreme measures and the population feared the consequences of uncontrolled infection for the Norwegian health care system. To date, there are vaccines approved for immunization against the disease around the world, but in the beginning when vaccines were not yet fully developed, it was important to reduce the spread of the disease. Professor Magnar Bjørnås and his research team at NTNU at the Department of Clinical and Molecular Medicine created something that could be employed to secure the test capacity. To accomplish this difficult task, the team required magnetic particles that could bind the virus's genetic material, called ribonucleic acid (RNA) of SARS-CoV-2 (5).

At the Department of Chemical Engineering at NTNU, Associate Professor Sulalit Bandyopadhyay developed magnetic nanoparticles (MNPs) that could be utilized for diagnostics and could efficiently capture RNA from the coronavirus. The collaboration between the research teams of Sulalit and Magnar, managed to produce effectively unlimited amounts of COVID-19 tests of what the health services in Norway required (5). Researchers at NTNU's Department of Chemical Engineering produced iron oxide nanoparticles (IONPs) coated with silica, which turned out to be quite useful. The tests used these MNPs to extract RNA from a solution containing a sample from the patient so that its genetic material could be extracted. RNA from the virus in the solution is actively attracted to the silica coating of IONPs

(IONPs@SiO₂) (6). This was the key to battle the COVID-19 pandemic with the diagnostic approach to minimize spread of infections in the community.

1.1 Why Applications of Iron Oxide Nanoparticles for Diagnosis?

Research on IONPs that are properly coated with silica may be of interest for use in molecular biology, particularly as a supplementary diagnostic material in biomedical applications (7). Since the IONPs@SiO₂ appear to have a strong affinity for RNA, other diagnostic applications such as deoxyribonucleic acid (DNA) extraction are also interesting. The development of nanotechnology, as well as other relevant methods and materials, has led to a great revolution in the field of medicine. With its unique benefits, this field of study is considered an essential role in diagnosis for the treatment of various medical purposes such as the treatment and prevention of illnesses. Thanks to the development of nanomaterials, nanoscience is receiving more attention (8). On the nanoscale, the nanomaterials have a diameter of nanometers and have smaller particles that have demonstrated exceptionally promising chemical, biological, and physical properties, depending on the size, morphology, and shape (9).

These nanomaterials draw many interests for fabrication and design including nucleic acid extraction for biomedical diagnosis. The involvement of MNPs such as IONPs is principal to prepare available systems for biomedical applications. In addition to silica as a coating agent, MNPs combinations with polymers also attracts the researcher's interest for participating in colloidal systems and the polymer which is interesting to highlight is polyvinylpyrrolidone (PVP). These MNPs combined with the right coating agent grasp many unique properties which provide applications such as COVID-19 diagnosis, biomedical separation, and nucleic acid/DNA separation or extraction (9).

Since the surface modification of IONPs can be modified by silica, the material is quite common in functionalizing nanoparticles (NPs) for DNA extraction and purification. DNA extraction and purification is contemplated to be important in biomedical applications such as clinical diagnosis (10). Thus, the nature of DNA interactions with silica is principal. The binding between DNA and silica is primarily based upon intermolecular electrostatic interactions, dehydration of the silica surface and DNA, and intermolecular hydrogen (H⁺) bond between DNA and silica contact layer. The influences of parameters on the DNA interactions with the silica surface are for example ionic strength, temperature, and pH, in which these can be considered as driving forces (11).

1.2 Key Problems with Iron Oxide Nanoparticles

In order to produce IONPs, there are many specific synthesis methods to consider, but only one of them is used for this project, and that is the co-precipitation method. One primary problem with synthesized IONPs is that these particles tend to aggregate, also in the form of clusters. The IONPs have the tendency to decrease the surface/interfacial energy to form these clusters due to large surface-to-volume-ratio (12-14), thus significantly reducing the colloidal stability of magnetic suspensions. The decrease in interfacial energy that causes aggregates usually arises because of the van der Waals forces. The IONPs may also aggregate because of strong magnetic dipole-dipole interactions in the absence of a hydrophilic layer. The IONPs are also vulnerable to aggregation due to the hydrophobic interactions. As in overall, the colloidal stability of IONPs can be controlled by van der Waals, magnetic dipolar, and hydrophobic-hydrophilic interactions (12, p. 71-72). Another problem that is significantly important is that IONPs have high chemical reactivity combined with high interfacial energy. In this way, the synthesized IONPs are highly susceptible to oxidation when exposed to air, and this may lead to a decrease in the magnetization value (13-15).

The prevention of aggregation, however, is not only a challenge associated with IONPs. A well-known problem with IONPs is the challenge of controlling the particle size, narrow particle size distribution, morphology, and magnetic properties with the purpose of providing desirable properties. These are considered the key factors of IONPs. To produce the particles in an appropriate way, with controlled particle size is the most significant challenge (12, p. 1, 5, 14).

Since IONPs provide potential applications in biomedicine, there are some specific challenges that is necessary to be addressed. Small average particle size/diameter along with very narrow particle size distribution are necessary for providing acceptable magnetization values, in which the particles offer uniform magnetic saturations with uniform chemical and physical properties. The NPs with various particle sizes and broad particle size distributions might cause undesirable properties, and this may also result in poor magnetic saturation performance. This means that the magnetization value of IONPs depends on the particle size to a large extent. Thus, monodispersed IONPs with a small average diameter combined with a high magnetization value, as well as functionalized particles with appropriate coating materials are required for this type of application (12, p. 5 and 11, 16).

1.3 Importance of Surface Modification of Iron Oxide Nanoparticles

The problem of reducing or preventing the aggregation of IONPs can potentially be solved by coating IONPs with specific materials. The reason for this is because the employed materials have the tendency to improve the colloidal stability, hydrophilicity, magnetic controllability, and biocompatibility of IONPs (17). The coating material method is commonly used to alter the surface of IONPs to prevent aggregation and oxidation of the particles. The purpose is to make them as biocompatible as possible. The method also provides functionalization of IONPs to improve their physiochemical features, which makes them strong candidates for biomedicine such as diagnostics (13, 14).

The most used surface modifications of IONPs are represented by polymers and inorganic materials. The IONPs can be functionalized during the synthesis or subsequently, but the focus is on the functionalization after the synthesis. This type of functionalization is often called *post-situ* functionalization of IONPs, which are considered as core-shell NPs. The most common *post-situ* functionalization is silanization for surface modification of IONPs (16). Silica (SiO_2) is the preferred material for modifying IONPs to produce IONPs@ SiO_2 because it has the capability to shield the repulsive electrostatic force and as well as rich in hydroxyl (OH^-) groups. These hydroxyl groups have the ability to participate in the formation of covalent bridges between IONPs and DNA or other bioactive molecules. The unique features of IONPs@ SiO_2 involve good dispersion, high magnetic saturation, as well as excellent acid resistance to provide better adsorption, elution, and purity for DNA extraction. The method of silanization is the Stöber method where the main objective is to synthesize monodispersed IONPs@ SiO_2 for biomedical applications (13). Other benefits of using silica are due to the fact that the shells arise from their chemical stability, simple surface modification, and as well as enhancing the biocompatibility of the particles in order to achieve new properties of the particle surface (18).

The polymer coating, on the other hand, is also used for improving the biocompatibility along with colloidal stabilization and an example of such a polymer is PVP (12, p. 72). PVP can be considered as a promising material because it has both hydrophilic and hydrophobic parts, and it is water-soluble, as well as un-charged, and more importantly non-toxic. The PVP coating of IONPs (IONPs@PVP) can be obtained by covalent bonds between hydrophilic parts of the polymer and OH^- group on the surface of IONPs in order to increase the stability of the dispersion. The main purpose with the use of PVP is to control the particle size, to reduce aggregation, and produce high monodisperse IONPs as a coating agent (19).

1.4 Aim and Objectives

The aim of the thesis is to control the particle size of IONPs coated with PVP and silica, which is referred to as IONPs@PVP@SiO₂, for diagnostics. The main idea is to study the interplay between various factors such as mass, molecular weight, concentration, pH, and zeta potential to achieve narrow size distribution and to prevent their aggregation for the purpose of controlling the size. It is hypothesized that the addition of PVP has the capability to increase stability, reduce aggregation, and obtain monodispersed IONPs for biomedical applications. Thus, three specific objectives are considered to achieve the desired result. The aim and objectives are related to the literature review section (*Section 7 – Literature Review*).

1st objective: Synthesis and characterization of IONPs

The 1st objective of the thesis is to synthesize and characterize IONPs. The following goal for performing this step:

- **1st goal:** To study the particle size and colloidal stability of non-functionalized (un-coated) IONPs with the comparison of functionalized IONPs.

2nd objective: *Post-situ* functionalization and characterization of IONPs@PVP

The 2nd objective of the thesis is to functionalize the IONPs with PVP as a surface modifier. The following goals for performing this step:

- **1st goal:** To compare the particle size and colloidal stability with non-functionalized IONPs and previous studies.
- **2nd goal:** To optimize the colloidal stability of IONPs@PVP.
- **3rd goal:** To study whether PVP is coated on the surface of IONPs or not and compare with previous studies.

3rd objective: *Post-situ* functionalization and characterization of IONPs@PVP@SiO₂

The 3rd objective of the thesis is to functionalize the optimized PVP coated IONPs with silica as an outer layer where PVP is considered an intermediate layer. The following goals for performing this step:

- **1st goal:** To control the particle size.
- **2nd goal:** To examine how PVP affects the silanization process by studying the particle size, particle size distribution, and morphology of IONPs@PVP@SiO₂.

1.5 Centre of the Work

This thesis involves the synthesis, surface functionalization and characterization of IONPs based on the aim and objectives. One approach to solve the problems associated with IONPs is primarily based on modifying the surface of IONPs by using the polymer and the inorganic material to produce IONPs@PVP@SiO₂. This is to examine whether the functionalized IONPs exhibit certain properties that can be used for the application in diagnostics. These surface modified IONPs may be used to demonstrate their performance in extracting DNA molecule from biological samples in longer term. A synthetic pathway for IONPs is prepared by a classical alkaline co-precipitation method of ferrous and ferric (Fe²⁺/Fe³⁺) chloride aqueous solution at ambient temperature followed by surface modifications on the surface of the IONPs with PVP and silica. A schematic illustration of the work is shown in **Figure 1.1**. The optimized surface functionalized IONPs can potentially be tested in collaboration with the Department of Clinical and Molecular Medicine.

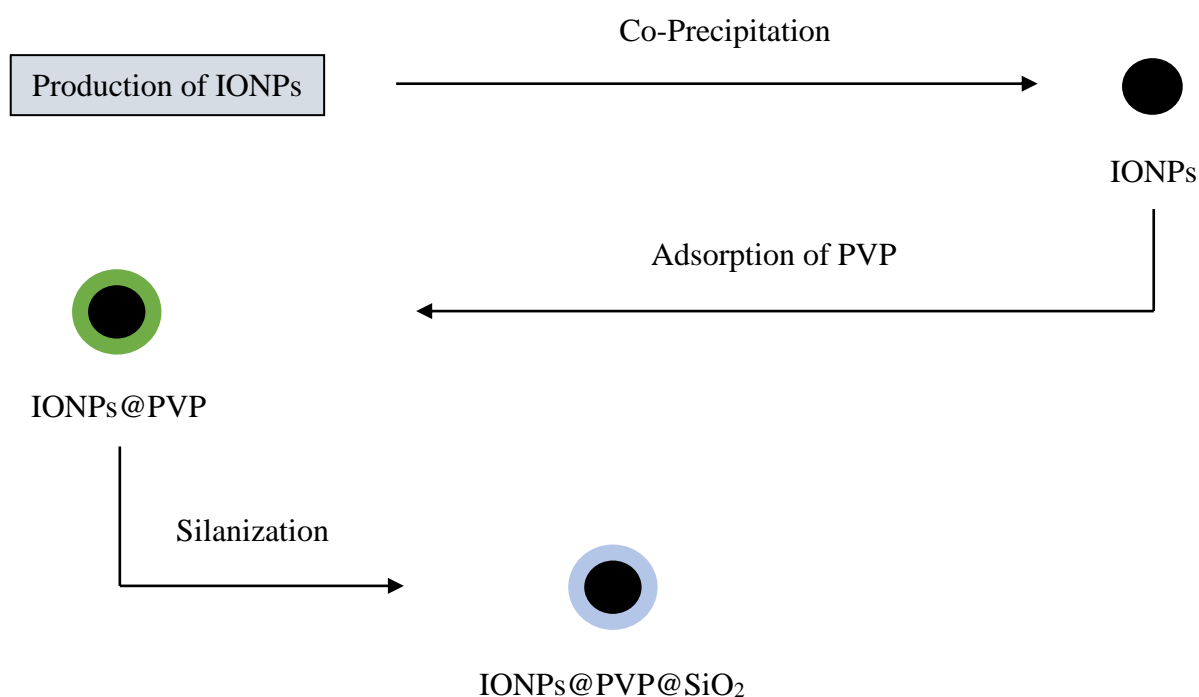


Figure 1. 1: Schematic illustration of work for the thesis.

1.6 Continuation of the Specialization Project

This master's thesis is a continuation of the work done in the specialization project in the Autumn 2021. The aim of the project was to control the particle size of IONPs@SiO₂ with PVP as a stabilizing agent. The study was to understand the effect of PVP on particle size control of IONPs@SiO₂ mostly in batch setting apart for a few experiments in semi-batch settings (20).

The methods for preparing IONPs with the surface modification of PVP appeared not to be efficient because there was nearly no change in particle size and agglomerates were found in all samples, which includes both *post-situ* and *in-situ* surface modification methods. The particle size of IONPs@SiO₂ in the absence of PVP was found to be the smallest compared to IONPs@SiO₂ with PVP. All methods showed approximately the same particle size for IONPs@SiO₂ ranging from 648 to 668 nm in the presence of PVP. The findings of the project also introduced that the number of agglomerates increased with increasing concentration of PVP by the *post-situ* method. The particle size distribution was explored to be narrow without the addition of PVP and the lowest concentration of PVP by the *post-situ* method, whereas the rest appeared to provide higher polydispersity in the system. The project also argued that PVP was potentially not coated on the surface of IONPs by the *in-situ* method (20).

These results appear to depend on the synthesis routes and how effective the methodology was. The methods used from the project was not optimal and the coating process between PVP and IONPs was not fully understood. Finding the solution for this thesis therefore depends on the experimental work (20).

1.7 Structure of the Thesis

This subsection presents an overview of the thesis, where it consists of a total 10 sections, including this one.

Section 1: This section describes the background of the topic which involves the use of PVP and silica as main coating materials to improve the physicochemical properties of IONPs.

Section 2: This section presents the theory related to IONPs.

Section 3: This section presents the importance of surface and colloid chemistry, as well as the colloidal stability.

Section 4: This section presents detailed information related to the adsorption of polymers at interface and why it is important to understand the coating process.

Section 5: This section provides a brief information of PVP as a coating agent.

Section 6: This section introduces the *post-situ* surface modification with the use of silica.

Section 7: This section discusses the gap in the literature associated with PVP coating of IONPs, followed by silanization.

Section 8: This section describes the materials and methods used for the experimental work.

Section 9: This section presents the main findings and the interpretation of the results.

Section 10: This section concludes the overall findings.

2 Introduction to Iron Oxide Nanoparticles

Detailed information of IONPs is considered in this section. The objective of this section is to understand what are exactly IONPs, why IONPs exhibit superparamagnetic behaviour along with other properties that are useful for biomedical applications, and how IONPs can be synthesized through the co-precipitation method.

2.1 The Rise of Nanotechnology and Magnetic Nanoparticles

The rise of nanotechnology has been studied extensively for human applications using of MNPs due to their ultrafine particle size, superparamagnetic properties, and biocompatibility. These MNPs have so far been accepted for various biomedical applications such as drug delivery, fluorescent biological labels, bio detection of pathogens, tissue engineering, magnetic resonance imaging (MRI), detection of proteins, probing of DNA structure, separation and purification of biological molecules and cells. All these applications of MNPs originate from the combination of their magnetic properties with biological circumstances. In biomedical applications, it is preferable that MNPs form stable suspensions in physiological media like water. As previously mentioned, MNPs such as IONPs have large surface area-to-volume ratios and possess high surface energies. In this way, they tend to aggregate to minimize surface energy. These MNPs also agglomerate because of strong magnetic dipole-dipole interactions in the absence of a hydrophilic layer. To improve the biocompatibility and the colloidal stability, and reduce the toxicity of the MNPs, a surface modification approach is essential to make the particles water dispersible, stable, as well as biocompatible. Among the MNPs, magnetite (Fe_3O_4) has been mostly studied (21).

2.2 Superparamagnetic Behaviour of Iron Oxide Nanoparticles

Superparamagnetic IONPs have been attracting various researchers because the particles own diverse potential applications and not just in biomedicine. Other applications such as catalysis, photocatalysis, pigments, magnetic recording technology, and environmental processes are considered important due to their adequate biocompatibility, simple preparation, vigorous superparamagnetic property, and low toxicity. In biomedicine, superparamagnetic IONPs have received an enormous interest in biomedical applications such as targeted drug delivery, cell separation, hyperthermal treatment, immunoassay, separation of biochemical products (22), therapy, magnetic separation, biosensing (23), and most importantly diagnostics (24). Moreover, the particles can also serve as MRI which provide tremendous benefit from diagnosis. Superparamagnetic IONPs demonstrate to have unique properties such as superparamagnetism, high saturation field, extra magnetic anisotropy contributions, and irreversibility of high field magnetization. Owing to these unique properties, superparamagnetic IONPs exhibit great potential in the treatment and detection of illnesses and other medical purposes (25).

2.2.1 Types of Iron Oxides with Different Magnetic Fields

Iron oxides are considered as a transition metal oxide that is capable of having more than one crystalline structure and in addition to various stoichiometric structures owing to the flexibility of their oxidation states such as ferrous ion (Fe^{2+}) and ferric ion (Fe^{3+}). This flexibility follows the formation of different single-crystalline phases including hematite ($\alpha\text{-Fe}_2\text{O}_3$), maghemite ($\gamma\text{-Fe}_2\text{O}_3$) and the commonly studied magnetite (Fe_3O_4). These three phases exhibit various chemical and physical properties (26). The magnetic materials are often dependent on the interaction with magnetic fields, and these can be classified as diamagnetic, paramagnetic, ferromagnetic, anti-ferromagnetic, and ferrimagnetic. Both diamagnetic and paramagnetic appear to demonstrate weak magnetism, in which the property of a certain material is weakly attracted to magnetic fields and exhibit magnetization only in the presence of an external field. Ferromagnetic, on the other hand, possesses a permanent magnetic moment in the absence of an external field and exhibit higher magnetizations than the previous magnetic fields. When a field is applied, magnetic domains of ferromagnetic materials demonstrate to be aligned in the same direction. The magnetic domains of anti-ferromagnetic, however, appear to be aligned in the opposite direction. Ferrimagnetism is quite similar to anti-ferromagnetism, but the difference is the magnitude of one set of parallel spins is not exactly equal to the magnitude of other one set of opposite spins (27).

2.2.2 Superparamagnetic State

Magnetite and maghemite exhibit superparamagnetic behaviour at room temperature. Superparamagnetic behaviour can be featured by the particle size of the NPs. An adequately small particle size of the nanoparticle can be less than 30 nm, in which the direction of magnetization of the NPs can be altered. The magnetic moment of the whole nanoparticle has the capability to arrange itself with an external magnetic field, and this concept is normally called superparamagnetism (12, p. 4). Theoretically, superparamagnetism appears in small ferromagnetic or ferrimagnetic NPs, and when the NPs are small, magnetization flips aimlessly in the direction where the time between two flips is known as the Néel relaxation time. The superparamagnetic state can be achieved when the time used to measure the magnetization value of NPs appears to be longer than the Néel relaxation time in the absence of an external magnetic field, which means their average magnetization value is equal to zero (27, 28).

2.3 The Nucleation Mechanism

Understanding the concepts of nucleation and growth provides a better comprehensive detail on the synthesis of IONPs and how to obtain highly monodisperse particles. Supersaturation is another term that is important to understand along with the nucleation and growth. The homogeneous precipitate in the aqueous medium can be reached where it involves the nucleation and growth of the nuclei, also stable NPs. The homogeneous reaction takes place due to the formation of supersaturated growth species (12, p. 11).

In order to achieve supersaturation, the concentration of solute in the solution exceeds the equilibrium concentration, which is shown in *Equation 2.1*. In this way, the negative amount of the Gibbs free energy is altered with respect to *Equation 2.2*, where the new species take place, where ΔG_v denotes the change in the Gibbs free energy per unit volume of the solid phase, k denotes the Boltzmann constant ($1.38 \cdot 10^{-23} \text{ J} \cdot \text{K}^{-1}$), T denotes the temperature, Ω denotes the atomic volume, C denotes the concentration of the solute, C_0 denotes the equilibrium concentration, while σ denotes the degree of supersaturation (12, p. 11-12).

$$C > C_0 \quad (2.1)$$

$$\Delta G_v = \frac{kT}{\Omega} \ln\left(\frac{C}{C_0}\right) = -\frac{kT}{\Omega} \ln(1 + \sigma) \quad (2.2)$$

$$\sigma = \left(\frac{C - C_0}{C_0}\right) \quad (2.3)$$

For obtaining IONPs with a narrow particle size distribution, both nucleation and growth stages must be separated and the nucleation stages should be suppressed during the growth stage. The control of separation between nucleation and growth stages can be regulated by the turbulent flow generated by an ultrasonic generator and addition to altering the homogenization rates of the solution. The following equations from 2.4 to 2.6 show the decrease of Gibbs free energy as a driving force for both nucleation and growth stages, where ΔG denotes the overall change in Gibbs free energy, ΔG_v and ΔG_γ denote the corresponding free energy changes related to the volume and surfaces changes of the nucleus with a radius of r , respectively, while A_1 and A_2 denote the model constants (12, p. 12).

$$\Delta G = \Delta G_v + \Delta G_\gamma \quad (2.4)$$

$$\Delta G_v = A_1 r^3 \quad (2.5)$$

$$\Delta G_\gamma = A_2 r^3 \quad (2.6)$$

The following equations 2.7 and 2.8 shown below can be expressed when the assumption is for spherical shapes, where $\Delta\mu_v$ and $\Delta\mu_s$ denote the corresponding changes in volume chemical potential and surface energy, while γ denotes the surface energy per unit area. The total Gibbs free energy is defined using *Equation 2.9* (12, p. 12).

$$\mu_v = \frac{4}{3} \pi r^3 \Delta G_v \quad (2.7)$$

$$\mu_s = 4\pi r^2 \gamma \quad (2.8)$$

$$\Delta G = \Delta\mu_v + \Delta\mu_s = \frac{4}{3} \pi r^3 \Delta G_v + 4\pi r^2 \gamma \quad (2.9)$$

According to *Equation 2.9*, the radius of embryo can be measured if the derivative function of total Gibbs free energy is equal to zero, which can be shown in *Equation 2.10* where r^* denotes the embryo radius. To create stable NPs, the critical energy is shown in Equation (2.12) where ΔG_c denotes the critical energy (12, p. 13).

$$4\pi r^{*2} \Delta G_v + 8\pi r^* \gamma = 0 \quad (2.10)$$

$$r^* = -2 \frac{\gamma}{\Delta G_v} \quad (2.11)$$

$$\Delta G_c = \frac{16\pi\gamma^3}{3\Delta G_v^2} \quad (2.12)$$

A schematic illustration of Gibbs free energy as a function of the radius of the nuclei is shown in **Figure 2.1** where it represents the significance of volume and surface energy with regards to the resulting curve. The diagram demonstrates for spherical shapes of the nuclei. Surface energy increases, while the volume energy appears to decrease as the radius of the nuclei increases. The energy barrier generated from this diagram is the critical energy (12, p. 13).

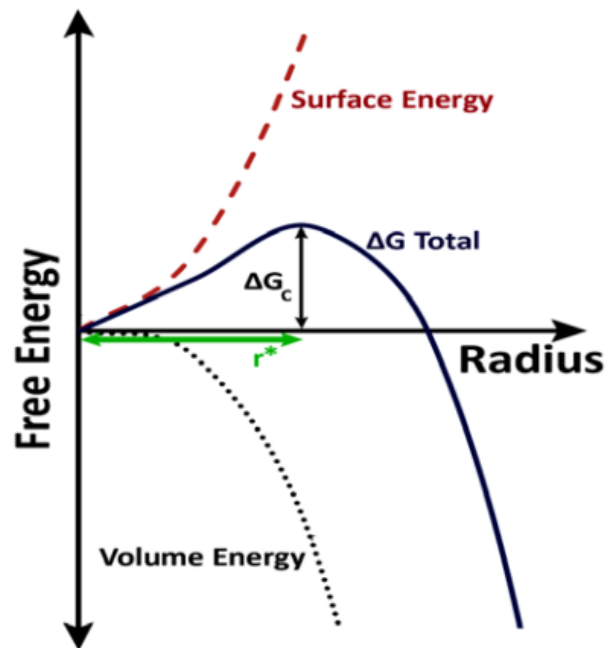


Figure 2. 1: A schematic illustration of the Gibbs free energy as a function of the radius of the nuclei.

The nucleation rate from the energy barrier based on the critical energy can be defined using **Equation 2.13**, where P denotes the probability of the thermodynamic fluctuation of critical energy (12, p. 13-14).

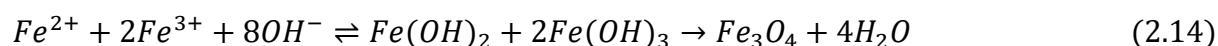
$$P = e^{\left(\frac{-\Delta G_c}{kT}\right)} \quad (2.13)$$

2.4 Synthesis of Iron Oxide Nanoparticles by Co-Precipitation

The most used synthesis method is primarily the co-precipitation owing to the simple route for obtaining the IONPs. The precipitation can be achieved by adding a weak base such as ammonium hydroxide (NH₄OH) to an aqueous solution followed by the addition of a stoichiometric mixture of Fe²⁺ and Fe³⁺ salts dropwise to the solution at ambient temperature. The reaction mechanism can be simplified using *Equation 2.14*. IONPs are prepared by dehydration of iron hydroxide intermediates, in which it forms a precipitate. Thus, IONPs contain OH⁻ groups on the surface, resulting in an adequate favourable suspension in aqueous solution. Narrow particle size distribution, however, is quite tough to obtain due to the rapid formation of the particles, and the control of morphology and particle size in this method is also limited (29, 30). The pH of the base should be in the range between 9 and 14 in addition to keep the molar ratio of iron salts to 2:1. Based on the nucleation theory, the IONPs nucleation takes place when the concentration of iron ions surpasses their solubility in solution (12, p. 14).

Many synthetic parameters affect the size, shape, and composition of the obtained IONPs such as the ratio between Fe²⁺/Fe³⁺, pH, temperature, type of salt used such as chloride (Cl⁻), nitrate (NO₃⁻), and sulphate (SO₄²⁻), and as well as type of base used such as sodium hydroxide (NaOH), and sodium carbonate (Na₂CO₃) (31). According to the methodology given in *section 8*, only one type of base used is NH₄OH, whereas the iron salts are ferrous and ferric ions.

Additionally, the relation between size, shape, and magnetism in IONPs plays an important role in exhibiting their properties. The particles tend to lose their diversity after long-term because of aggregation. Their magnetism also gets reduced due to oxidation in air. Thereby, the surface engineering of IONPs can be employed by few methods through layering a coating material over the core of the IONPs in order to generate a core-shell structure (24), which is primarily discussed in the next few sections. Because of the kinetic factors involved during crystal growth, the limited control of the particle size uniformity is an all-inclusive drawback. The NPs surfaces are reactive, so agglomeration processes take over. Hence, silica is an option to prevent this phenomenon. As in overall, the synthesise method is cost-effective and versatile for biomedical applications if it is coated with the right material (10).



3 Introduction to Surface and Colloid Chemistry

The objective of this section is to introduce the most essential principles and theories associated with surface and colloid chemistry. To identify the problem related to the thesis, it is quite useful to understand this topic, and in addition to finding practical solutions to solve the problem. This section is written with the purpose to balance theory and applications, to present the fundamental principles and theories of surface and colloid chemistry in a simple approach. Although some principles and theories are not entirely covered, it is important to have an adequate understanding of research aspects in surface and colloid chemistry.

3.1 Why are Surfaces and Colloids Important?

First and foremost, the term “colloid” was originally invented by Thomas Graham in 1861 where he measured the diffusion rate to different chemical compounds in water. It was discovered that a class of natural macromolecules took place where they diffused quite leisurely in comparison to ordinary inorganic salts. These macromolecules are considered polymers (32, p. 1). He first thought that the unique properties of colloids were because of the nature of the compounds involved, however he realized that the size of particles is simply responsible for the unique properties of colloidal systems. The distinctive term “colloid” was in fact derived from the Greek word for glue (“colla”), meaning glue-like molecules (33, p. 1-2).

When the term “colloid” is used, the term “surface” is also used to understand the most common surface and colloid phenomena. Surface and interface can sometimes be interchangeable, but in fact there is no difference between the terms. However, the term “interface” is mostly recommended when describing a phase boundary between two condensed phases such as molecules in liquid and solid states of matter, meaning between liquid-liquid, liquid-solid and solid-solid phases. Thus, interface is perhaps the most used keyword rather than surface (32, p. 1, 33, p. 4). The connection between surfaces and colloids is interesting to study due to the extensive difference in surface (interfacial) area which is one of the reasons why the properties of the interface become highly essential for colloidal solutions (= colloidal dispersions). The unique properties of colloidal dispersions are somehow associated with the high interfacial area of the dispersed phase, and in addition to the chemical nature of the surface of the particle (33, p. 3, 34, p. 1, 6).

Why are surfaces and colloids just important to study? It is an immensely interdisciplinary topic because surface and colloid chemistry provide diverse fields of science and engineering perspective such as medicine, food, cosmetics, detergents, pharmaceuticals, materials, and microelectronics. Colloids have various useful properties where stability is perhaps the most important factor. The study of both interfaces and colloids is the knowledge between molecules and particles or surfaces which is principal to the problem statement of this thesis (33, p. 7). Particle interactions dispersed in a medium are primarily one of the main keys of understanding how IONPs and functionalized IONPs interact with one another in aqueous media.

3.2 Colloidal Systems

To refer to colloidal systems, but what is it? These types of systems may be a bit complicated to understand. In colloid chemistry, colloidal systems are primarily systems of particles or normally droplets with the proper dimensions “the dispersed phase”, which are dispersed in a medium such as liquid, solid or gas, and this medium is often called “the continuous phase”. Simply put, it is basically “particles” dispersed in a medium. A colloid fall somewhere between homogeneous and heterogenous mixture. A homogeneous mixture provides a uniform appearance where the particles do not separate out and the mixture is considered a solution. A heterogenous mixture has parts that do not dissolve, and these may suspend, but they always settle out, which means that the mixture is non-uniform. Therefore, a colloidal system presents an intermediate state which particles have intermediate or medium sizes and do not settle down but remain suspended (33, p. 1).

Since colloidal systems are found to have intermediate particles, it is important to note that the system depends on the particle size of the solute in the medium. The particles have dimensions between 1 nm and 1 μm (10^{-9} and 10^{-6} m). Their unique properties arise from the large surfaces owing to these dimensions. In simpler terms, the characteristic properties of colloidal systems depend on the particle size such as the dispersed phase and not to any unique nature of the particles or solvent. In colloidal systems, particles exhibit spherical shapes, but on some occasions the colloidal particles are not always spherical such as rod- or disk-like shapes. With respect to polymers, they are considered as colloid particles and their shape is affected to a certain degree of hydration. This phenomenon is usually used when the solvent molecules are linked or attached to the particles, which leads to the influence of their final properties. Polymers are usually categorized as lyophilic colloids (33, p. 2).

3.2.1 Classification of Colloids

Based on colloidal systems, it can be classified as the state of dispersed phase and the continuous phase like liquid, solid and gas according to their stability (33, p. 5). Colloidal systems can be divided into subgroups on the basis of chemical and physical properties. Based on lyophilic colloids (lyo = liquid and phileous = love), they refer to high attraction (affinity) between the particles of dispersed phase and the surrounding liquid phase, which means that they have attached interface groups that are wetted/solvated by the liquid in the case of water due to diversity of hydrogen bonds. As mentioned earlier, polymers are lyophilic macromolecules, and such systems are thermodynamically stable and reversible. Oppositely, lyophobic colloids (lyo = liquid and phobia = not loving) do not refer to high affinity between the particles and the liquid phase. Example of such systems are colloidal dispersions where the system is thermodynamically not stable and irreversible because of their high specific interfacial area, which means they have the tendency to aggregate (32, p. 3-4).

The terms hydrophilic and hydrophobic are also used due to the fact that aqueous dispersions are commonly referred to as colloidal systems where water is the main medium. Simply expressed, hydrophilic is defined as water-loving where the colloidal particles are attracted to water, whereas hydrophobic is defined as water-scaring. If a molecule is bonded with groups such as OH^- , they have the ability to interact with water by intermolecular force like hydrogen bonding. Hydrophobic molecules, on the other hand, do not have any form of intermolecular bonding with water molecules. Thus, these molecules do not dissolve or mix well with water unlike hydrophilic molecules (32, p. 3).

3.2.2 Types and Applications of Colloidal Systems

Colloidal systems can also be divided into different systems shown in **Table 3.1**. Examples of such systems are liquid-gas, gas-liquid, liquid-liquid, solid-liquid, gas-liquid, liquid-solid, and solid-solid systems. From the table, each combination exhibits different properties and colloids. There are eight various colloidal systems, and these colloids depend on the physical state of dispersed phase and continuous phase. However, why are there no gas-gas combinations? Two gas phases do not create a colloidal system due to the fact that the dispersed phase is already at the molecular level and thus there is a homogeneous mixture of different gases. But as shown in the table, various combinations are possible to obtain depending on the phase of the colloidal particles and the medium (32, p. 5, 33, p. 6, 34, p. 6).

Table 3. 1: Various types of colloidal systems (34, p. 6).

Dispersed Phase	Dispersion Medium	Name	Examples
Liquid	Gas	Liquid Aerosol	Fogs, Sprays, Smoke, Dust
Solid	Gas	Solid Aerosol	Foams
Gas	Liquid	Foam	Milk, Mayonnaise
Liquid	Liquid	Emulsion	Au Sol, AgI Sol
Solid	Liquid	Colloidal Solution “Sol”	Toothpaste
Gas	Solid	Solid Foam	Expanded Polystyrene
Liquid	Solid	Solid Emulsion	Opal, Pearl
Solid	Solid	Solid Suspension	Pigmented Plastics

Various applications of surface and colloid chemistry are very important, ranging from these fields of study such as materials and nanotechnology, biotechnology, food science, environment, separations, chemical industries to oil industries, which are shown in **Table 3.2**. The most relevant field of study for this thesis is materials and nanotechnology because of surface modifications of NPs where surface chemistry plays a huge role (33, p. 4).

Table 3. 2: Various applications of surface and colloid chemistry (33, p. 4).

Surface and Colloid Chemistry	
Field of Study	Application
Materials and Nanotechnology	Nanoporous Materials Surfaces with Unique Properties Surface Manipulation and Analysis Electronics, Semiconductors Extreme Applications such as Space
Biotechnology	Cell Membranes Lung Surfactant Drug Delivery Proteins and Surfactants in Detergents Protein Analysis Pharmaceutical Emulsions
Food Science	Food Emulsions and Dispersions
Environment	Air Chemistry, Aerosols Water Purification Natural Phenomena, Soil Structure
Separations	Adsorption Membranes Filtering Flotation
Chemical Industries	Paints and Coatings Glues such as Adhesives, Lubricants Detergents-Cleaning Photo-Emulsions Catalysts Mineral Processing and Separations in Mining Industry
Oil Industries	Oil Recovery Porous Materials Capillary Condensation

3.2.3 Terminology in Colloidal Systems

In colloidal systems, the terminology is very important to understand the colloidal stability. Aggregation is the most used term when the system is not stable. Other terms such as coagulation, agglomeration, coalescence, and flocculation can sometimes be interchangeable. The definitions, however, are sometimes used in different circumstances and these are elucidated below (32, p. 212, 33, p. 235).

Aggregation

The most used terminology is aggregation and often refers to the cohesion between two or more particles, which means that these particles are attracted to each other, resulting in clusters, but they do not merge into a new particle. The total surface area is not significantly decreased (32, p. 212). The term agglomeration can be replaceable depends on the conditions of the system.

Coagulation

Another term to use is coagulation which refers to the formation of aggregates owing to the clash between solid particles, which results in a significant decrease in the total surface of particles, and it is considered an irreversible phenomenon (32, p. 212, 33, p. 235).

Coalescence

The term coalescence is mostly used when the individual particles completely lose their identity or original shape where droplets or bubbles fuse together to form a single larger drop or bubble, in which the total surface area is decreased (32, p. 212).

Flocculation

The term flocculation, on the other hand, refers to the formation of loose and simple reversible networks of particles, and this term is usually linked to the secondary minimum energy region in the DLVO theory (32, p. 212, 33, p. 235).

3.3 Colloidal Stability

The presentation of colloidal stability is one of the most important topics in colloid chemistry. The most commonly concepts are van der Waals (vdW) and electrical forces between colloid particles. Other important concepts to include are zeta potential and electrical double-layer thickness. The DLVO theory of colloidal stability is also presented. This is an important theory to include because of how stability is affected by controlling the parameters. Hamaker is also a concept from the colloidal stability, but it is not covered in this thesis. The aim of this subsection is to understand the importance of each concept and theory associated with the classical DLVO and their role in colloidal stability (33, p. 211).

In the preceding subsections, the properties of colloidal dispersions are related to the high interfacial area of the dispersed phase. Colloidal dispersions are not stable owing to the high interfacial area and thus the system is required to be somewhat stabilized. The question is how? When colloidal stability is mentioned, various types of forces between the colloidal particles can be considered. The various forces are shown in **Table 3.3**, and these are vdW, electric, and steric forces. Due to Brownian motion, interactions between particles dispersed in water take place regularly. The vdW forces become dominant when the distance between two particles has a short separation distance. The force of attraction tends to overcome the repulsive forces such as electrostatic or steric forces. To this extent, the particles aggregate, in which the particles remain close to one another temporarily or permanently without merging into a new particle. Even though the total interfacial area is not significantly reduced (32, p. 212). However, stable dispersions are attained when the repulsive forces dominate over the attractive vdW forces, which means the separation distance is longer (35, p. 53).

Table 3. 3: Various types of forces between the colloidal particles (33, p. 212).

Colloidal Stability	
Forces	Effect
van der Waals	Attractive
Electrical (Ions)	Repulsive
Steric (Polymers)	Repulsive

3.3.1 The van der Waals Forces

Colloidal stability depends crucially on the vdW forces. The vdW force is a general term to define intermolecular forces between molecules and the distance between the molecules has a short range. The vdW force between two molecules are given by the fundamental expression given in **Equation 3.1** where the single contributions are due to polar (p), induction (ind), and dispersion (disp) forces. The attractive vdW force can be explained by understanding the attractive force originating from induced or permanent dipoles in atoms or molecules (33, p. 15).

$$V_{12} = -\frac{C}{r^6} = -\frac{C^p + C^{ind} + C^{disp}}{r^6} \quad (3.1)$$

The vdW force is the result of the interaction between a permanent dipole and other dipoles or a polarizable atom that tends to produce an induced dipole or produced instantaneous dipoles because of fluctuations in the distribution of electronic charge in the absence of permanent dipoles. These three contributions are polar (Keesom), induced (Debye), and dispersion (London) interactions. To understand these three contributions, the following equations are expressed to understand each interaction. **Equation 3.2** defines the polar interactions due to the dipole-dipole interaction between two permanent dipoles on a surface. **Equation 3.3** defines Debye interactions that arises from interactions between a molecule with permanent dipole that induces a dipole in the other molecule. **Equation 3.4** defines dispersion interactions, in which no permanent dipole is required for attraction between molecules (33, p. 15, 35, p. 54). In these equations, V denotes the potential energy (J), C denotes the electric charge, r denotes the distance between the positive and negative charge within a certain molecule (m), μ denotes the dipole moment ($\mu = ql$) where the Debye length is $3.336 \cdot 10^{-30} Cm$, α_{0i} denotes electronic polarizability ($C^2 m^2 J^{-1}$), k_B is the Boltzmann's constant ($1.38 \cdot 10^{-23} J \cdot K^{-1}$), ϵ_0 denotes vacuum permittivity ($8.854 \cdot 10^{-12} C^2 J^{-1} m^{-1}$), while I denotes the 1st ionization potential (J) (33, p. 15).

$$V_{12} = -\frac{C^p}{r^6} = -\frac{1}{3} \left[\frac{\mu_1^2 \cdot \mu_2^2}{k_B T (4\pi\epsilon_0)^2} \right] r^6 \quad (3.2)$$

$$V_{12} = -\frac{C^{ind}}{r^6} = -\left[\frac{\alpha_{01} \mu_2^2 \cdot \alpha_{02} \mu_1^2}{(4\pi\epsilon_0)^2} \right] r^6 \quad (3.3)$$

$$V_{12} = -\frac{C^{disp}}{r^6} = -\left[\frac{3\alpha_{01}\alpha_{02}}{2(4\pi\epsilon_0)^2} \right] \left[\frac{\alpha_{01}\mu_2^2 \cdot \alpha_{02}\mu_1^2}{(4\pi\epsilon_0)^2} \right] r^6 \quad (3.4)$$

3.3.2 The Electrostatic Forces

Another force that is important to include is the electrostatic force. This force arises because of the attraction of opposite charges or the repulsion of similar charges. When defining the electrostatic interaction, the electrical force can be elucidated by the electrical double layer (EDL) present around the particles in almost all colloidal dispersions. In aqueous media, nearly all particles are charged, in which the interfaces consist of either a positive or negative charge. However, most interfaces are negatively charged once they are dispersed in water due to the fact that the smaller cations (positively charged) are more hydrated than anions (negatively charged). Thus, the cations remain in the aqueous media, whereas the anions adsorb at the interface. With regards to the hydration number, divalent and trivalent cations have the tendency to be more hydrated than monovalent cations, while monovalent anions tend to be poorly hydrated (33, p. 219).

To get into the details of EDL, charged interface is an important term to consider. The charge at the interface (σ) is provided by a distribution of ions with oppositely charged particles called “counterions” and ions with similar charge, the so-called “co-ions”. The EDL formation is illustrated through the Stern modification of the Gouy-Chapman theory from *Figure 3.1*. The illustration reveals that there is a monolayer of counterions adsorbed on the interface and a diffuse layer in which the concentration of counterions decreases as the separation distance increases (35, p. 56). The counterions are electrically attracted to the interface, but the charges also have the tendency to diffuse away, somewhat resulting in a diffuse double layer of ions dispersed in a medium. Simply put, in this model it consists of two regions which are the Stern layer and the diffuse layer (33, p. 219).

The Stern layer presents the distance between the interface and the counterions is close together owing to the attractions with the charged interface, as illustrated from the figure. In the diffuse layer, the concentrations of counterions are moderately reduced due to random movements of counterions until an electroneutral solution is achieved. The attractive force of the anionic charges becomes weaker with the distance and thereby the 2nd is less ordered, structured, and mobile compared to the 1st layer. The diffuse layer is considered the Gouy-Chapman layer. From the figure, the boundary line between the Stern and the diffuse layer is contemplated as the shear plane. The potential distance dependency is linear in the Stern layer and exponential in the diffuse layer (33, p. 219-220, 223).

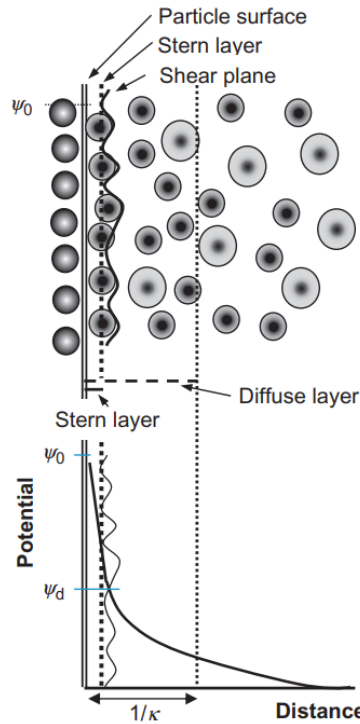


Figure 3. 1: The electrical double layer (35, p. 54).

An example of a schematic illustration of the EDL on the surface of a nanoparticle based on the Gouy-Chapman-Stern model is presented in **Figure 3.2**. The interface between a metal oxide and aqueous solution is interesting to explore. As demonstrated in the figure, the surface complexation of the metal oxide is strongly affected by the development of the surface charge which results in the EDL. This tends to create around the surface of the metal oxide of each particle. The energy potentials represented in the figure display that the surface potential is located at the charged particle, and the Stern potential is located at the Stern layer, while the zeta potential (ζ) is located at the shear plane (slipping plane). It is important to note that the EDL presented for nanoparticles is also closely related to the **Figure 3.1**, because the particle interface has ions distributed in the surrounding interfacial area, which results in an increased concentration of counterions near the interface of the charged particle (36).

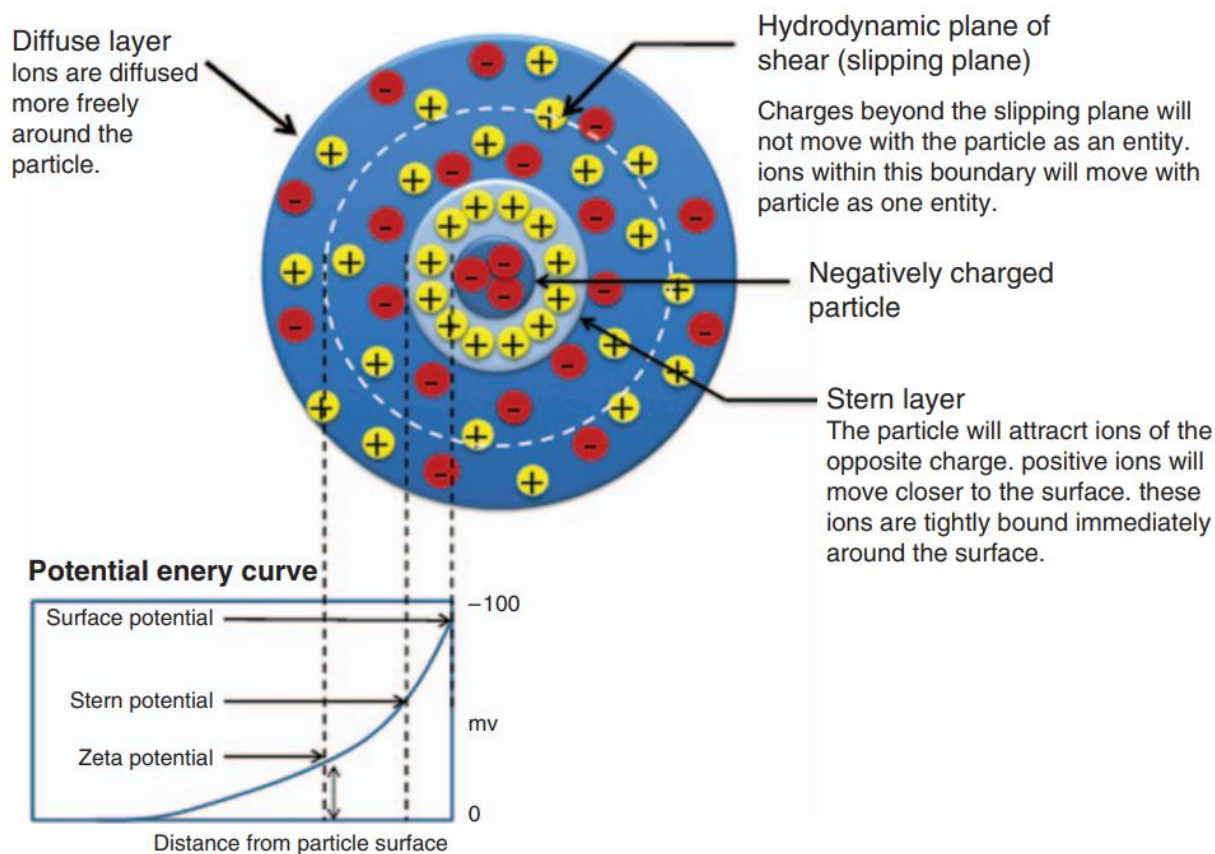


Figure 3. 2: The electrical double layer on the surface of a nanoparticle based on the Gouy-Chapman-Stern model with the various energy potentials represented (36).

The Stern model divides the EDL into two parts which are the inner part due to immobile ions and specific adsorption and the outer part due to mobile ions. The electrical forces of particles arise because of overlap of their diffuse electrical double layers, and this can also be illustrated in **Figure 3.3**. The double layers start to overlap when two charged particles approach each other which results in electrostatic repulsion. The schematic representation of EDL can be shown in **(a)**, while the schematic representation of steric stabilization can be shown in **(b)**, in which the stabilization is achieved using adsorption of polymers (33, p. 214).

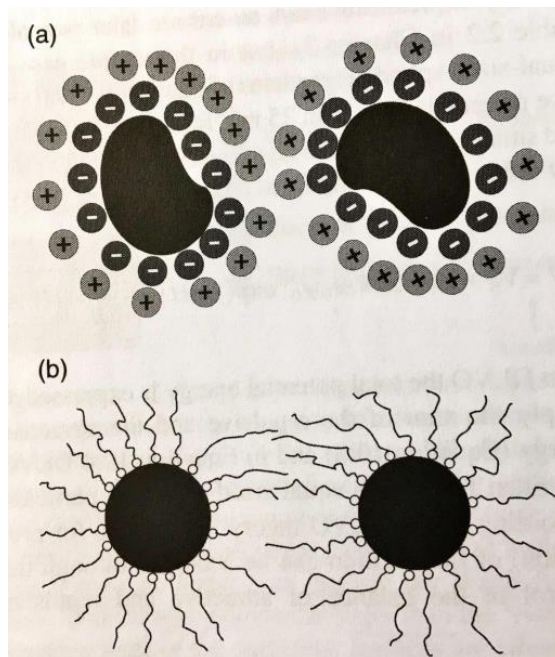


Figure 3. 3: Schematic illustration of (a) the electrical double layer forces and (b) the steric stabilization adsorbed by polymers (33, p. 214).

3.3.3 Key Parameters of Electrical Forces

Regarding electrostatic or electric forces, the understanding and control of the electrical interactions and the stability of a colloidal dispersion depends extensively on the Debye length (λ_D) and the zeta potential. The commonly used parameter is the zeta potential because it provides more detail about the surface charge which is quite related to the objectives given in this thesis. In colloidal stability, it is essential to regulate the diffuse double layer through regulation of the ionic strength of the solution, as well as the adsorption of charged molecules such as ionic surfactants and polyelectrolytes. Polyelectrolytes are commonly used when steric interactions are applied in colloid chemistry (33, p. 222, 234).

The Debye (double layer) length is a measure of the length (thickness) of the EDL. This layer usually depends on the solvent, the temperature and in particular the ionic strength of the solution. The Debye parameter is expressed in *Equation 3.5*, where e denotes the elementary charge ($1.602 \cdot 10^{-19}C$), $C_{i(B)}$ denotes the concentration of ion i in the bulk solution, z_i denotes the ionic valency of ion i , while I denotes the ionic strength. The Debye length plays an important role in the stability of colloidal dispersions. Some key points for applying the Debye thickness involve the measurement of the thickness of EDL, and as well as increasing the stability when the Debye has a high value. The higher the Debye thickness, the better the colloidal stability of the system (33, p. 222, 225, 234-235).

$$\kappa^{-1} = \sqrt{\frac{\epsilon\epsilon_0 k_B T}{e^2 N_A \sum_i C_{i(B)} z_i^2}} = \sqrt{\frac{\epsilon\epsilon_0 k_B T}{e^2 N_A 2I}} \quad (3.5)$$

The zeta potential, on the other hand, is the electrical point at the shear plane, which means the boundary line between the Stern and diffuse layer. The parameter may also be defined as the measurement of the magnitude of the electrostatic of charge attraction or the repulsion between particles. The zeta potential is one of the fundamental parameters that is known to affect stability to a high degree. The measurement of zeta potential provides details of the dispersion, aggregation, or flocculation. From the previous subsection, the other various potentials are considered such as surface and Stern potential. All three potentials are different because they are located at different locations. This means that the zeta potential is not equal to the surface or the Stern potential in the EDL. The zeta and Stern potentials are close to each other, but theoretically the zeta potential is, in fact, the lowest of the three. When performing calculations, all three potentials are assumed to be identical. However, the error presented using the zeta potential turns out to be small except for a few occasions (32, p. 250, 33, p. 223).

In colloidal dispersions, zeta potential is known to be under the category of electrokinetic potential. Electrokinetics is simply defined by movement caused by electric interactions. The term is commonly used with the combination of effects of motion and charge. With respect to colloidal particles, motion is affected by EDL. The measurement of zeta potential can be performed via the so-called electrophoresis experiment (32, p. 250). In order to achieve higher colloidal stability, the high absolute value of the zeta potential produces a repulsive electrostatic interaction between particles. This is also the key to resisting agglomeration or aggregation in the dispersion. Theoretically, the higher the zeta potential, the more stable the dispersion. A specific value for colloidal stability is when the electrostatic stability of the absolute zeta potential is 30 mV or higher, whether it is -30 or +30 mV (37). Zeta potential analyzes are often considered important with regards to NPs because it is used to improve the dispersion and suspension of a system. This means that highly dispersed NPs have zeta potential less than -30 mV or greater than +30 mV. Another important fact is that NPs is quite sensitive to variation in pH and ionic strength (38). Since pH is an important factor affecting the zeta potential, it can affect the surface charge and thus the extent of the repulsion between particles dispersed in the medium (39). Theoretically, a plot of zeta potential versus pH is positive at low pH, but negative at high pH (40).

3.3.4 The DLVO Theory

To conclude from the previous subsections, the colloidal stability depends on the balance between the attractive vdW and the repulsive electrostatic interactions. The electrostatic double-layer interaction dominates at longer separation distances, whereas the attractive vdW interaction dominates at shorter distances. However, the attractive vdW forces between particles/surfaces are of much longer range than the corresponding forces between molecules, whereas the repulsive electrostatic forces between particles/surfaces are also long range but on many occasions with various distance dependence. Simply put, the distance between surfaces/particles of vdW forces can also be very long, but theoretically, when the surfaces are brought relatively close to each other, the vdW forces have the tendency to overcome the repulsive electrostatic forces resulting in dominance of the attractive force over the repulsion force. However, that is unlikely to occur when the distance becomes longer where stability may be obtained in the region where the repulsion forces dominate. Stable colloidal systems are achieved if the colloidal particles have very low or negative Hamaker constants, high Debye length (double layer thickness), and high absolute zeta potential. Therefore, the stability of colloidal systems can be quantified with the DLVO theory. The theory is commonly used that evaluates the interaction between dispersed particles in a liquid medium such as water (33, p. 12, 243).

The DLVO theory was developed by Deryaguin, Landau, Verwey, and Overbeek. The theory assumes that when the particles are dispersed in a medium, they experience both attractive and repulsive forces. The overall interaction between particles is the product or a combination of the attraction and the repulsive forces. It is based upon the energy changes arises when two charged surfaces encounter, resulting in the total interaction energy given in the **Equation 3.6** where V_T denotes the overall interaction energy, V_A denotes the attractive London-vdW forces, while V_R denotes the repulsive potential energy due to electrical double layers overlap. The attractive V_A is defined as negative, while the repulsion force V_R is defined as positive (32, p. 213).

$$V_T = V_A + V_R \quad (3.6)$$

A schematic illustration is shown in **Figure 3.4** where it represents how all interaction such as V_T , V_A , and V_R can depend on the distance between particles, H . In terms of theory, there are three main regions for interaction between particles, namely the primary minimum, the primary maximum, and the secondary minimum regions. When V_T reaches the primary minimum region, there is a high attraction between the particles because the particles approach very close to each other, which results in coagulation or agglomeration. This region causes an instability in the system. However, when V_T reaches the primary maximum region, high repulsion exists which is usually regulated by the zeta potential. The effect of the parameter prevents the particles from coming closer to each other and the particles remain individually dispersed. When V_T reaches the secondary minimum region, the attraction force is not as strong as in the primary minimum because the particles do not agglomerate, but rather flocculate. Note that V_T increases as H decreases until the repulsive energy maximum is reached in the primary maximum region. Beyond this point, the attractive force becomes dominant, and the total interaction energy decreases quickly until the primary minimum is reached. Thus, controlling the zeta potential is one of the most important parameters to overcome the agglomeration (32, p. 213-214).

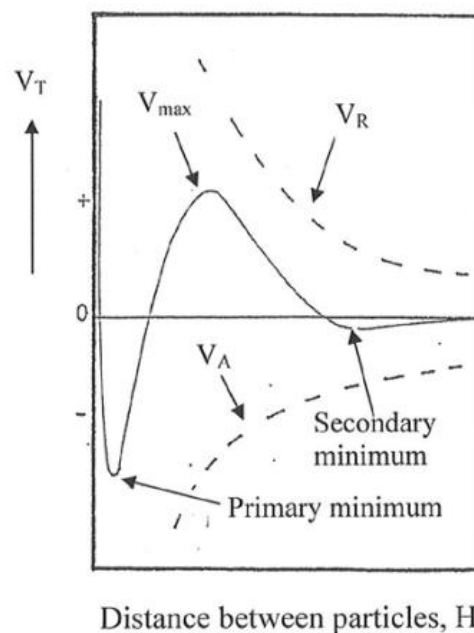


Figure 3. 4: Schematic illustration of the total interaction energy as a function of the distance (H) between the particles (32, p. 213).

3.3.5 The Steric Forces

Another force that is important is the steric interaction (or electrosteric). This interaction provides stability to a suspension through the adsorption of polymers onto the particle's interface. As previously mentioned, electrostatic interaction is the type of force that takes place with charged interfaces such as EDL. However, the steric interaction can also take place with charged interfaces with adsorbed polymers. Systems that consist of electrical double layers or adsorbed polymers tend to develop a repulsive interaction as the colloidal particles approach each other. The electrical and adsorbed layers begin to overlap. If the double layer of two particles overlaps the negative or positive charge at the Stern plane repels each other. In the case of steric interactions, particles contain adsorbed polymers or non-ionic surfactants which have the tendency to penetrate as the particles approach, resulting in an increase in the density of polymer segments and steric repulsion arises (35, p. 53, 58).

Adsorbed polymers can be uncharged or charged (the so-called polyelectrolytes), in which the steric hindrance or barrier related to the adsorbed polymer is strengthened by electrostatic repulsion because of the presence of charges surrounding the molecule. The steric repulsion is introduced where the steric effect is dominating at short range colloidal stability and the electrostatic repulsion occurs at higher distances (35, p. 58). However, there is always an attractive interaction due to the vdW force, which has the ability to attract particles to each other at short separation distances (35, p. 53). Thereby, an approach to stabilize the colloidal system is to increase the steric repulsions by adding a polymer layer or increase the repulsive forces owing to the EDL interactions (39). The steric interaction is an important concept to include in this work because of the effect of polymers adsorbed on the surface of particles dispersed in water.

Steric interactions are short-range, and the layers are preferably to be thick due to the reason that the forces have small distances. The adsorption of polymers on the surfaces/particles must be strong to prevent displacement during bridging or depletion phenomena. To avoid coagulation, the repulsive interaction of the lyophilic segments and particles is considered (33, p. 277-278).

3.3.6 Steric Stabilization

From the previous subsections, the DLVO theory is built on a balance of the attractive vdW and repulsive electrostatic forces. The focus of this subsection is to understand the stabilization method which is based on an additional compound such as polymers known as steric stabilization. For protecting particles against agglomeration or coagulation, this stabilization method is considered. Polyelectrolytes provide particles with both electrostatic and steric stability against coagulation, whereas uncharged polymers only provide steric stabilization. In the case of steric stabilization, the total interaction energy can be expressed using *Equation 3.7* where the new term V_S denotes as the steric interaction energy (41).

The steric forces are not taken into consideration from the DLVO theory in *Figure 3.4*, but the theory can be extended by introducing the effect of steric interactions. The potential energy diagram for a steric stabilized colloidal system with and without EDL repulsion is shown in *Figure 3.5*. To understand the diagram, the potential energy of interaction is dependent on the particle distance. On the left side of the diagram, the repulsive force is not considered, whereas on the right side of the diagram, the repulsive force is introduced. The illustration shows that the total interaction energy V_T with and without EDL repulsion decreases as the distance between the particles increases. This also applies for the V_S . When the steric interaction energy reaches the primary maximum region, coagulation is not possible to obtain due to the energy barrier created. However, flocculation might arise in the secondary minimum region (32, p. 233-234).

$$V_T = V_A + V_R + V_S \quad (3.7)$$

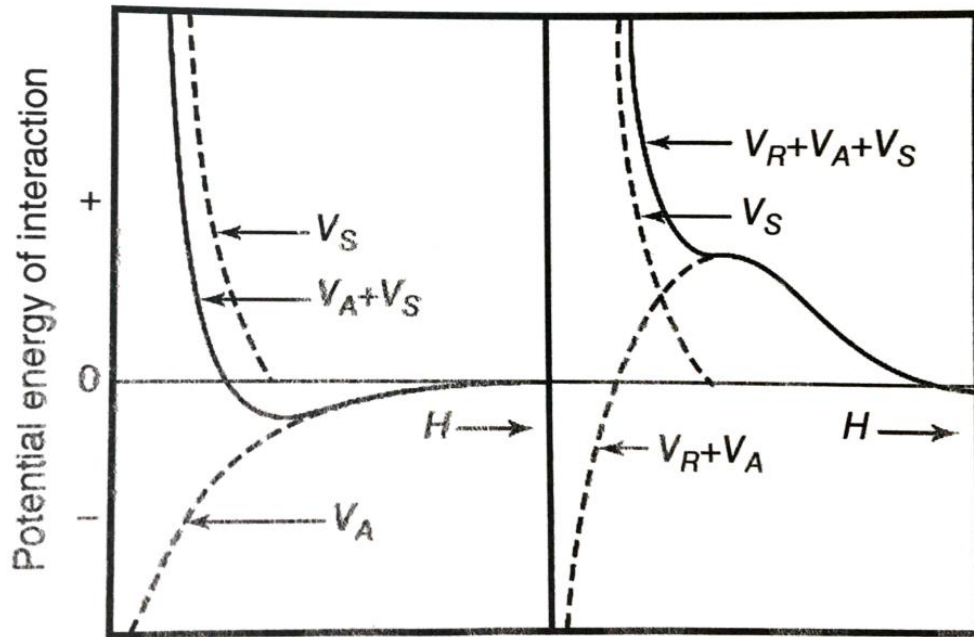


Figure 3. 5: Representation of the potential energy diagram for a steric stabilized colloidal system with and without electrical double layer repulsion (33, p. 275).

An important fact with respect to repulsive electrostatic forces is the high repulsive interactions between the particles, which results in a reduction of aggregation in the system. However, there is an instability problem related to the primary maximum region from the DLVO plot. For colloidal systems stabilized by only electrostatic forces, there is a reduction in the energy barrier that results in rapid coagulation. Therefore, a combination of repulsive electrostatic and electrosteric forces is required for better stability owing to the adsorption of polymers at the particle's interface. If the polymers are charged, there might be a change in the electrostatic repulsion. For long chain of polymers, steric repulsion arises when the adsorbed layers penetrate (33, p. 275).

Addition of polymers can not only result in stabilization but also destabilization of colloidal systems due to either depletion or bridging flocculation, which can be illustrated in **Figure 3.6**. Adding polymers to the system may also alter the hydrodynamic characteristics of the colloidal system. If no adsorption of polymer chains is covered at the interface because of lower polymer concentration near the interface, this results in depletion flocculation. However, if the particle's interface is not completely covered by the adsorbed polymer, this can lead to bridging flocculation and is considered as partial interface coverage (33, p. 277).

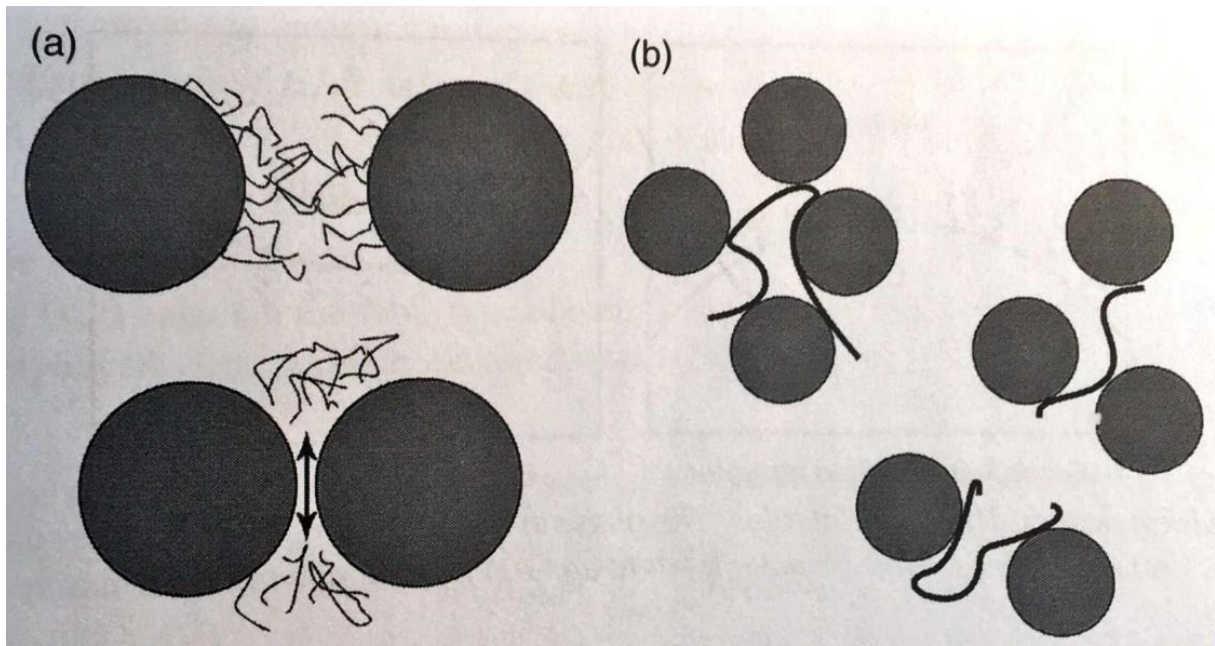


Figure 3. 6: Schematic illustration of steric destabilization of colloidal systems of (a) depletion flocculation and (b) bridging flocculation (33, p. 277).

4 Introduction to Polymers at Interface

Introduction of polymers adsorbed at the interface of particles is explained in more detail. This section is the continuation of steric stabilization from previous section. This topic is important to understand how polymers interact on surfaces or interfaces of particles.

4.1 Adsorption of Polymers in Colloidal Systems

From earlier sections of steric repulsion force, polymers are the center of attention. The idea is to understand how polymers are dispersed in a liquid media, as well as to study the interaction between the interfaces with the aim to enhance particle dispersion along with flocculation process and interface properties. How polymers are adsorbed onto the interface of particles can be elucidated through diffusion, attachment, and rearrangement. The role of diffusion is to transfer the polymer from the bulk to the interface, whereas the role of attachment is to attach the polymer to the interface, and the role of rearrangement is to improve polymer segments at the interface site. The adsorption process of the polymer is depending on the molecular weight of the polymer, the quality of the solvent, interface-to-volume-ratio, the polymer density, pressure and temperature, pH, and the ionic strength (42).

4.2 Adsorbed Polymers with Various Interactions

From previously mentioned section, preventing aggregation in the colloidal system depends on different forces. The adsorbed surface includes with and without a polymer. A summary of important forces can be shown in *Figure 4.1*. The interactions between colloidal particles depend on a balance between vdW and electrostatic forces without the adsorption of polymer. The depletion effect, however, is another attractive force that has the capability to expel polymer chains from the interface due to osmotic attraction between the colloidal particles, and this may lead to aggregation. This means that no polymers are adsorbed on the interface of the particle, which results in poor stability. Bridging flocculation, however, involves the adsorption of some polymer chains on two or more various particles simultaneously, but this force does not allow complete interface coverage. Steric repulsion, on the other hand, has the ability to protect the particles from interacting with each other at the high concentration of polymer chains, resulting in complete interface coverage. To achieve highly colloidal stability in the system is not simple (43).

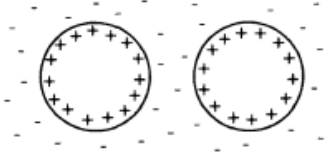
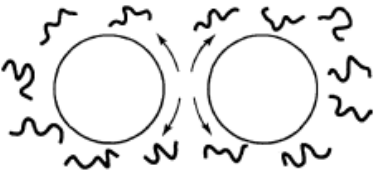
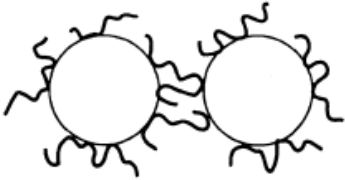
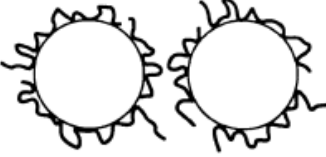
MECHANISM	FORCE LAW
<p>(A) bare particles</p> 	<p><u>Van der Waals attraction</u></p> <p><u>electrostatic repulsion</u></p>
<p>(B) particles + non-adsorbing polymer</p> 	<p>weak (osmotic) attraction</p> <p><u>"depletion attraction"</u></p>
<p>(C) particles + low polymer dose adsorbed</p> 	<p>strong attraction</p> <p><u>"bridging"</u></p>
<p>(D) particles + excess adsorbing polymer</p> 	<p>strong repulsion</p> <p><u>"steric repulsion"</u></p>

Figure 4. 1: Schematic overview of various interactions between colloidal particles with and without polymer (43).

4.3 Polymer Adsorption and the Control of Steric Stabilization

As polymers enter the liquid and as the particles approach close to each other, the polymer layers tend to hinder the particles from interacting with each other, which results in steric repulsion. The steric repulsion depends on the properties of the polymer and the solvent. The dependence on the molecular weight of the polymer has an effect on steric stabilization and determines the final properties of the polymer. Thus, the amount of polymer adsorbed on the interface depends on the molecular weight (33, p.174-176).

To achieve good adsorption, higher molecular weight of polymer is recommended. Adsorption of polymers is higher at high polymer molecular weight in comparison to lower molecular weight. However, adsorption of higher molecular weight of polymers is not quick, but rather slow due to the fact that it takes many hours to days to reach equilibrium and the desired constant plateau. The plateau term is used to describe a complete coverage of adsorbed polymers, the so-called maximum adsorption of the plateau of Langmuir isotherms (33, p. 174-176).

Additionally, having a good solvent has the tendency to make the polymer layers more efficient and expanded. If there are charged polymers, electrical effects may arise. Theoretically, the adsorption depends on the changes in the polymer configurations and the stability of the solution on the solvent quality. A polymer adsorbed at an interface has the tendency to occupy larger interfacial area in a good solvent compared to a poor solvent (33, p. 174-176).

4.3.1 Various Surface Configurations of Polymer Adsorption

Polymers have the tendency to change their surface configurations when adsorbed on the particle interface. Various surface configurations of polymer adsorption can only be tails or with loops, tails, and trains. These surface configurations are demonstrated in **Figure 4.2**. The task of the tails determines the thickness of the adsorbed layer of the polymer even though they contribute less to the adsorbed amount. The thickness of these layers can be measured using the gyration radius, which is shown in **Equation 4.1**. Steric stabilization can be achieved if two particles only repel each other when the distance is approximately $\leq 2R_g$. The R_g is proportional to the square root of the molecular weight of the polymer (33, p. 177).

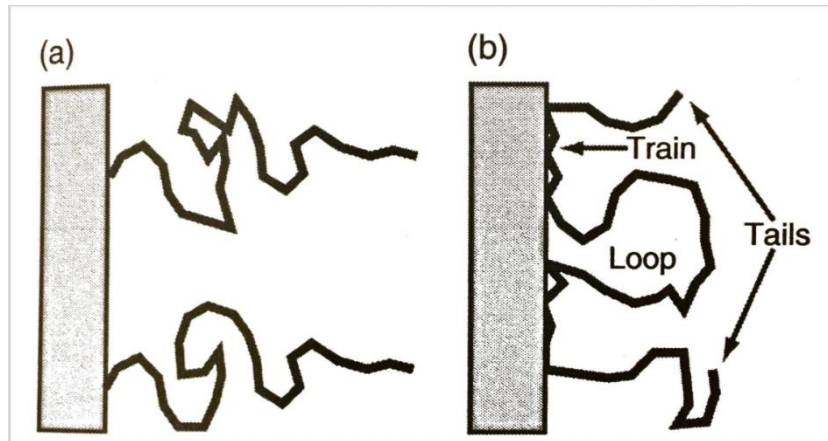


Figure 4. 2: Surface configurations of polymer adsorption with (a) only tails or (b) with loops, tails, and trains (33, p. 177).

$$R_g = \frac{a\sqrt{nl}}{\sqrt{6}} = \frac{6\sqrt{\frac{M}{M_0}}l}{\sqrt{6}} \quad (4.1)$$

R_g : Radius of gyration

a : Solvent interaction

= 1 for ideal solvent, meaning no interactions with segment.

> 1 for good solvent

< 1 for poor solvent

n : Number of segments

l : Length of the segment

$\frac{M}{M_0}$: Segment number

4.4 Positive and Negative Adsorption

In terms of adsorption, there are two types of adsorptions of polymers onto colloidal particles such as positive and negative adsorption. The effects of positive and negative adsorption influence the final colloidal stability based on various interactions. A schematic illustration shown in **Figure 4.3** illustrates scenarios/frameworks when adding polymers to the interface of colloidal particles with respect to positive and negative adsorption of polymers. The colloidal stability of aqueous dispersions is the most significant to study (44).

In terms of negative adsorption or depletion, the concentration of polymer segments close to the colloidal particles is lower than in the bulk concentration. The extent of this range is referred to as the depletion thickness and is in a dilute polymer solution near the gyration radius of the polymer chains, which is elucidated from the previous subsection. When there are extremely low concentrations of the polymer, the attraction becomes weak and this results in instability in the system, shown in **(a)**. However, when increasing the concentration of the polymer, the attraction becomes rather strong, but also results in instability in the system, shown in **(b)**. At very high concentrations which is above the polymer overlap concentration, the depletion thickness decreases, resulting in restabilization, shown in **(c)**. Hence, this type of adsorption is not the optimal result to achieve colloidal stability (44).

In terms of positive adsorption or accumulation, the scenario is different in comparison to negative adsorption. When there is a fairly small amount of positively adsorbed polymer chains, the chains tend to adsorb at multiple interfaces, which results in bridging flocculation, shown in **(d)**. When there are more positively adsorbed polymer chains to completely cover all particle interfaces, the stabilization may be achieved in the dispersion of the system, shown in **(e)**. However, excess of positively adsorbed polymer chains may result in depletion interactions, although the adsorbed polymer layers may protect the particles from interacting with each other, shown in **(f)**. Thus, a better understanding of colloidal stability is very important when adding polymers to the interface of particles (44).

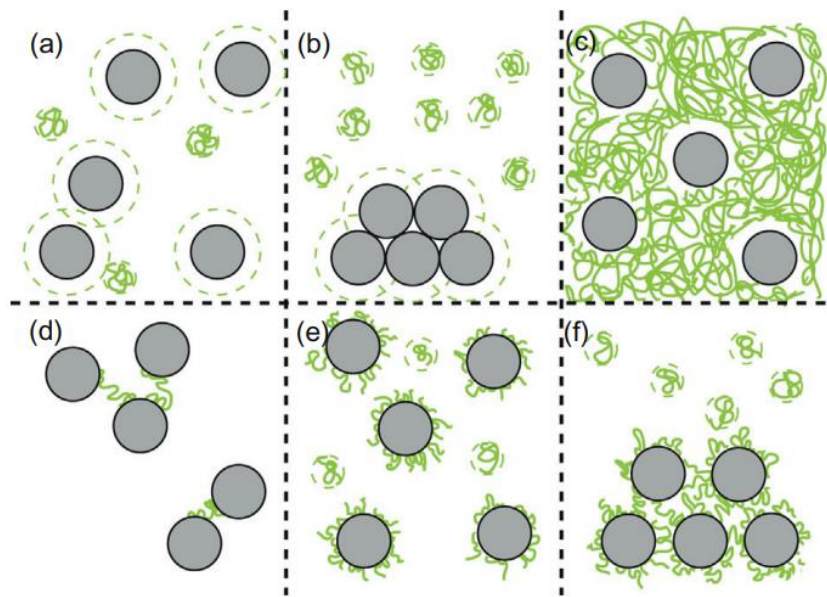


Figure 4. 3: Schematic illustration of various framework when adding polymers to the interface of the particles in terms of **(a-c)** negative adsorption (depletion) of polymers or **(d-f)** positive adsorption (accumulation) of polymers (44).

5 Introduction to Polyvinylpyrrolidone

This section introduces the most important aspects of using PVP as a potential surface coating material. Theory about the mechanism of PVP is not covered since the synthesis of polymer is not part of the experimental work in this thesis, but the use of PVP itself is essential to solve the problem associated with the thesis statement. Therefore, some theories related to the polymer are required to understand.

5.1 Features of Polyvinylpyrrolidone

PVP is a polymer which is non-charged, stable, and non-toxic. The polymer consists of C=O, C-N and CH₂ functional groups. The polymer consists of a hydrophilic component which is the pyrrolidone moiety. The molecule does also contain a hydrophobic group such as the alkyl group. Water and alcohols are excellent solvents for dissolving PVP. This is due to the amide group within the pyrrolidone ring which is polar. Additionally, the PVP molecule has the non-polar methylene and methine groups in the ring and along its backbone and can be dissolved in many organic solvents such as ethanol (EtOH) and isopropanol (IPA) (45).

The polymer is considered as a stabilizer and has the ability to prevent aggregation of NPs through repulsive forces owing to its hydrophobic carbon chains extending into solvents and interacting with each other. This effect is called for steric hindrance, which is closely linked to the previous section related to polymers at interface. PVP can also be considered as a dispersant, in which the polymer is typically a surfactant that can be added to a suspension of liquid or solid particles for improving the dissociation of the NPs and preventing their settling. Moreover, the length of PVP is contemplated to be quite essential for stabilization of the particles. The polymer is often known as a shape control agent, in which it promotes the growth of crystal facets while preventing others. PVP is also a lenient reductant or reducing agent where the hydrophilic groups are located (45). The scheme of the monomer N-vinylpyrrolidone is shown in **Figure 5.1** (46), whereas the scheme of the polymer is shown in **Figure 5.2** (47).

PVP is overall an amphiphilic polymer that has an alkyl hydrophilic pyrrolidone group and hydrophobic side group. It is easily soluble in water and many organic solvents due to the formation of hydrogen bonds between carbonyl group in PVP and the solvent (48).

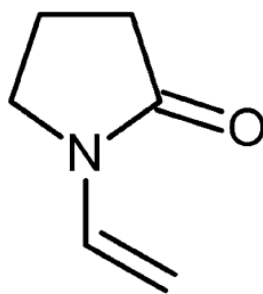


Figure 5. 1: The molecular structure of *N*-vinylpyrrolidone (46).

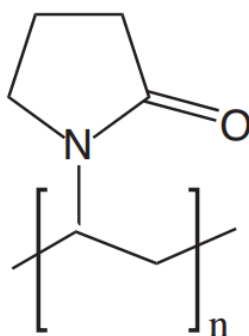


Figure 5. 2: The chemical structure of PVP (47).

5.2 Physicochemical Properties of Polyvinylpyrrolidone

The polymer has physicochemical properties that are appropriate for a range of applications such as biomedical, pharmaceutical, and cosmetic industries. The physicochemical properties are shown in **Table 5.1**, introduced by Kurakula *et al.* (49). The table introduces the most important physicochemical properties of PVP such as physical description, melting point, pH, solubility, K-range, chemistry perspective, and stability and storage.

Table 5. 1: Physicochemical properties of PVP (49).

Number	Physicochemical Property	Description
1	Physical Form	Fine, white to off white odorless, very hygroscopic, amorphous powder.
2	Molecular Formula	(C ₆ H ₉ NO) _n
3	Molecular Weight	2500-30 000 000 g/mol (Da)
4	CAS Number	9003-39-8
5	Non-proprietary Name	Povidone
6	Synonyms	Povidone, Polyvinylpyrrolidone, Polyvidone, Plasdone, Kollidon, Poly[1-(2-oxo-1-pyrrolidinyl)ethylene], 1-vinyl-2-pyrrolidone polymer, 2-pyrrolidone-1-ethenyl-homopolymer.
7	IUPAC Name	1-ethenylpyrrolidin-2-one
8	Melting Point	Softens at 150 °C and decomposes at 180 °C.
9	pH	3-7 (varies with K-value and concentration of solution).
10	Solubility	Soluble in water, ethanol, methanol, chloroform, acids, and amines. Insoluble in ethers, hydrocarbons, some esters, some ketones, and mineral oil.
11	K-Value Range	10-120
12	Chemistry Perspective	The polymer consists of C=O, C-N, and CH ₂ with a strong hydrophilic moiety pyrrolidone alkyl group. The highest solubility of PVP in both water and non-aqueous solvents is characterized by the existence of highly polar amide moiety in pyrrolidone ring and apolar methylene and methine groups within the ring and along its backbone. The steric hindrance effect is due to the hydrophobic carbon chains.
13	Compatibility	Compatibility in solution with a wide range of hydrophilic and hydrophobic, natural and synthetic resins; inorganic salts and other chemicals. PVP forms adducts in solution with sodium salicylate, salicylic acid, sulfathiazole, phenobarbital, tannin, and some other compounds. Because of the complex nature of thimerosal with povidone, the preservative action of the previous agent is affected.
14	Stability and Storage	PVP is chemically stable in dried form, and can be stored in ordinary conditions, however in a tightly closed container owing to the high hygroscopic physical property.
15	Relative Viscosity in Water [m.Pa.s]	PVP-K12 (5 %): 1.222-1.361 PVP-K17 (5 %): 1.430-1.596 PVP-K25 (1 %): 1.146-1.201 PVP-K30 (1 %): 1.201-1.281 PVP-K90 (1 %): 3.310-5.195
16	Particle Size Distribution	Kollidon 25/30: 90 % > 50 µm, 50 % > 100 µm, 5% > 200 µm; Kollidon 90: 90 % > 200 µm, 95 % > 250 µm.
17	Water Sorption	As the relative humidity increases, the water sorption and weight of PVP increases.

6 Introduction to *Post-Situ* Surface Modification

Understanding the *post-situ* surface modification method is the most important topic for this thesis. The functionalization approach improves the properties and characteristics of IONPs through surface modification, and this allows the particles with new functional groups to play a major role in the field of diagnostics. This section introduces a brief theory about *post-situ* surface modification strategy along with silica as the coating material used in this thesis.

6.1 *Post-Situ* Surface Modification Strategy and Mechanisms

Since the focus of this thesis is to apply *post-situ* surface modifications for experimental work, it is principal to understand how this modification really works theoretically. This type of surface modification is based upon the synthesis of NPs followed by modification of the surface of these particles through various mechanisms. *Post-situ* functionalization of MNPs such as IONPs is performed mainly via three mechanisms, also ligand addition, ligand exchange and encapsulation (17).

The 1st mechanism which is ligand addition involves the addition of a ligand to the outer surface of the obtained IONPs. This ligand addition does not remove existing ligands such as OH⁻ or other surface groups depending on the synthesis route. An example of such a mechanism is shown in **Figure 6.1**. However, the 2nd mechanism is different from the previous one due to the fact that the functional groups attached to the surface of IONPs are replaced by another ligand, as shown in **Figure 6.2**. This mechanism is called ligand exchange. The 3rd mechanism, however, involves the use of biocompatible polymer or inorganic materials to obtain stabilization as a surface modification strategy, which is shown in **Figure 6.3**. This mechanism is called encapsulation. Biocompatible hydrophilic shell encapsulation is a beneficial method for surface modification of IONPs. Example of shell materials to consider are amphiphilic ligands, water-soluble polymer matrixes, and hydrophilic inorganic materials (17).

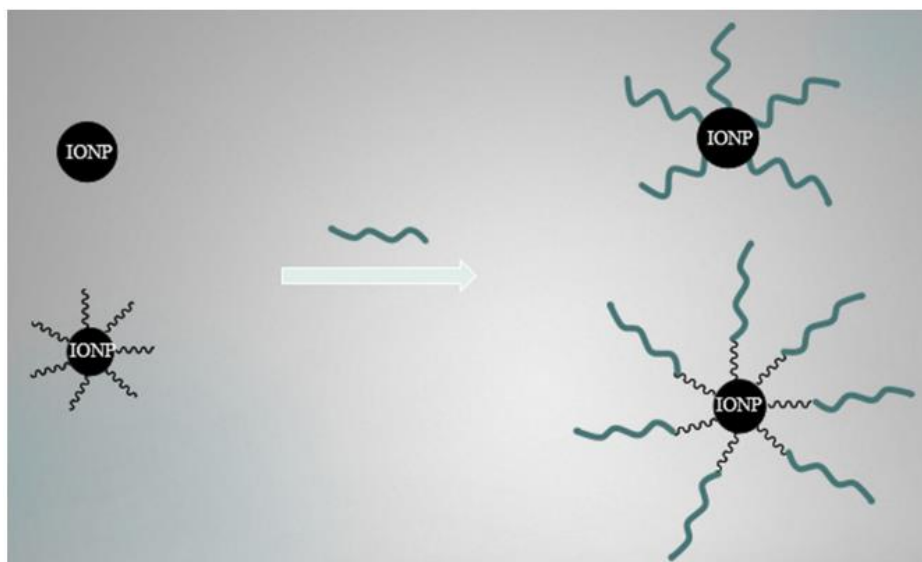


Figure 6. 1: Surface Modification of IONPs by ligand addition (17).

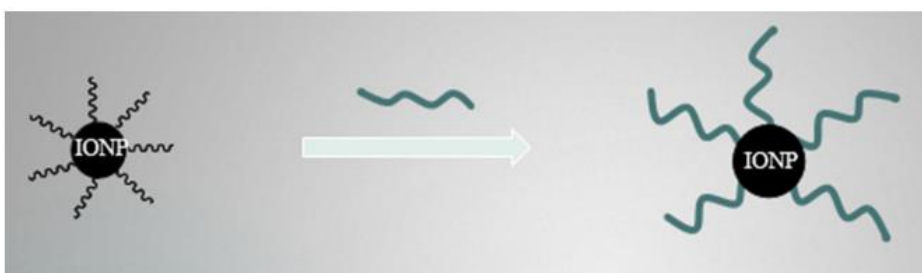


Figure 6. 2: Surface modification of IONPs by ligand exchange (17).

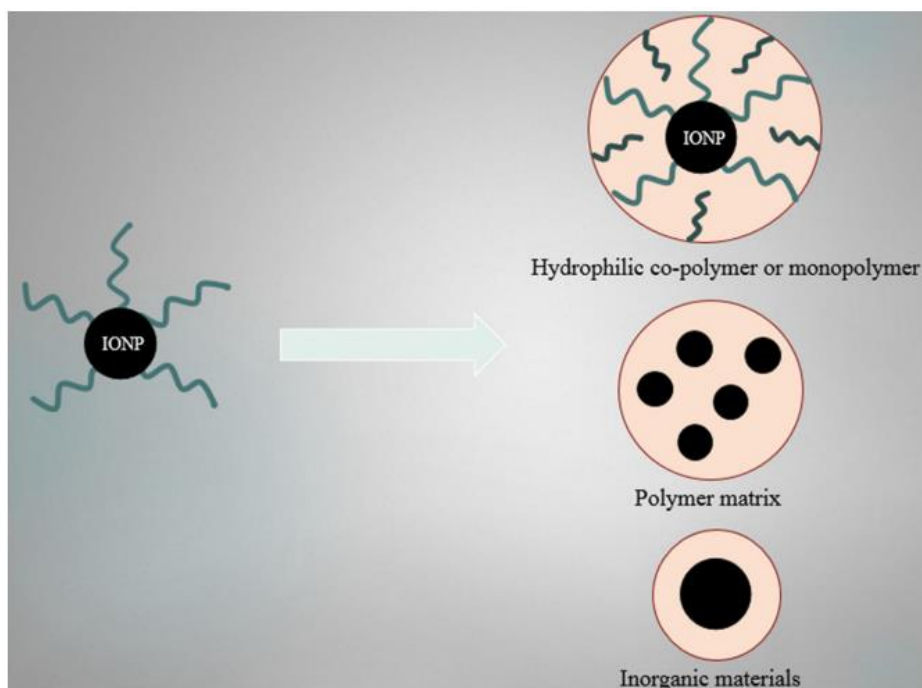


Figure 6. 3: Surface modification of IONPs by encapsulation method (17).

6.2 Coating with Silica

It was previously mentioned in the introduction section that the use of silica provides desirable materials as a coating material. The *post-situ* surface modification can be employed by using silica. The coating material silica yields robust water-soluble NPs with good colloidal stability and biocompatibility. Using silica includes simple control of the coating process, optical, low cost, and magnetic transparency. Providing efficient surface coatings and the development of effective protection methods to retain the stability of these particles is foremost important. The surface of IONPs modified by silica demonstrates to have high dispersibility and stability (50).

Silica coating has the capacity to enhance the dispersion in solution due to the layer of the material, in which it has the capability to screen the magnetic dipolar attraction between magnetic IONPs. Silica coating has the potential to increase the stability of IONPs which is quite favourable for application in biomedicine. Inorganic materials do maintain many various properties and silica is one of them. Also, owing to the existence of abundant silanol groups on the silica layer, IONPs@SiO₂ can be triggered for providing the surface of IONPs with distinct functional groups (30). On top of that, silica assists in binding the miscellaneous biological or the other ligands at the IONPs surface.

The Stöber method is the selection functionalization method for coating IONPs with silica, which is explained in the next subsection. It is, in fact, significant to note that the thickness of silica shell from 5 to 200 nm can be altered by varying the amount of TEOS precursor and the concentration of the catalysts NH₄OH. This strategy results in better dispersion and minimize the aggregation of IONPs (51). A modified scheme for the preparation of silica functionalized IONPs is shown in **Figure 6.4**.

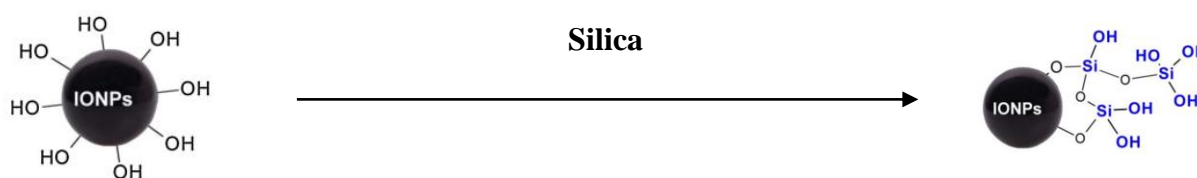
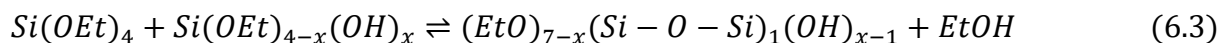
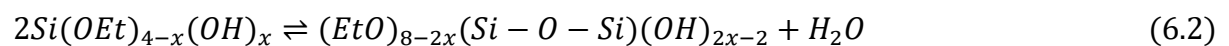


Figure 6. 4: Post-Synthesis scheme of silica functionalized IONPs (Modified) (10).

6.2.1 The Stöber Method

The silanization process can be performed through the Stöber process which is the method for obtaining IONPs@SiO₂. In the Stöber process, there are two approaches for controlling the growth of silica particles which are hydrolysis of tetraorthosilicate (TEOS) [Si(OEt)₄] into silanol monomers [Si(OEt)_{4-x}(OH)_x], and followed by condensation of the silanol monomers into a siloxane network, in which x and 4-x embody the numbers of silanol and ethoxy groups, respectively (x = 1 - 4). This is prominent as the sol-gel chemistry where it has been centralized in research area of kinetic balance between TEOS hydrolysis and subsequential condensation of silanol monomers (52).

Three equations exemplify the overall reaction of the Stöber process. Here, TEOS encounters hydrolysis in a mixed ethanol/ammonia solution for obtaining silanol monomers, which is shown in **Equation (6.1)**. The ethoxyl groups (-Si-OEt) are substituted with predominantly silanol groups, (-Si-OH). Subsequently, the silanol monomers engage in the condensation enclosed by two silanol groups for generating branched silanol clusters, which is shown in **Equation (6.2)**. The reaction is further connected to activate the nucleation and growth of silica particles. Contemporaneously, the silanol monomers have the capability to proceed with the unhydrolyzed ethoxyl groups of TEOS through condensation within ethoxyl and silanol groups, which is shown in **Equation (6.3)**. This is to get in on the act of nucleation and growth of silica particles (52).



7 Literature Review

This section discusses what previous studies have reported associated with the theory highlighted in earlier sections. The purpose of this section is to review the work that has already been done in terms of controlling the particle size of functionalized IONPs by studying the colloidal stability, the various functionalization methods, and the effect of PVP on IONPs. The motive is to analyze gaps in literature research and present why these gaps require to be explored.

7.1 Surface Modification of Iron Oxide Nanoparticles with Polyvinylpyrrolidone

A study performed by Abu Noqta *et al.* (53) synthesized IONPs@PVP by the *in-situ* co-precipitation method at room temperature in the presence of PVP as a stabilizing agent. The study dissolved 4.1 g of PVP in distilled water with stirring speed at 500 rpm and heated the mixture at 50 °C for 5 h. The iron salts 2M Fe³⁺ and 2M Fe²⁺ were co-precipitated in the presence of PVP at ratio 2/1 in order to produce the IONPs followed by washing with water occasionally. According to the study, it was discovered that the presence of PVP during co-precipitation reaction has a significantly role in reducing the agglomeration, as well as controlling the particle size, which affects the magnetization value of IONPs. The transmission electron microscope (TEM) showed in the study was reported to be 15.6 nm with narrow particle size distribution, as shown in **Figure 7.1**. However, this study does not report the zeta potential of IONPs@PVP and discusses why PVP potentially reduces the agglomeration and decreases polydispersity of the NPs.

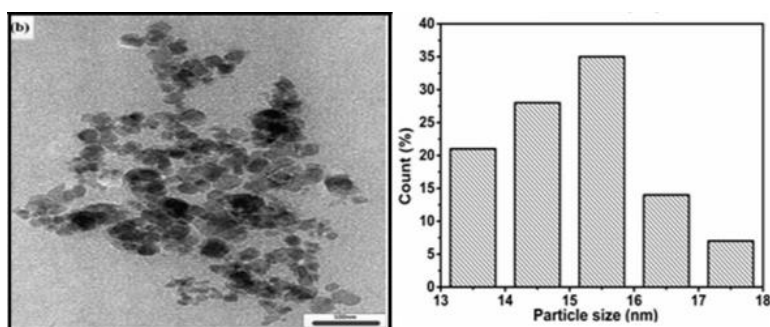


Figure 7. 1: TEM images and histogram of PVP coated IONPs (53).

The study performed by Zare *et al.* (54), prepared *post-situ* functionalization of IONPs using PVP as a coating agent. The synthesized IONPs were prepared by dissolving the iron salts ferrous chloride tetrahydrate ($\text{FeCl}_2 \cdot 4\text{H}_2\text{O}$) and ferric chloride hexahydrate ($\text{FeCl}_3 \cdot 6\text{H}_2\text{O}$) in 200 mL of deaerated distilled water in a round bottom flask and keeping at a desired temperature. The mixture was purged using nitrogen for 30 min followed by the addition of NaOH dropwise into the solution. The nitrogen was used to prevent oxidation of the ion Fe^{2+} in the system, meanwhile the addition of the base formed the IONPs precipitates. The functionalization of IONP@PVP was prepared by adding the IONPs to a solution of PVP (10 % w/w) previously purged with nitrogen. The product was centrifuged and washed 3 times with deionized water and acetone. **Figure 7.2** shows the TEM images of IONPs@PVP, in which the morphology shows spherical particles with a particle size of 10 nm. The study indicates that the presence of PVP prevented aggregation of IONPs in the system.

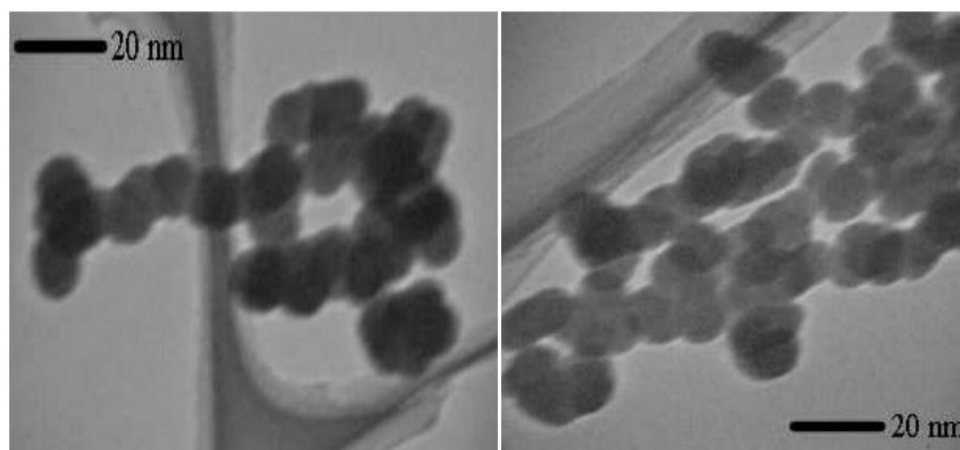


Figure 7. 2: TEM images of IONPs@PVP (54).

The study reported by Zulfiqar *et al.* (55) modified the surface of IONPs with PVP through the *in-situ* co-precipitation method. The study dissolved 7 g of PVP in 100 mL of distilled water and heated at 90 °C for 1 h with continuous agitation at 1000 rot/min followed by the addition of the mixture to 350 ml of 1 M NaOH solution. The stoichiometric ratio of 1:2 FeCl₂·4H₂O to ferric chloride hexahydrate FeCl₃·6H₂O was added dropwise to the solution in 30 min, in which the addition rate was set to 1.6 mL/min. The obtained precipitates were centrifuged and washed with water 6 or 7 times. **Figure 7.3 (a)**, and **(b)** show SEM images of un-coated IONPs and IONPs@PVP, respectively. The study reported that without the presence of PVP the particles were formed in the form of agglomerates to a large degree. With respect to IONPs@PVP, the number of agglomerates was still found in the presence of PVP, but the agglomeration appears to be reduced owing to the polymer coating. **Figure 7.4 (a)** and **(b)** shows TEM images of un-coated IONPs and IONPs@PVP, respectively, whereas **(c)** and **(d)** represent the corresponding particle size distribution of un-coated IONPs and PVP coated IONPs. The study reported that the mean particle size was found to be 10.36 ± 1.97 nm with a particle size distribution of 5-15 nm and 6.91 ± 1.89 nm with a particle size distribution of 4-10 nm for un-coated IONPs and PVP coated IONPs, respectively.

The study discovered that the presence of PVP resulted in a decrease in particle size and reduced the agglomeration of IONPs. Although agglomeration of IONPs was reduced, there are still particles interacting very closely with each other. Reduced agglomerations are discovered in both SEM and TEM for IONPs@PVP, but agglomerations are not completely prevented. The study presents no data regarding the colloidal stability of un-coated IONPs and PVP coated IONPs, which is crucial in determining whether the particles are relatively stable or not. Therefore, the stability study is not known for this particular study.

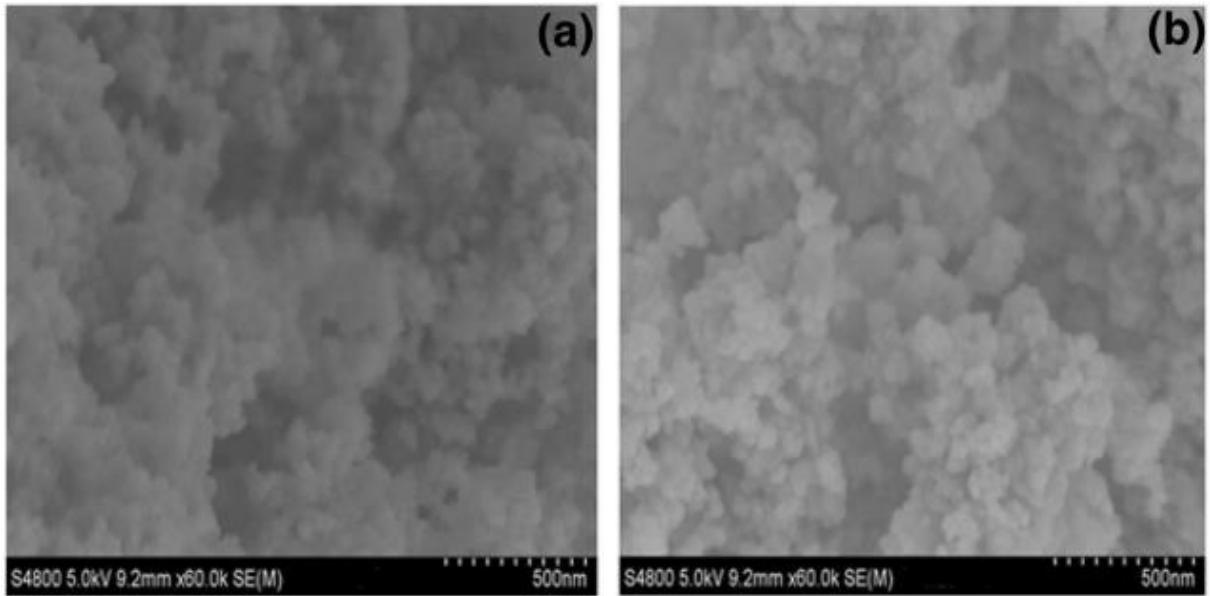


Figure 7. 3: SEM images of (a) uncoated IONPs and (b) PVP coated IONPs (modified) (55).

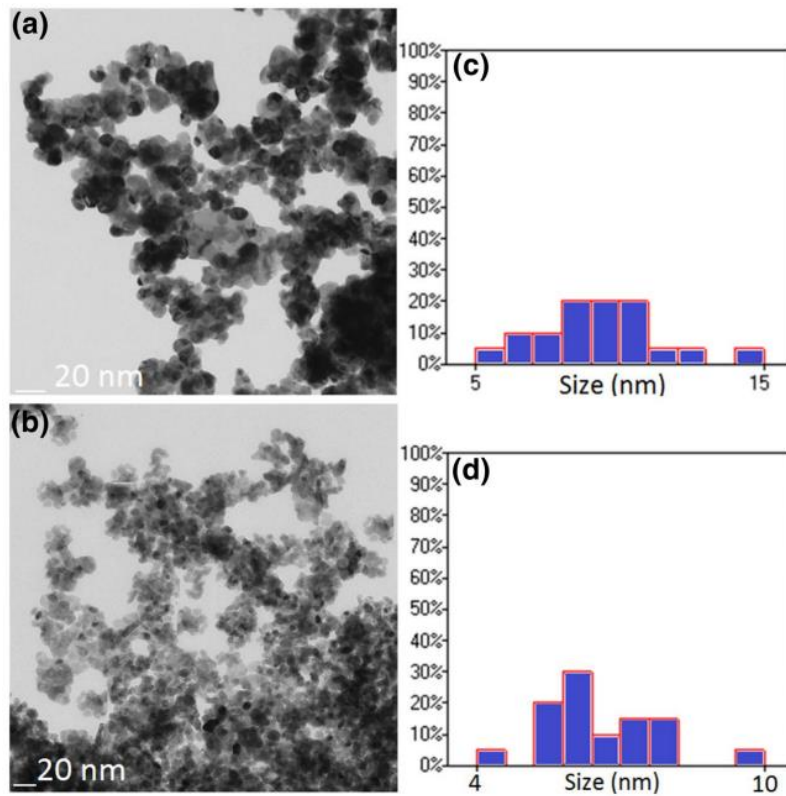


Figure 7. 4: TEM images of (a) un-coated IONPs and (b) PVP coated IONPs, and particle size distribution of (c) un-coated IONPs and (d) PVP coated IONPs (55).

The study performed by Heiran *et al.* (56), synthesized PVP coated IONPs through the *in-situ* co-precipitation to examine the effect of PVP content/amount on its properties. The study prepared IONPs@PVP by dissolving three various amounts of PVP with 0.5 g of FeCl₂ and 1.35 g of FeCl₃ in 600 mL nitrogen degassed distilled water in a three-necked flask followed by the addition of NH₄OH dropwise to the solution under vigorous stirring at 70 °C. The obtained IONPs@PVP were washed with ethanol. The PVP coated IONPs can be illustrated in **Figure 7.5**, where the study represents the binding between the polymer and the surface of IONPs. **Figure 7.6** shows the field-emission scanning electron microscope (FE-SEM) images of IONPs@PVP, in which three various amounts of PVP are 0.32, 0.745, and 1.74 g are used. The results found by the study discovered that the particle size range was between 30 and 40 nm. According to the study, the final morphologies were shown to be spherical particles and somehow monodispersed.

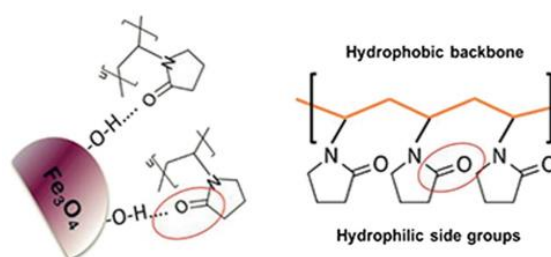


Figure 7. 5: Schematic illustration of IONPs@PVP nanospherical shapes and the chemical formula of PVP (56).

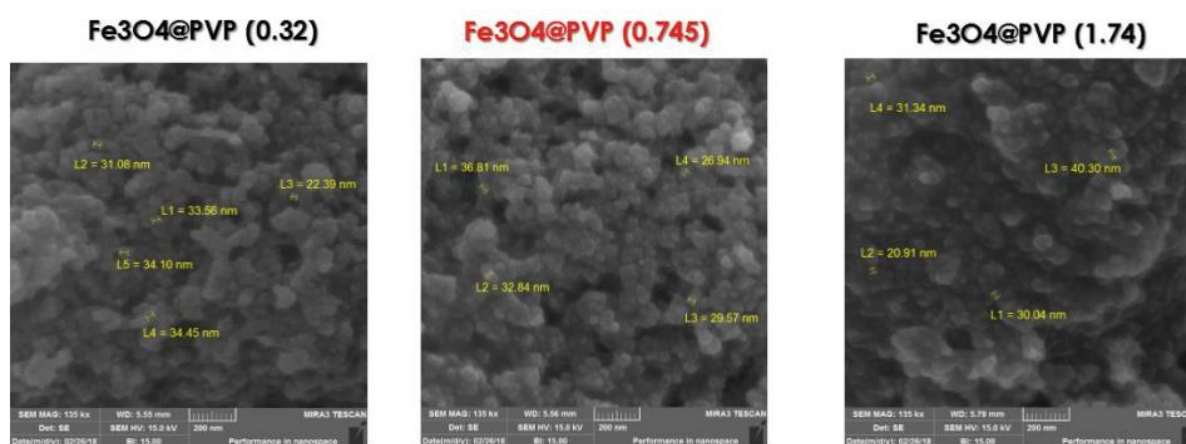


Figure 7. 6: FE-SEM images of three various contents of PVP coated on the surface of IONPs (56).

Another study reported by Pandey *et al.* (57) also studied the effect of various amounts of PVP on the surface of IONPs. The synthesis method used in this work was primarily based on *in-situ* co-precipitation method, in which PVP was mixed with 50 mL aqueous solution of 0.017 M of ferric chloride and 50 mL aqueous solution of 0.033 M of ferrous sulphate in 250 mL lessened flask. The mixture was stirred for 30 min to obtain a standardized solution followed by the addition of 0.25 M NH_4OH in 50 mL of distilled water moderately to the solution mixture until the pH reached 11. The whole solution was vigorously stirred on motorized stirrer for 3 h at ambient temperature. The obtained IONPs@PVP were washed with methanol four times to remove the amount of amine molecules remaining.

In **Figure 7.7** reported by Pandey *et al.*, number of spherical particles were discovered to some extent, but mostly agglomerates were found due to the magnetic dipole-dipole interaction between IONPs. Three various amounts of PVP were analyzed using FE-SEM of the samples IONPs@PVP (1 g), IONPs@PVP (2 g), and IONPs@PVP (3 g). It appears that the addition of PVP does not really reduce agglomerations.

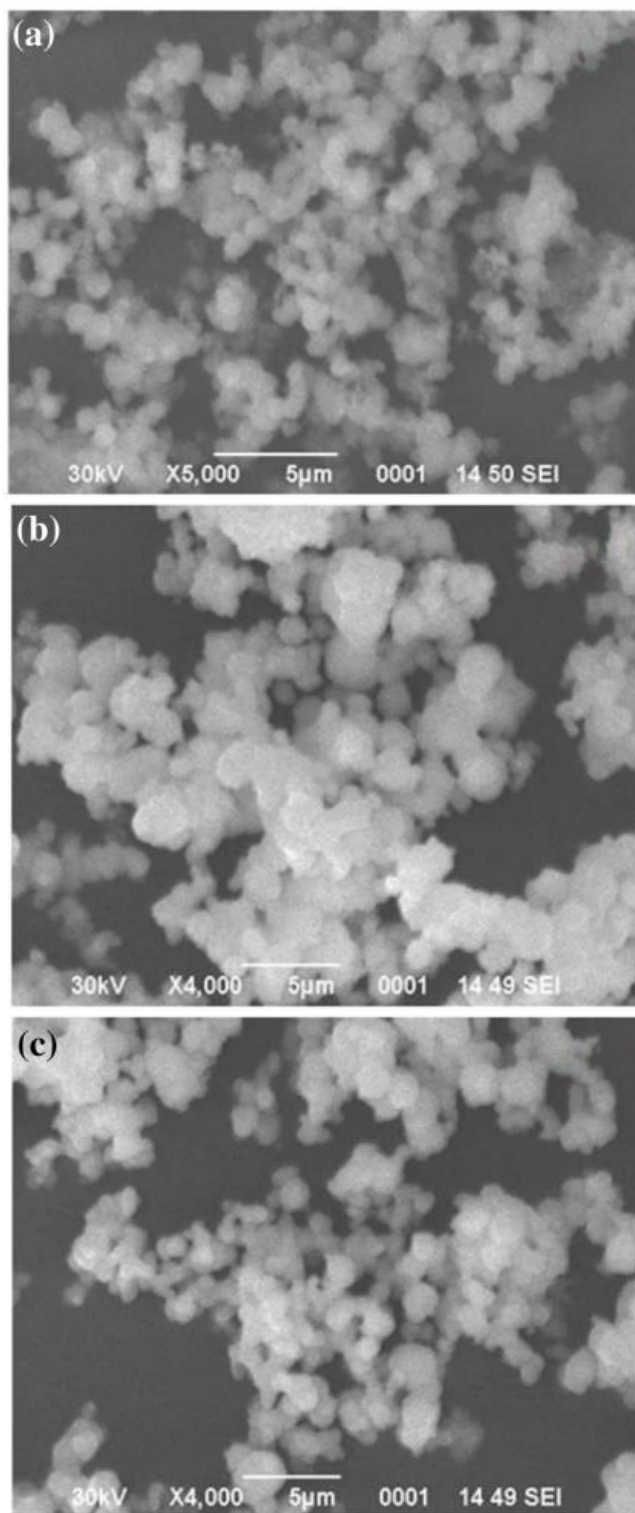


Figure 7. 7: SEM images of IONPs@PVP (a) 1 g PVP, (b) 2 g PVP, and (c) 3 g PVP (57).

A study performed by Isci *et al.* (58), has done research on the effect of zeta potential by adding PVP to the surface of IONPs. The preparation of IONPs@PVP was performed by mixing various concentrations of PVP from 10^{-5} to 1 g/l with IONPs in water dispersions at room temperature followed by shaking the mixture overnight and subsequently ultrasonicated for 5 minutes. This is the study where *post-situ* surface modification is used to study how the colloidal stability of IONPs@PVP differs from un-coated IONPs.

The zeta potential of IONPs with various PVP concentration is shown in **Figure 7.8**. The results show the changes in zeta potential of IONPs in water system with various amounts of PVP added to the dispersions. The zeta potential of IONPs in the absence of PVP was found to be -18.6 mV, in which the dispersion is not very stable and behaves in an aggregative state. The study reported that the addition of PVP to the IONPs surface decreased the absolute value of zeta potential by steric interactions owing to the bridging flocculation. Increasing the concentration of PVP, however, caused steric repulsions between PVP polymers even though the concentration was still low. By adding more PVP resulted in flocculation due to the depletion stabilization, which means that there were free PVP chains moving in the dispersion rather than being attached to the particle's surface. The study also found out that the isoelectric point was reached when higher concentration of PVP were added, resulting in flocculation (58).

The synthesized method of IONPs from this particular study, however, is not known and therefore it is unclear whether the co-precipitation method has been used or not. Additionally, the study does not report the effect of various molecular weights of PVP on the zeta potential apart from 360 000 g/ mol PVP. The results of various mass of IONPs have also not been reported, which means that it is unclear whether the mass of the NPs has any effect on the final colloidal stability or not.

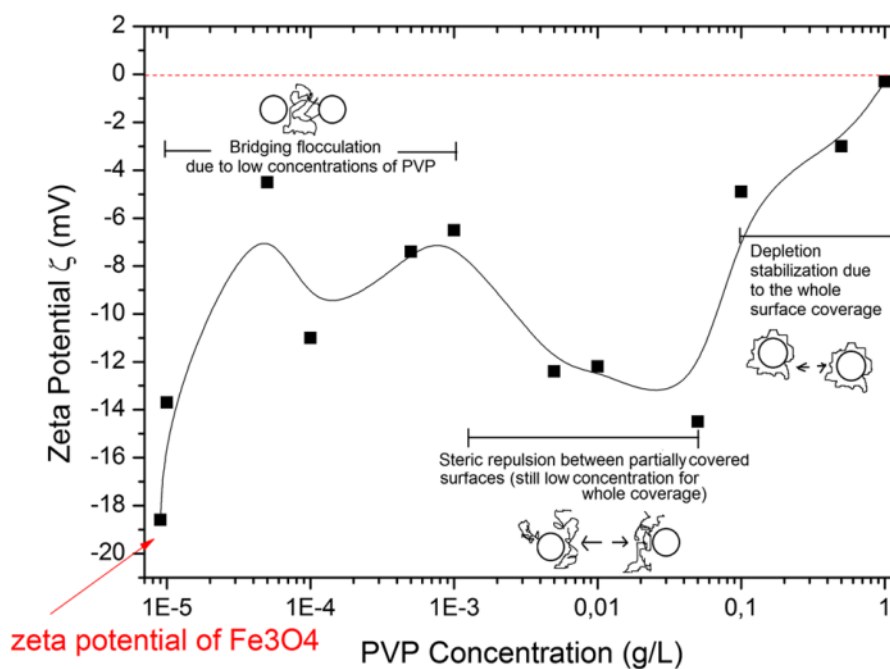


Figure 7. 8: The changes in zeta potential of IONPs in water system with various amounts of PVP added to the dispersions (58).

Another study performed by Abu-Noqta *et al.* (59) has done research on the colloidal stability of IONPs@PVP. The synthesise of IONPs by the *in-situ* co-precipitation method was to precipitate ferric and ferrous salts in the presence of PVP as a capping agent. The preparation was to mix 0.2 g PVP, 1.0 mmol of iron (II) chloride and 2.0 mmol iron (III) chloride in 30 mL distilled water at ambient temperature. The addition of reactant solutions was controlled using three various peristaltic pumps at the same flow rate into a reactor which contains 1 M of sodium chloride solution. In order to regulate the pH value of the solution at 10, 2 M of sodium hydroxide solution was added. The reaction was kept for 2 h for obtaining IONPs@PVP. The washing step was proceeded by using distilled water few times.

The study explored that the zeta potential value of IONPs@PVP was found to be -10 mV. The zeta potential exhibited poor stability, resulting in aggregation and precipitation of suspension. Thereby, the result indicates that the PVP used in this work was not an appropriate coating agent and did not provide acceptable colloidal dispersion of IONPs in the system. The hydrodynamic size of IONPs coated with PVP, however, was found to be 136.1 nm. The obtain NPs was synthesized through the *in-situ* co-precipitation method in the presence of PVP as a coating agent instead of modifying the surface of IONPs after the synthesis (59).

7.2 *Post-Situ* Functionalization with Silica

Previously reported of generating silica NPs has been studied using the Stöber method. Most of the experiments are conducted either in a batch or semi-batch settings or a combination of both, but mostly in a batch setting.

The research conducted by Han *et al.* (52), represents the synthesis of colloidal spherical silica particles which are primarily dependent on NH_4OH -catalyzed hydrolysis of silicon alkoxide, also particularly TEOS which is followed by condensation of silanol monomers which again are conventional as the Stöber process. The size of the silica particles can be altered in a wide range from 10 to 500 nm by controlling the NH_4OH concentration. In this particular study, the Stöber method is divided into two consecutively occurring stages. The 1st is the incubation stage, in which the nucleation and growth of silica particles is determined principally by TEOS hydrolysis (pathway I). The 2nd is the stage of size magnification/enlargement of silica particles produced at the incubation stage by adding newly created silanol monomers on the top via condensation (pathway II).

Another study conducted by Kim *et al.* (60), prepared silica NPs from the hydrolysis of alkoxide to set up the optimal conditions. The purpose of this study was to prepare the particles and to discover the main parameters affecting the properties of silica NPs. The synthesise method for preparing silica NPs consists of a two-stage semi-batch/batch hydrolysis reaction of TEOS. An illustration of this process is shown in **Figure 7.9**, in which the experimental procedure and the schematic diagram of a semi-batch and batch setting are presented, respectively.

According to the study, a micro feed syringe pump with a constant flow rate (0.3-5.0 mL/min) feeds the starting reactant (TEOS/ethanol) into the process containing the other reactant ($\text{H}_2\text{O}/\text{NH}_4\text{OH}/\text{EtOH}$). This 1st stage of the process is called semi-batch setting. After the initial stage, the 2nd stage of process takes place, called batch setting. The reactants (TEOS/EtOH) and ($\text{H}_2\text{O}/\text{NH}_4\text{OH}/\text{EtOH}$) are added again into the process system containing the solution and the particles prepared by the 1st stage reaction. In this study, the optimal reaction conditions for the silica NPs using this mixed method are found to be 0.5 M TEOS, 0.2 M NH_4OH and 6.0 M H_2O with corresponding feed rate and temperature at 5.0 mL/min and 42.5 °C. This mixed method suggests a new path of likelihood for the synthesis of silica NPs (60).

With respect to the study performed by Kim *et al.*, the benefits of a batch process/setting are that the process is simple and efficient to carry out and the process itself provides high conversion. However, the process may lead to potentially increased storage costs for a large quantity of product produced, coupled with inefficient production of nanophase particles with a narrow size (60).

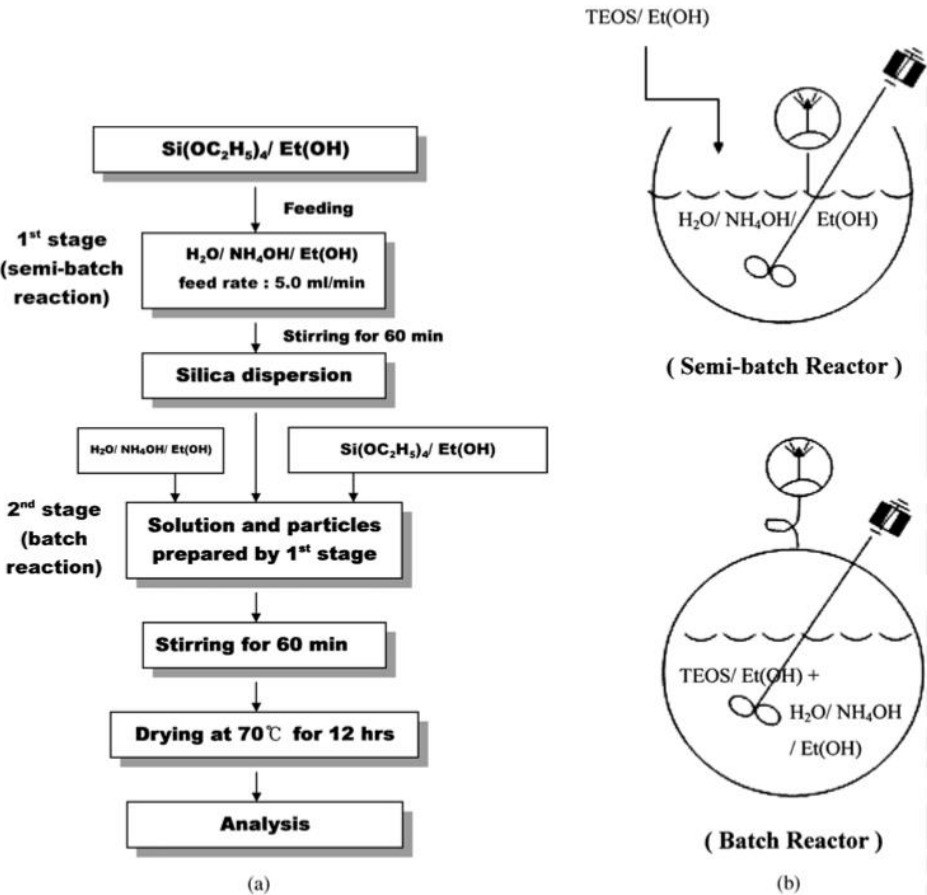


Figure 7. 9: Experimental procedure of silica NPs preparation by two-stage mixed method (a) and schematic diagram of semi-batch and batch process system (b) (60).

Another study performed by Nozawa *et al.* (61), prepared monodisperse silica particles by proceeding the hydrolysis and condensation of alkoxy silanes in a mixture of alcohol, water, and ammonia used as a catalyst. Importantly, alkoxy silanes is often called for TEOS with a chemical formula $\text{Si}(\text{OR})_4$ with $\text{R} = \text{C}_2\text{H}_5$. Many studies have been investigating this synthesis based on the Stöber method. A Stöber-like synthesis of silica particles are performed in which the control of the addition rate of one of the reactants, TEOS, is the main varying parameter. As opposed to the Stöber method, also known as a batch process, the use of so-called semi-batch process where one reactant (TEOS/ethanol) is added into a system containing the other solution containing ($\text{H}_2\text{O}/\text{NH}_4\text{OH}/\text{EtOH}$) at a constant feed rate. The study of this system is presented to provide greater control over particle size, particle size distribution, and morphology. As claimed by this study, the addition rate is the dominant factor compared to other reaction parameters such as TEOS/ H_2O ratio, pH, and temperature on final size and polydispersity of the particles.

In the following experiment, the monodispersed silica NPs is prepared by the hydrolysis of TEOS, which is shown in **Figure 7.10**. Solution of TEOS in EtOH and ammonia in EtOH are prepared separately. The volumes of TEOS, NH_4OH and EtOH are 5, 30 (solution I)/50 (solution II), and 9.5 mL, respectively. Solution I contains the mixture between TEOS and EtOH, while solution II contains EtOH in NH_4OH . As shown in the illustration, solution I is added to the round-bottom flask that contains solution II at a constant flow rate between 0.005 and 1.0 mL/min.

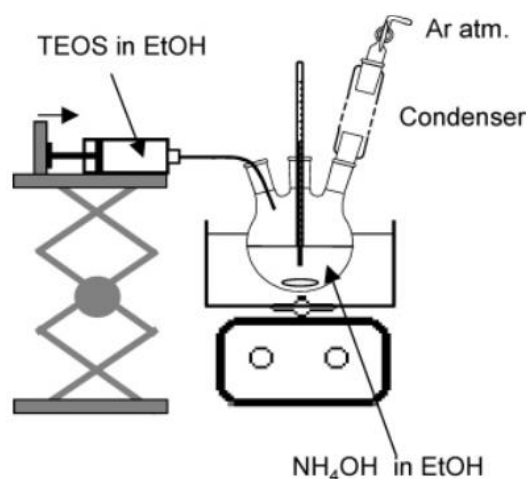


Figure 7. 10: Illustration of the experimental set-up used for the preparation of the controlled particle growth at a constant addition rate by Nozawa *et al* (61).

7.2.1 Previously Studied Thesis at NTNU

Silanization via the Stöber process has also been performed at NTNU with the purpose of studying the effect of various parameters to understand the final properties of functionalized IONPs such as particle size, particle size distribution, and morphology. The study performed by Ali (62), studied the effect of batch setting to introduce different parameters in the system and examine how these parameters may affect the final results. The study explored that the particle size and particle size distribution of IONPs@SiO₂ could be altered by changing the type of solvent, the mass of IONPs, the surface coating of IONPs, and the concentration of NH₄OH.

With respect to solvent, it was discovered that ethanol provided smaller particle size and narrower particle size distribution of IONPs@SiO₂ in comparison to isopropanol. It was also found that altering the mass of IONPs affected the particle size, particle size distribution, and morphology. The effect of the concentration of NH₄OH also affected the final particle size and particle size distribution by increasing the concentration from 0.98 to 1.53 M. The study also compared un-functionalized IONPs with functionalized IONPs, in which the IONPs were functionalized using citric acid as a surface modifier. The *in-situ* surface modification was the main method for modifying the surface of IONPs followed by silanization. The study discovered that the citrate coating of IONPs somehow resulted in the increase in particle size but provided a narrow particle size distribution of IONPs@SiO₂ (62).

The effect of all these parameters resulted in four various morphologies, which were considered as spherical particles, incompletely fused particles, irregular shapes, and agglomerates. The desired results were to obtain mostly spherical particles, and these could be obtained by using the concentration of NH₄OH greater than or equal to 0.98 M. The other undesirable morphologies were also obtained but with different amounts of catalyst and use of solvent. By using the concentration of NH₄OH equal to 1.53 M with ethanol as a solvent, incompletely fused particles were observed. By decreasing the concentration of NH₄OH less than 0.98 M, irregular shapes were observed, but these shapes could also be considered as non-spherical shapes. Perhaps, the most undesirable morphology to obtain were agglomerates because these were observed in all the experiments (62).

According to the study, it appears that altering the various parameters provides different results based on the particle size, particle size distribution, and morphology.

In the study performed by Nissen-Sollie (63), a semi-batch setting was examined, where the purpose was to compare with the batch setting conducted by Ali. The study also examined the effect of various parameters on the final particle size, particle size distribution, and morphology. The parameters that varied in this study were the type of solvent, the mass of IONPs, the flow rates of both NH_4OH and TEOS. It was also explored that the combination of all these parameters resulted in spherical shapes, incompletely fused particles, irregular shapes, and agglomerates. It appears that the type of solvent significantly affected the final morphology, where ethanol and isopropanol were used. In this study, ethanol provided mostly irregular shapes, whereas isopropanol provided mostly spherical shapes. The particle size, however, was discovered to be smaller in ethanol where spherical particles were observed even with the existence of other undesirable morphologies in comparison to isopropanol.

7.3 Iron Oxide Nanoparticles with Silica and Polyvinylpyrrolidone

A study performed by Kermanian *et al.* (64) prepared mesoporous IONPs@SiO₂ with PVP through sol/gel surface protected etching mechanism. The study also used co-precipitation to synthesize IONPs, in which FeCl₂·4H₂O and FeCl₃·6H₂O were mixed in 50 mL distilled water at 70 °C under the flow of nitrogen followed by the addition of NH₄OH dropwise to the solution. The precipitates obtained were washed with water and ethanol. The preparation of IONPs@SiO₂@PVP was to disperse the IONPs in a mixture of PVP in deionized water followed by sonication at 40 °C for an hour. The mixture was centrifuged and subsequently re-dispersed the precipitate in 90 mL ethanol followed by the addition of 14 mL water and 2.5 mL NH₄OH under stirring. Then 3.5 mL of TEOS was added to the mixture at ambient temperature and left the reaction for 4 h. The mixture was then centrifuged, and the precipitate was re-dispersed in about 40 mL of deionized water. Then 3 g of PVP was added to the dispersion and heated at 100 °C overnight for filling the non-etching sample with PVP. Then 6 mL of NaOH was added to the mixture when it was cooled down to ambient temperature. The final product was obtained after another 4 h and washed with deionized water and ethanol few times.

The TEM and FE-SEM images of IONPs@SiO₂ with PVP are shown in **Figure 7.11 (A)** and **(B)**, respectively, meanwhile **(C)** shows the particle size distribution. The morphology analysis of both images represents spherical shapes of nanocomposite with an average particle size of 11.8 ± 2.2 nm and particle size distribution between 5 and 20 nm. The histogram shows that the particle sizes are quite narrow in terms of monodisperse particles.

The study, however, did not present why there were also agglomerations in the images, as the particles were very close to each other, and this might be due to the attractive force. The uncertainty about the stability of the particles were not measured, and hence the colloidal stability was not reported in this study.

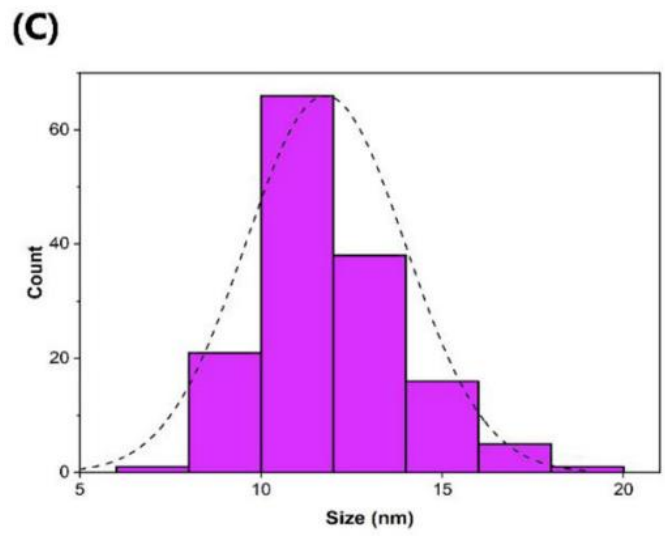
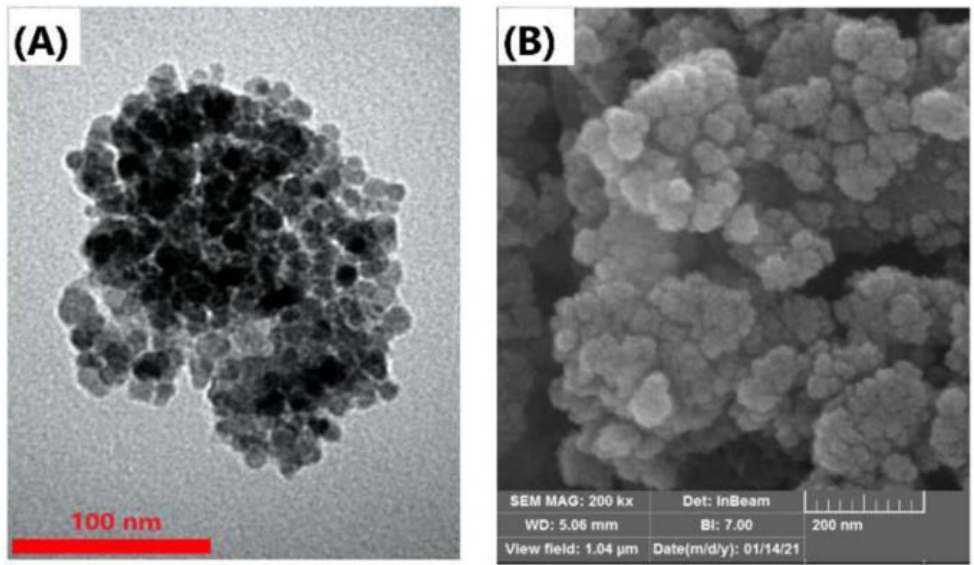


Figure 7. 11: Results of (A) TEM image, (B) FE-SEM image, and (C) particle size distribution of IONPs@SiO₂@PVP nanocomposite (modified) (64).

The study performed by Gao *et al.* (65), prepared silica coating of EMG308 which is a commercially available IONPs. In this study, the Stöber method was used to modify the surface of IONPs with silica shell. They have also reported the use of PVP coating material as an intermediate layer for colloidal particles with silica on IONPs. The protocol for preparing the IONPs@PVP@SiO₂ was to mix 0.6 g PVP in distilled water in a 150 Erlenmyer flask to probe sonicate the mixture for 5 min. After the addition of 18 mg of Fe stock EMG308 to the PVP solution and ensuring that the total volume of water was 5.4 mL, the mixture was probe sonicated for 10 min. The solution was then added to a flask with 40 mL ethanol followed by an additional 10 min of probe sonication. Subsequently, 2 mL of NH₄OH was added to the solution followed by the addition of 0.5-8 mL of TEOS to the solution while stirring at ambient temperature. An additional polymer such as polyethylene glycol (PEG) was added to the solution after 1 h followed by the addition of 0.0375 mL trimethyl silane (TMS) after another half an hour. The reaction was kept overnight to allow complete condensation. The product obtained was collected by ultracentrifugation at 30 000 rpm for 15 min. The product was then washed with ethanol, mixture of ethanol and water, and water few times to remove unreacted reagents. The final product was re-dispersed in water and filtered for the removal of micrometer-sized impurities or aggregates. The overall scheme of the process is shown in **Figure 12 (a)**.

According to the study, other groups have reported direct silica coating on EMG304 which is another type of IONPs, where they attempted to produce a silica shell on EMG308 without the presence of PVP. This resulted in free or excess of silica in addition to EMG308 cores in the absence of coating layers. EMG308 is naturally polydisperse and contains small agglomerates of IONPs in the system. By coating EMG308 with silica, the silica shell thickness could be altered by varying the amount of TEOS, as shown **Figure 7.12 (b)**. The study reported that the thin silica shell thickness resulted in relatively polydisperse. When the silica shell thickness was thicker the core polydispersity was somehow hidden and IONPs@SiO₂ became more spherical and monodisperse. Increasing the amount of TEOS, however, increased the volume occupied per particle and the total iron (Fe) could be suspended in the system. Silica shell thickness with 45 nm for IONPs@SiO₂ could only be concentrated up to 5 mg Fe mL⁻¹ in water, which is low. However, silica shell thickness with 18 nm could be concentrated up to 40 mg Fe mL⁻¹ which are monodisperse (65).

The study reported that the porous structure in the silica shell was due to the addition of PVP as a coating agent, which can be observed in the TEM images from **Figure 7.12 (b)**. In **Figure 7.12 (c)**, pure silica nanoparticles (NPs@SiO₂) were synthesized with and without PVP. In the presence of PVP, the surface coated NPs were shown to be less electrically dense and resulted in a porous structure in TEM. Without the presence of PVP, the surface coated NPs were shown to be more electrically dense and solid. The study indicated that the addition of PVP to the surface of NPs caused porous structure. As an overall result, both IONPs@SiO₂ and NPs@SiO₂ in the presence of PVP caused porosity structure (65).

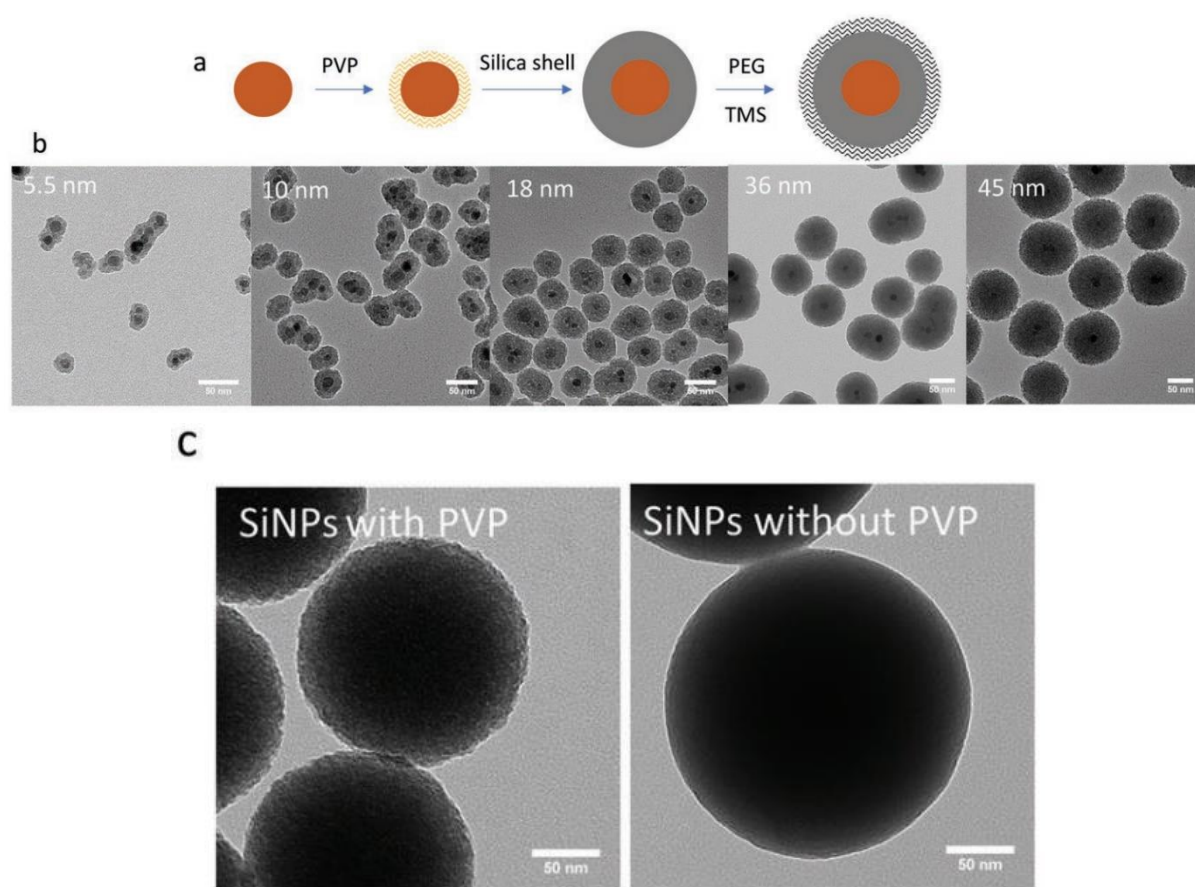


Figure 7. 12: A schematic illustration of surface modification of IONPs@SiO₂. (b) TEM images of IONPs@SiO₂ with various TEOS amount added to the coating process, where the number on the top to left identifies the average silica shell thickness for each image. (c) TEM images of NPs@SiO₂ with and without the presence of PVP (modified) (65).

7.4 Gaps in Literature

To this knowledge, other studies have reported the synthesis of IONPs by co-precipitation using PVP as a stabilizing agent to control the particle size of IONPs. As far as the literature presents, most of the research has done experiments with *in-situ* surface modification of IONPs with PVP as the surface modifier, and studies have explored the benefits of using the polymer as a coating material. Most of the studies have discovered that PVP decreases the particle size and provides narrow particle size distributions, as well as a decrease in agglomeration except for a study conducted by Pandey *et al.*, in which the agglomerations were not decreased. The study performed by Abu-Noqta *et al.* discovered that the presence of PVP caused instability in the system by studying the colloidal stability. Therefore, this raises the question whether PVP really provides the desired results or not. There is also a controversy regarding the study of morphology because previous studies have shown various images where the particles appeared to interact very close to each other, usually as a form of clusters. If observed closely, the images show the existence of mostly agglomerates.

Moreover, a study has focused on the synthesis of IONPs through co-precipitation to functionalize the particles with PVP and silica to produce mesoporous IONPs@PVP@SiO₂, which was discussed by Kermanian *et al.* from the previous subsection. Meanwhile, another study has done experiments on surface modification of IONPs with PVP and silica, but the method used was not co-precipitation. In particular, not many studies have so far reported the synthesis of IONPs through the co-precipitation method to study the effect of PVP on particle size control of IONPs@SiO₂.

No study to date has reported the interaction between mass, molecular weight, concentration, pH, and zeta potential with the aim of controlling the particle size of IONPs@PVP. There has been less reporting of *post-situ* functionalization of IONPs with PVP for application in diagnostics. Thus, the method used by Isci *et al.* is an interesting study to explore by studying the effect of the mass of IONPs, and the molecular weight and concentration of PVP. The optimization of the colloidal stability of IONPs@PVP is the main study followed by silanization to control the particle size of IONPs@PVP@SiO₂. It is interesting to explore whether mass, molecular weight and concentration have any influence on the results. To solve the problem of the thesis, the aim and objectives are assessed in the introductory section (***Section 1.4 – Aim and Objectives***).

8 Materials and Methods

A detailed description of materials and methods followed in carrying out the experiments is introduced. It describes the materials used, how the materials are prepared, what calculations are used and how the experiments are conducted regarding various protocols. The main point for using the methodology and methods is for data collection and analysis which involves qualitative and quantitative methods. The methodology is linked to the thesis statement and is oriented around obtaining an acceptable solution for the thesis.

8.1 Formulas

In order to perform the experiments, the following formulas are required. The formula for calculation of the concentration of IONPs is shown in **Formula 8.1**. The formula for calculation of the volume required depending on the mass of IONPs desired is shown in **Formula 8.2**. This estimation was based on the procedure of silanization of small-scale magnetic beads, meaning IONPs@SiO₂. Mass of IONPs was measured in mg, while volume of IONPs was quantified as mL. The formulas presented have the parameters C, m and V denote as concentration, mass, and volume, respectively.

$$C_{IONPs} = \frac{(m_{dry\ IONPs} - m_{Eppendorf\ tube}) [mg]}{V_{desired\ IONPs} [mL]} \quad (8.1)$$

$$V_{IONPs} = \frac{(Mass_{IONPs}) [mg]}{(C_{IONPs}) \left[\frac{mg}{mL} \right]} \quad (8.2)$$

8.2 Instruments

Various characterization techniques are utilized for data collection and observation, and these are considered instruments. The instruments are of high quality and provide accurate measurements results. The most commonly used instruments are nanoparticle characterization techniques which include dynamic light scattering (DLS), scanning electron microscope (SEM), and LumiSizer. The measurement of hydrodynamic size and zeta potential can be determined using DLS. The analysis of particle size, particle size distribution, and morphology can be determined using SEM. The particle size distribution and stability, on the other hand, can be analyzed using LumiSizer. These characterization techniques are considered quantitative methods. For other qualitative methods, Fourier-transform infrared (FT-IR) spectroscopy is mostly used to identify the functional groups of the materials where one of the goals is to examine whether PVP is coated on the surface of IONPs or not. Below is a list of the various characterization techniques used to analyze, observe, and identify IONPs and functionalized IONPs that are coated with polymer and silica.

Dynamic Light Scattering (DLS)

- Type: Anton Paar Litesizer 500 NTNU-IKP1150
- Core: IKP – Particle Engineering Core Facility
- Department: NV – Department of Chemical Engineering
- Category: Measuring and Characterization

Scanning Electron Microscope (SEM)

- Type: FEI APREO
- Core: Nanolab
- Department: NTNU Nanolab
- Category: Characterization

Fourier-Transform Infrared Spectroscopy (FT-IR)

- Type: Bruker Vertex 80v – FT-IR Spectroscopy
- Core: IMA – Electrochemistry
- Department: NV – Department of Materials Science and Engineering
- Category: Measuring and Characterization

LumiSizer

- Type: LumiSizer Dispersion Analyzer (SEPView) NTNU-IKP1002
- Core: IKP – Particle Engineering Core Facility
- Department: NV – Department of Chemical Engineering
- Category: Measuring and Characterization

8.3 Equipment

Equipment used is obtained from NTNU at the Faculty of Natural Sciences and Technology and the Department of Chemical Engineering. **Table 8.1** shows all the equipment used in this thesis. The equipment is used regarding the synthesis route of IONPs and *post-situ* functionalization of PVP and silica.

Table 8. 1: List of equipment.

Equipment for the synthesis of IONPs by the co-precipitation method
Beaker
Weighing boat
50 mL volumetric flask
25 mL burette
Plastic funnel
Mortal pestle
Magnetic stirrer bar
Magnetic bar retriever
50 mL centrifuge tube
Disc magnet (magnetic separation)
Timekeeper (stopwatch)
Finnpipette
Equipment for <i>post-situ</i> functionalization of IONPs with PVP
Weighing boat
500 ml volumetric flask
Beaker
Glass funnel
Disc magnet (magnetic separation)
Timekeeper (stopwatch)
Pasteur pipette
Micropipette
Finnpipette
Equipment for <i>post-situ</i> functionalization of IONPs with silica
Pasteur pipette
Glass pipette
Glass vial
Disc magnet (magnetic separation)
Timekeeper (stopwatch)
Magnetic stirrer bar
Magnetic bar retriever
Micropipette
Finnpipette

8.4 Chemicals and Solutions

All chemicals and solutions are obtained from NTNU at the Faculty of Natural Sciences and Technology and the Department of Chemical Engineering. **Table 8.2** shows the chemicals and solutions used for the entire thesis. Iron (III) chloride hexahydrate ($\text{FeCl}_3 \cdot 6\text{H}_2\text{O}$), ammonium hydroxide solution (NH_4OH , 25 % by weight), and polyvinylpyrrolidone (PVP, Mw: 10 000, 40 000 and 360 000 g/mol) were purchased from Merck. Tetraethyl orthosilicate (TEOS) for synthesis was purchased from Sigma-Aldrich which was produced in Germany. Hydrochloric acid for pH analysis was purchased from Thermo Fischer. Iron (II) chloride tetrahydrate ($\text{FeCl}_2 \cdot 4\text{H}_2\text{O}$, $\geq 99.0\%$), isopropanol (IPA, technical grade, $\geq 98.0\%$), and sodium hydroxide for pH analysis (NaOH, pellets) were purchased from VWR. All the chemicals were taken advantage of without any supplemental purifications. Distilled de-ionized water purified using a Millipore water purification system (MQ water) was used for the experimental work.

Table 8. 2: List of chemicals and solutions.

Chemical	Phase	Manufacturer	Chemical formula	Molecular weight [g/mol]
Iron (II) Chloride Tetrahydrate	s	VWR	$\text{FeCl}_2 \cdot 4\text{H}_2\text{O}$	198.81
Iron (III) Chloride Hexahydrate	s	Merck	$\text{FeCl}_3 \cdot 6\text{H}_2\text{O}$	270.33
Ammonium Hydroxide	aq	Merck	NH_4OH	35.04
Tetraethyl Orthosilicate (TEOS)	l	Sigma-Aldrich	$\text{SiC}_8\text{H}_{20}\text{O}_4$	208.33
Hydrochloric acid	aq	Thermo Fischer	HCl	36.50
Sodium hydroxide	aq	VWR	NaOH	40.00
Isopropanol (Isopropyl Alcohol)	l	VWR	$\text{C}_3\text{H}_8\text{O}$	60.10
Polyvinyl- pyrrolidone	s	Merck	$(\text{C}_6\text{H}_9\text{NO})_n$	10 000 40 000 360 000

8.5 Procedure

A method is used to synthesize IONPs followed by adsorption of PVP on the surface of IONPs and subsequently silanization by the Stöber method. These methods are used to solve the objectives given in the introduction section. Below is the list of all the methods that were performed.

8.5.1 Synthesis of Iron Oxide Nanoparticles by the Co-Precipitation Method

Step 1 – Stock Solution

4.0 g of $\text{FeCl}_2 \cdot 4\text{H}_2\text{O}$ and 10.8 g of $\text{FeCl}_3 \cdot 6\text{H}_2\text{O}$ were prepared in a weighing boat and transferred to a 50 mL volumetric flask. 20 mL of MQ water was added to the volumetric flask and shaken for obtaining a uniform solution. The remaining of MQ water was added up to the mark.

Step 2 – Reaction

84.6 g of MQ water was added to a beaker and stirred at 380 rpm. A 25 mL burette attached to the stand was filled with the stock solution. 15.4 mL of 25 wt % NH_4OH was added straight into the beaker (the base was added quickly to minimize loss from the pipette during addition). 10 mL of the iron salt solution was added to the beaker dropwise (~3 drops per second). After addition was completed, less than 2 mL of MQ water was used from a squirt bottle to wash the particles from the magnetic bar into the beaker.

Step 3 – Transferring content from beaker to centrifuge tube

45 mL of the suspension was transferred from the beaker to a 50 mL centrifuge and a disc magnet was placed on the side of the tube for 2 minutes in order to discard the supernatant (this step was repeated 3x).

MQ water was added to the tube using a squirt bottle so that the level in the tube was at 25 mL mark (the squirt water bottle was used to get the particles into dispersion).

After all the 4 reaction beakers had gone through step 2 and 3, the washing step was followed.

Step 4 – Washing

The centrifuge tube containing 25 mL of IONPs dispersion was shaken briefly with hands followed by 5-10 seconds of vortexing and placed on top of the disc magnet for 2 minutes in order to discard the supernatant (this step was repeated 3x).

Finally, 12 mL of MQ water was added to the centrifuge tube using a finnpipette. The sample was marked and stored at 4 °C.

The other reactions were repeated the same, so there were 4 batches in total.

Concentration test was calculated using *Formula 8.1*.

8.5.2 *Post-Situ* Functionalization of Iron Oxide Nanoparticles with Polyvinylpyrrolidone

Step 1 – Stock Solution

Desired amount of PVP was prepared in a weighing boat and transferred to a 500 mL volumetric flask depending on the concentration. MQ water was added to the volumetric flask using a squirt bottle and the solution was shaken to dissolve PVP for obtaining a uniform solution. The remaining of MQ water was added up to the mark.

Step 2 – Preparation of Polyvinylpyrrolidone with Iron Oxide Nanoparticles Dispersion

The prepared IONPs from *subsection 8.5.1* was vortexed for 20-25 seconds. The desired amount of IONPs was added to a small glass vial using *Formula 8.2*. The water was separated by magnetic separation for 2 minutes. 10 mL of the stock solution was added to the vial containing IONPs followed by 20 seconds of vortexing. Finally, the solution was shaken overnight at 230 rpm at ambient temperature.

Step 3 – Washing

The supernatant was discarded by magnetic separation for 3 minutes. The PVP coated IONPs was cleaned thrice using magnetic separation by adding 3-5 mL with MQ water for the washing step. The PVP coated IONPs were re-dispersed in 3 mL of MQ water followed by 20 seconds of vortexing. Finally, the PVP coated IONPs were ultrasonicated for 5 minutes using a probe sonicator.

The sample was ready for DLS and FT-IR characterization, and in addition to pH measurement.

8.5.3 Batch Silanization of Iron Oxide Nanoparticles

Step 1 – Preparation of IONPs in Solvent

19 mL of solvent was added to a glass vial and stirred at 580 rpm. In the meantime, the volume required depending on the mass of IONPs desired was added to an Eppendorf tube using *Formula 8.2*. The water was removed by magnetic separation for 2 minutes. The IONPs were cleaned thrice with the solvent in the Eppendorf tube by magnetic separation for 2 minutes. Eventually, the IONPs were re-dispersed in 1 mL of the solvent followed by 20 seconds of vortexing.

Step 2 - Reaction

2 mL of TEOS was added to the vial and left the reaction for 15 minutes. In the meantime, the IONPs were vortexed for 20 seconds followed by 2 minutes sonication using a sonicator bath. The IONPs were vortexed for another 20 seconds followed by 1 minute pipette flush while sonicating (the Eppendorf tube was held in the corner of the sonication bath and shielded the content from water drops). Eventually, the IONPs were loaded slowly into the vial. The solution was stirred for another 15 minutes to ensure complete mixing. 6 mL of NH₄OH was added to the reaction while stirring. The reaction was left for 5 hours.

Step 3 – Washing

When the reaction time approached 5 hours, a 50 mL centrifuge tube was taken out and labelled with the name of the sample, name of one making it, and date. The magnet was kept stirring until the magnet retrieve has removed the magnet stirrer from outside. The content was then transferred from the vial to the centrifuge tube as fast as possible. The supernatant was removed by magnetic separation for 2 minutes. The particles were cleaned by adding approximately 25 mL of MQ water/solvent using a squirt bottle. The tube was shaken and vortexed for 20 seconds followed by magnetic separation for 2 minutes in order to discard the supernatant. This was repeated twice with MQ water, and then twice with solvent and eventually five times with MQ water.

- 2 x MQ water
- 2 x solvent
- 5 x MQ water

Finally, the IONPs were re-dispersed in 25 mL MQ water followed by 20 seconds of vortexing and stored at 4 °C.

8.5.4 Batch Silanization of Iron Oxide Nanoparticles with Polyvinylpyrrolidone

Steps 1 and 2 were repeated from *subsection 8.5.2*.

Step 3 – Preparation of IONPs@PVP in solvent

19 mL of solvent was added to a glass vial and stirred at 580 rpm. In the meantime, the supernatant of IONPs@PVP was discarded by magnetic separation for 3 minutes. The PVP coated IONPs were cleaned thrice with the solvent by magnetic separation. Subsequently, the PVP coated IONPs were re-dispersed in 1 mL of solvent followed by 20 seconds of vortexing. Any IONPs sticking to the wall were sonicated for 1-2 minutes using a sonicator bath.

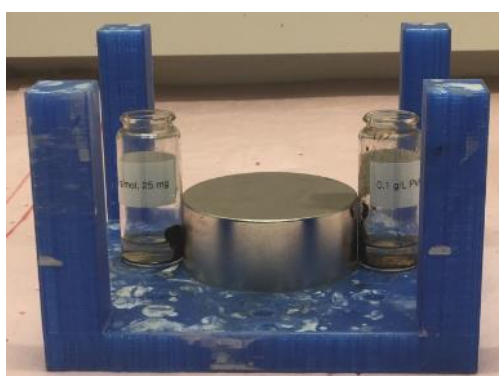


Figure 8. 1: Photo of magnetic separation from experimental work.

Step 4 – Reaction

Step 2 was repeated from *subsection 8.5.3*.

Step 5 – Washing

Step 3 was repeated from *subsection 8.5.3*.

8.6 Sample Preparation for Characterization Techniques

This subsection introduces the sample preparation for all the characterization techniques used in this thesis. Before samples can be analyzed using the various characterization techniques, the samples must be processed and prepared properly. Sample preparation is very important to obtain accurate data.

8.6.1 Sample Preparation for Dynamic Light Scattering

The sample was sonicated for 1 minute to ensure homogeneous mixture. The sample preparation for IONPs and IONPs@PVP was prepared at 1:30 dilution and 1:100, respectively. The diluted sample was vortexed for 30 seconds followed by pipette flushing during sonication for 1 minute. The vortex and sonication + pipette flush of the sample was repeated thrice. Finally, the dispersion was filled into a folded capillary cell and inserted in the LiteSizer. After every measurement, the cell was cleaned by injecting MQ water inside with a syringe, in which the syringe was attached to one of the openings of the cell. The injection step was repeated three times to ensure that the cell was cleaned. Then a second syringe was filled with MQ water and attached to the other opening of the cell. The cell was rinsed using both syringes a few times. The cell was then dried by shaking it a few times.

8.6.2 Sample Preparation for Fourier-Transform Infrared Spectroscopy

The sample preparation for FT-IR was prepared using the attenuated total reflection (ATR) method which allowed direct measurement of the sample. A background spectrum for air was first recorded. The sample was prepared without pre-treatment. For liquid samples, the FT-IR spectrum was collected by adding a drop of the sample directly on the diamond in the device. For powder samples, the FT-IR spectra was collected by adding the sample on the diamond at an external pressure using the tip. For each measurement, the diamond and tip were cleaned with ethanol and water before analysis.

8.6.3 Sample Preparation for Scanning Electron Microscope

The sample preparation for SEM was prepared by diluting 20 μL of the sample with 980 μL of MQ water in an Eppendorf tube. The diluted sample was vortexed for 20 seconds followed by 10 minutes of sonication. The prepared sample was taken to the nanolab. A silicon wafer was cut into to small square pieces followed by cleaning in a plasma chamber in order to remove organic and inorganic contaminants from the surface. The sample was then vortexed for 20 seconds followed by 4 minutes of sonication to achieve greater dispersion. Eventually, 20 μL of the sample was added to the silicon wafer on a hot stirrer plate. The stirrer plate was heated to dry the sample quicker. Finally, the silicon wafer that contains the sample was placed on a copper conductive tape followed by insertion into the chamber of the instrument for image analysis.

8.6.4 Sample Preparation for LumiSizer

The sample was vortexed for 20-25 seconds. The sample preparation for IONPs was prepared at 1:100 dilution in an Eppendorf tube. The diluted sample was vortexed for 20 seconds followed by 10 seconds of sonication (the vortex and sonication step were repeated 3x). 0.5 mL of the diluted sample was transferred to a polyacrylamide (PA) type cuvette cell. The diluted sample was inserted into the instrument.

8.7 pH Measurement

This subsection includes the procedure for measuring pH of the potential samples to study the effect of pH on the zeta potential.

8.7.1 Direct pH Measurement

Step 1 – Cleaning of electrode

The electrode of the pH meter was taken out of its storage solution that contains potassium chloride (KCl). The electrode was then rinsed with MQ water under an empty waste beaker. Once rinsed, the electrode was dried using wipes. It was important to avoid rubbing the electrode because it had a sensitive membrane around it.

Step 2 – Calibration

The electrode was placed in the buffer solutions starting from the pH value 7, then the pH value 4 and lastly the pH value 10 (the electrode was cleaned between each calibration).

Step 3 – pH reading

After the calibration was completed, the electrode was taken out to rinse it with MQ water followed by drying with wipes. The electrode was then inserted into the sample to start the reading. The pH reading was left for approximately 1 minute to ensure that the reading was accurate.

Step 4 – Cleaning after use

When the pH reading was completed, the electrode was rinsed with MQ water and dried using wipes. The electrode was then placed in the same storage solution containing KCl.

8.7.2 pH Change

Steps 1 and 2 were repeated from *subsection 8.7.1*.

Step 3 – Sample preparation

In prior to the calibration of the pH meter, the sample was diluted by a factor of 1:20. The diluted sample was scaled up to 20 mL to have enough volumes for 7 readings.

Step 4 – pH validation

The electrode was directly inserted into the sample to validate the pH level at initial point before pH adjustment.

Step 5- pH adjustment

The pH adjustment was performed using 0.1 M NaOH and 0.1 M HCl to change the pH of the diluted sample that contains 20 mL (it was important not to mix both base and acid together as neutralization might take place). A few drops from the acid or base were added to the sample followed by 5-10 seconds of vortexing. The pH reading was left for approximately 1 minute to ensure accurate reading. Then 2 mL of the diluted sample was added to a small glass vial followed by DLS measurement.

This step (**Step 5**) was repeated until 7 readings have been measured.

Step 6 – Cleaning after use

Step 4 was repeated from *subsection 8.7.1*.

8.8 Experimental Design

8.8.1 Design for Polyvinylpyrrolidone Coating of Iron Oxide Nanoparticles

Based on the aim and objectives of the thesis, an experimental design was created manually to examine the colloidal stability of IONPs@PVP. **Table 8.3** represents the experimental design of IONPs@PVP, in which the mass of IONPs, and the molecular weight and the concentration of PVP are the main factors. These are considered inner parameters. The selected masses of IONPs are 25, 50 and 100 mg. The selected molecular weights of PVP are 10 000, 40 000 and 360 000 g/mol. The selected concentrations of PVP are 0.1 and 0.5 g/L. Additional experiments were also included based on the results obtained from DLS to examine whether an increase or decrease in concentration provided the optimal results.

Table 8. 3: Experimental design for IONPs@PVP.

Mass of IONPs [mg]	Molecular Weight of PVP [g/mol]	Concentration of PVP [g/L]
25	10 000	0.1
50	10 000	0.1
100	10 000	0.1
25	40 000	0.1
50	40 000	0.1
100	40 000	0.1
25	360 000	0.1
50	360 000	0.1
100	360 000	0.1
25	10 000	0.5
50	10 000	0.5
100	10 000	0.5
25	40 000	0.5
50	40 000	0.5
100	40 000	0.5
25	360 000	0.5
50	360 000	0.5
100	360 000	0.5
Additional Experiments		
25	10 000	1.0
50	10 000	1.0
100	10 000	1.0
25	40 000	0.05
25	360 000	0.05

8.8.2 Design for Silica Coating of Iron Oxide Nanoparticles

Based on the aim and objectives of the thesis, an experimental design was also created manually to examine the effect of PVP on IONPs@SiO₂ to study the particle size, particle size distribution, and morphology. **Table 8.4** represents the experimental design of IONPs@SiO₂, in which the mass of IONPs, the molecular weight and the concentration of PVP, and the amounts of NH₄OH, TEOS, and solvent are the main factors. These are considered inner parameters. The selected masses of IONPs are 25, 50 and 100 mg. The selected molecular weights of PVP are 10 000 and 360 000 g/mol. The selected concentrations of PVP are 0.1 and 0.5 g/L. The selected amounts of NH₄OH, TEOS, and solvent are 6, 2, and 20 mL, respectively.

Table 8. 4: Experimental design for IONPs@SiO₂ in the presence of with and without PVP.

Mass of IONPs [mg]	Molecular Weight of PVP [g/mol]	Concentration of PVP [g/L]	Amount of NH ₄ OH [mL]	Amount of TEOS [mL]	Amount of Solvent (IPA) [mL]
25	0	0	6	2	20
50	0	0	6	2	20
100	0	0	6	2	20
25	10 000	0.5	6	2	20
50	10 000	0.5	6	2	20
100	10 000	0.5	6	2	20
25	360 000	0.1	6	2	20
50	360 000	0.1	6	2	20
100	360 000	0.1	6	2	20

9 Results and Discussion

9.1 Iron Oxide Nanoparticles by the Co-Precipitation Method

The objective of this subsection is to validate the IONPs sample without any additional layer adsorbed on the surface. This is to examine whether the IONPs can be used for *post-situ* functionalization. The validation of the sample is to study the particle size and stability of the particles.

9.1.1 Concentration Test Analysis

The concentration analysis of IONPs by the co-precipitation method is shown in **Figure 9.1**, where the error bars indicate the standard deviation of three concentration measurements for each batch. The synthesis of IONPs developed at NTNU provides 4 batches by this particular method according to the methodology. The results indicate that the batches provide similar results. The mixture of all the batches gives a final product, and it is referred to as mixed IONPs. The concentration of the mixed IONPs appears to be 55.70 ± 1.50 mg/mL. The sample is used for the entire thesis and is considered as the main sample for studying the hydrodynamic size and zeta potential (ZP) and in addition to surface modification with PVP and silica. The sample name for mixed IONPs is named as IONPs when compared to functionalized IONPs.

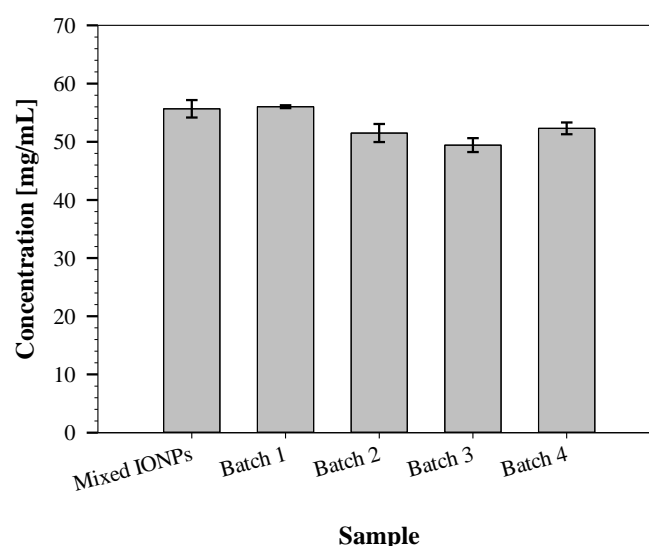


Figure 9. 1: Concentration test of IONPs. The synthesized method for IONPs by the co-precipitation gives 4 batches. The mixed IONPs are a result of these corresponding batches. The error bars represent the standard deviation calculated from the triplicate measurement of the specific sample.

9.1.2 Particle Size Distribution Analysis

The particle size of IONPs by the co-precipitation method is shown in **Figure 9.2**, where the error bars indicate the standard deviation of three hydrodynamic size measurements for each batch. The DLS value refers to the size of a sphere diffused at the same rate as the particle being measured. The size includes the additional hydration layer of the particles (core + hydration shell/layer). In DLS measurement, the sphere contains the core particle in addition to ions or adsorbed polymers attached to its surface/interface. The results indicate that the sizes of each batch vary to a certain extent. The findings at least hint that batch 3 provides the smallest hydrodynamic diameter (H_d), whereas batch 4 shows the highest H_d . Although the batches show variations in sizes, the range is between 116 and 190 nm which is considered acceptable. The H_d of the mixed IONPs appears to be 192.10 ± 4.50 nm, which is relatively closed to the H_d of batch 4.

Another method of measuring the particle size of IONPs is the use of a dispersion analyzer called LumiSizer. This method is quite similar to DLS which measures the diffusion of particle's movement under Brownian motion. The difference, however, is the use of a centrifugal technology where it detects changes in light transmission that characterizes processes such as sedimentation. The particle size of IONPs calculated from the dispersion is found to be 43.44 ± 21.49 nm, which is shown in **Table 9.1**. The sample name IONPs is from the mixture of all the batches.

The particle distribution calculated from the dispersion is shown in **Table 9.2**. The particle size interval of IONPs is shown to have a distribution between 29 and 67 nm, which is an indication that the polydispersity of the system is not significantly high. The results show that the percentage of particles of 29.90, 34.37, 43.44, 60.01, and 66.90 nm are equal to or less than 10, 16, 50, 84 and 90 %, respectively. Thus, the calculated average particle size appears to be 43.44 nm. This sample is from the mixed IONPs, but it is referred to as IONPs. The objective was to produce smaller particle size interval as much as possible to have highly monodisperse particles. The overall findings of particle size distribution of IONPs are satisfactory to some extent.

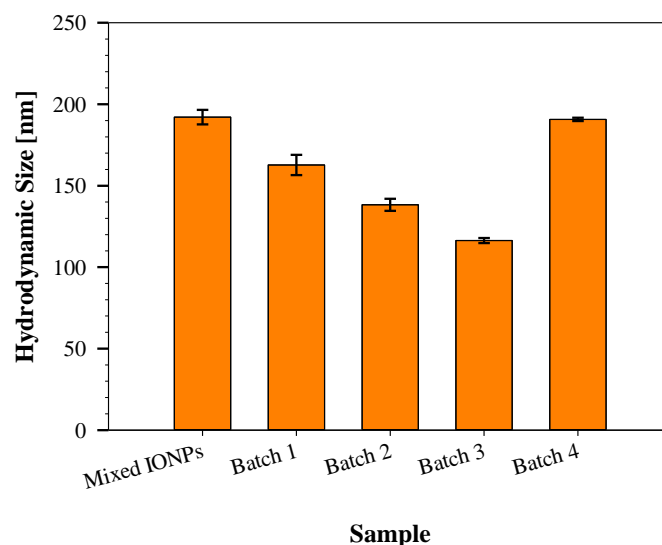


Figure 9. 2: Hydrodynamic size of IONPs. The synthesized method for IONPs by the co-precipitation gives 4 batches. The mixed IONPs are a result of these corresponding batches. The error bars represent the standard deviation calculated from the triplicate measurement of the specific sample.

Table 9. 1: Particle size of IONPs.

Sample	Particle Size [nm]	Standard Deviation
IONPs	43.40	21.50

Table 9. 2: Particle size distribution of IONPs.

Sample	10 % ≤ [nm]	16 % ≤ [nm]	50 % ≤ [nm]	84 % ≤ [nm]	90 % ≤ [nm]
IONPs	29.90	34.40	43.40	60.00	66.90

9.1.3 Surface Charge and Stability Analysis

The zeta potential of IONPs by the co-precipitation method is shown in **Figure 9.3**, where the error bars indicate the standard deviation of three ZP measurements for each batch. The results indicate that the ZP of each batch does not vary significantly. The findings show that the particles are stable in terms of colloidal stability which is in good agreement with the literature (37). The ZP of the mixed IONPs appears to be -34.40 ± 0.30 nm. The surface charge of all samples is negative owing to the OH^- groups attached to the surface of IONPs. The instability index of IONPs characterized by LumiSizer, on the other hand, is found to be 0.496, which is shown in **Table 9.3**. The sample is considered relatively stable and is in good agreement with the results obtained from DLS. This is the sample from the mixed IONPs, but it is referred to as IONPs in this context. The overall results demonstrate that the IONPs are somehow colloiddally stable and is considered acceptable for further characterizations.

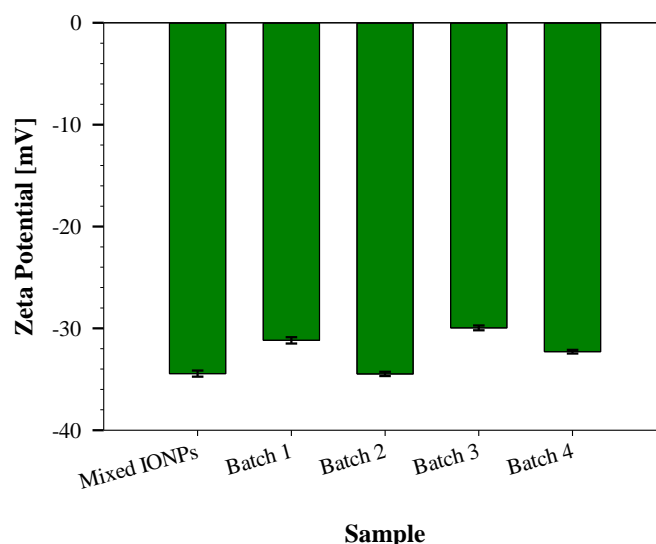


Figure 9. 3: Zeta Potential of IONPs. The synthesized method for IONPs by the co-precipitation gives 4 batches. The mixed IONPs are a result of these corresponding batches. The error bars represent the standard deviation calculated from the triplicate measurement of the specific sample.

Table 9.3: Instability index of IONPs.

Sample	Instability Index
IONPs	0.496

9.2 Polyvinylpyrrolidone Coating of Iron Oxide Nanoparticles

The findings obtained for non-functionalized IONPs were considered valid and stable, and it was to ensure that the particles were appropriate for the *post-situ* surface modification. Therefore, the purpose of this subsection is to understand the coating process of IONPs@PVP by studying the particle size, ZP, surface charge, structural detection, and pH.

9.2.1 Control of Particle Size and Stability Analysis

The Effect of Mass, Molecular Weight, and Concentration

According to the experimental design shown in **Table 8.3**, all samples were characterized using DLS to study how PVP affects the final particle size and colloidal stability of IONPs. **Figure 9.4** shows the effect of IONPs and the effect of molecular weight and concentration of PVP on the hydrodynamic size and ZP of IONPs@PVP, where the error bars represent the standard deviation of DLS measurements for each sample. The findings are compared with non-functionalized IONPs.

Figure 9.4-A shows the hydrodynamic size of IONPs@PVP with various molecular weights of PVP for 0.1 g/L PVP in water dispersion. This report describes the result of hydrodynamic size, which shows that there is nearly no variation in sizes apart from the sample named 25-IONPs@PVP for 10 000 g/mol PVP where the H_d appears to be quite large. There is a certain possibility that the polydispersity of the particle distribution is because of the aggregation of clusters measured as a single particle. However, the comparison with other samples is demonstrated to be different because the H_d range is between 177 and 225 nm for all samples apart from the particular sample mentioned above. The samples 50-IONPs@PVP and 100-IONPs@PVP for 10 000 g/mol PVP appear to have a much smaller H_d in comparison to 25 mg IONPs. The results highlight that increasing the mass of the IONPs decreases the H_d to a small degree, but the effect of molecular weight of PVP does not affect the final H_d .

Figure 9.4-B shows the hydrodynamic size of IONPs@PVP with various molecular weights of PVP for 0.5 g/L PVP in water dispersion. The findings clearly demonstrate that increasing the concentration of PVP results in an increase in hydrodynamic size for 40 000 and 360 000 g/mol PVP. There are variations in sizes except for 10 000 g/mol PVP. In comparison to 0.1 g/L PVP where the H_d increases significantly for 25 mg IONPs, it seems that the increase in concentration does not affect the H_d for 10 000 g/mol PVP. However, the results for 40 000 g/mol PVP indicate that increasing the mass to 100 mg results in large H_d . It is an indication that the polydispersity of the particle distribution is due to the aggregation of clusters measured as a single particle. For 360 000 g/mol PVP, all samples show large H_d . The results demonstrate that the effect of the mass of IONPs does not influence the lowest molecular weight of PVP, but it affects 40 000 g/mol PVP to a small degree, whereas it affects 360 000 g/mol PVP to a large degree. The effect of the molecular weight of PVP, on the other hand, seems to influence the final H_d to a greater extent. The overall findings show that the concentration of PVP at 0.5 g/L favours 10 000 g/mol PVP.

The hydrodynamic size is also dependent on the stability of the particles. The dispersed particles can be measured using ZP to determine the colloidal stability. **Figure 9.4-C** shows the ZP of IONPs@PVP with various molecular weights of PVP for 0.1 g/L PVP in water dispersion. The results show that the ZP increases slightly as the mass increases for the lowest molecular weight of PVP. For higher molecular weights such as 40 000 g/mol PVP, the ZP decreases slightly as the mass increases, which seems to be the opposite compared to the lowest molecular weight. The highest molecular weight with 360 000 g/mol PVP shows that the masses of 25 and 50 mg of IONPs provide nearly the same results, but the ZP decreases as the mass is 100 mg. From these overall findings, the masses of 25 and 50 mg for 10 000 g/mol PVP demonstrate to have a lower ZP in comparison to the highest mass. The masses of 25 and 50 mg of the IONPs for 40 000 and 360 000 g/mol PVP show higher ZP compared to 10 000 g/mol PVP. However, the highest mass of IONPs appears to decrease the ZP for both 40 000 and 360 000 g/mol PVP. This clearly shows that the effect of the mass of IONPs and the effect of molecular weight of PVP have an influence on the ZP.

Figure 9.4-D shows the ZP of IONPs@PVP with various molecular weights of PVP for 0.5 g/L PVP in water dispersion. By increasing the concentration of PVP, the results favour the lowest molecular weight of PVP due to the high ZP. This result ties well with the H_d because the samples show the lowest size compared to 40 000 and 360 000 g/mol PVP. There are nearly no variations in the ZP between mass of 25 and 50 mg of IONPs for 10 000 g/mol PVP, but the ZP has a slight decrease when 100 mg of the IONPs are used. There are also nearly no variations in ZP for 40 000 and 360 000 g/mol PVP. The results indicate that the effect of the mass of IONPs does not appear to influence the ZP to a great extent, but the effect of the molecular weight of PVP seems to influence the final ZP to a certain extent.

The overall findings in **Figure 9.4** demonstrate that the H_d is between 177 and 1915 nm. The mass of IONPs, the molecular weight and concentration of PVP appear to affect the size of the particles to some extent. Few of the samples provide a smaller size than non-functionalized IONPs, but the stability is not as high as IONPs without the presence of PVP. The results clearly show that the addition of PVP does not increase the stability compared to non-functionalized IONPs. The particles are considered not stable because the ZP value is not high enough to overcome attractive forces and the particles tend to flocculate in the system. The particles settle very quickly at low dilution, and therefore higher dilutions were required for DLS characterization. The samples demonstrate to have a ZP between 6 and 20 mV, but to stabilize them remains a challenge. The study reported by Isci *et al.* (58) demonstrates that the presence of PVP decreases the absolute value of IONPs, resulting in poor colloidal stability. The study reported by Abu-Noqta *et al.* (59), also demonstrates that the ZP of IONPs@PVP results in poor stability. The results are somehow in line with these studies because PVP shows to be not an appropriate coating agent and does not provide a good colloidal dispersion of IONPs in the system.

It is also important to highlight the fact that the presence of PVP causes positive surface charge. The results are not in good agreement with Isci *et al.* since the study reports negative surface charge in the presence of PVP. It is confirmed that the surface charge of IONPs without the presence of PVP shows to be negative, and this does appear to depend on the functional group attached to the surface of IONPs. It is notable that PVP is known to be an un-charged polymer. Therefore, it was speculated that the addition of PVP would not change the surface charge. However, since the results show that the addition of polymer neutralized the negative to positive charge might be because of other factors such as the concentration of the solution, the nature of the solvent, and the pH. The pH of a solution may have the tendency to influence the surface

charge owing to the functional groups present on the surface of IONPs that contain oxygen atoms. The atom can either be protonated or deprotonated, meaning that the oxygen atom has the ability to capture or remove a proton (H^+) with the interaction between a PVP molecule.

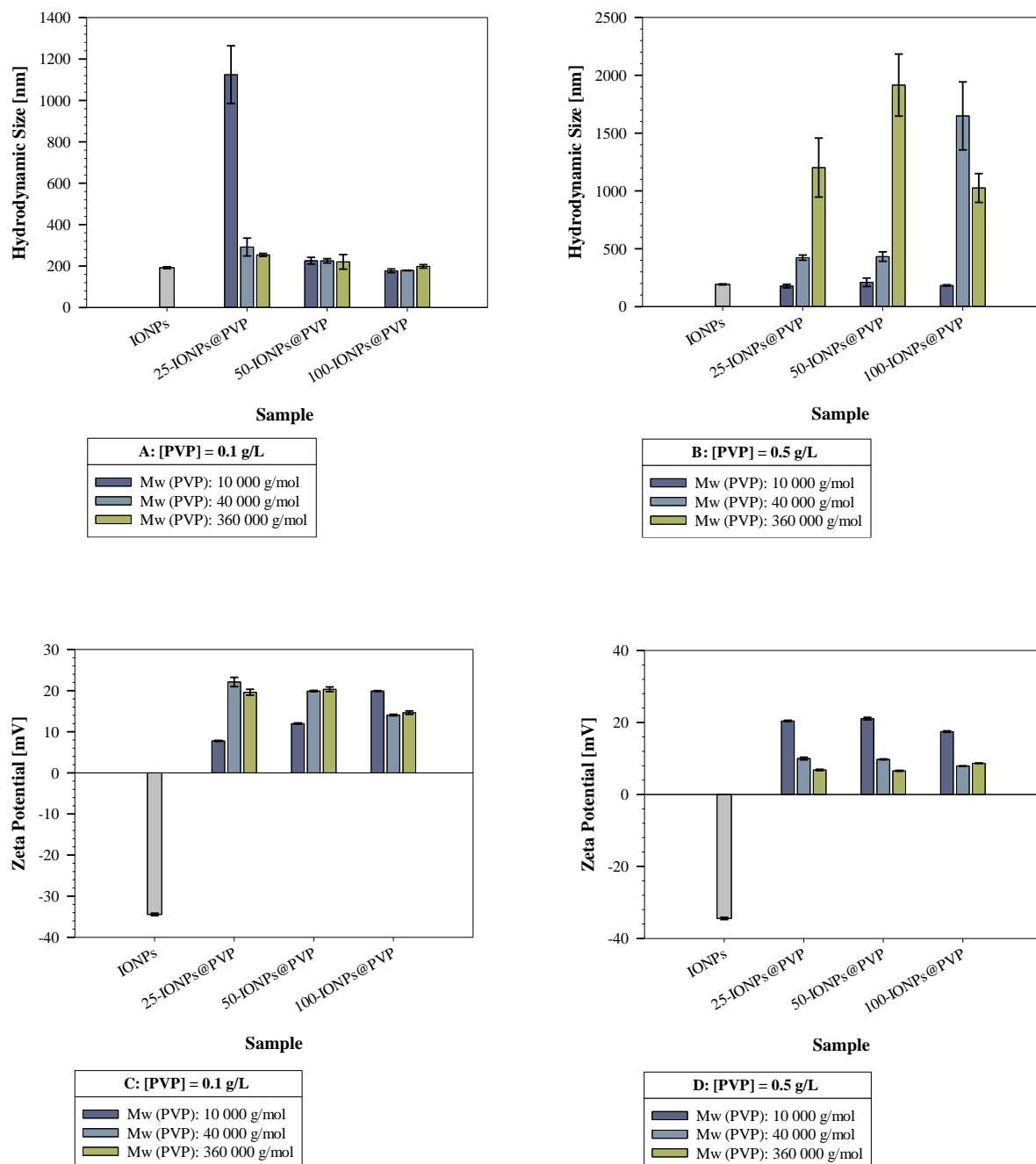


Figure 9. 4: Hydrodynamic size of x -IONPs@PVP: (A) 0.1 g/L and (B) 0.5 g/L PVP in water dispersion with various molecular weights of PVP. Zeta potential of x -IONPs@PVP: (C) 0.1 g/L and (D) 0.5 g/L PVP in water dispersion with various molecular weights of PVP. The letter x represents the mass of IONPs used for the characterization ($x = 25, 50, \text{ or } 100 \text{ mg}$). The sample for non-functionalized IONPs is from the mixed IONPs batch. The error bars indicate the standard deviation calculated from the triplicate measurement of the specific sample.

Study of Concentration Change

From **Figure 9.4**, it appears that the lowest concentration of PVP mostly favours the higher molecular weights of PVP, whereas the highest concentration of PVP favours the lowest molecular weight of PVP. **Figure 9.5** considers 0.05 and 1.0 g/L PVP for the highest and lowest molecular weights of PVP, respectively, in addition to 0.1 and 0.5 g/L PVP from **Figure 9.4**. The purpose of decreasing and increasing the concentration of PVP is to examine whether the effect of concentration has a large influence on the H_d and ZP. The masses of IONPs are selected as 25, 50, and 100 mg for 10 000 g/mol PVP, while only the mass of 25 mg of IONPs are considered for 40 000 and 360 000 g/mol PVP.

An increase in concentration of PVP does not provide better results for 10 000 g/mol PVP, as shown in **Figure 9.5-A**. It was speculated that higher concentrations of PVP with lower molecular weight might decrease the size, but the findings show the opposite. Increasing the concentration to 1.0 g/L appears to provide higher H_d in comparison to 0.1 and 0.5 g/L PVP except of 25 mg IONPs from 0.1 g/L PVP. The ZP, on the other hand, appears to provide better results when the masses 25 and 50 mg of IONPs are used compared to 100 mg, as shown in **Figure 9.5-B**. At this concentration, the ZP seems to demonstrate higher values than 0.1 g/L PVP for 25 and 50 mg of IONPs to a certain degree. This might be because of the effect of bridging flocculation at low concentration. However, when 0.5 g/L PVP is added to the dispersion, the ZP appears to be higher, and this may be due to the steric interactions. At 1.0 g/L PVP, the ZP decreases, and the reason for this may be that the existence of PVP molecule chains is not adsorbed on the surface of IONPs, as it can result in depletion stabilization. The attractive force starts to dominate because there is a possibility that the polymer chains do not protect the particles from getting close to each other, is likely to be high.

A decrease in concentration of PVP does not provide the expected results based upon 40 000 and 360 000 g/mol PVP, as shown in **Figure 9.5-C**. It was speculated that lower concentrations for higher molecular weights of PVP may lead to decrease in size, but the results do not appear to be true. The H_d for 0.5 g/L PVP shows the highest size, but the concentration at 0.1 g/L shows the lowest size. The ZP shown in **Figure 9.5-D**, corresponds well with the H_d because the highest concentration provides the lowest ZP, whereas the concentration at 0.1 g/L provides the highest ZP. The results also appear to demonstrate that the lowest concentration of PVP at 0.05 g/L might cause bridging flocculation, whereas the highest concentration of PVP may result in depletion effect, as it is unfavourable. The concentration at 0.1 g/L PVP provides the better results.

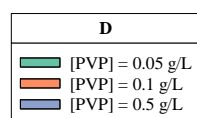
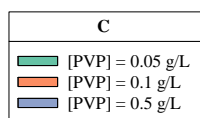
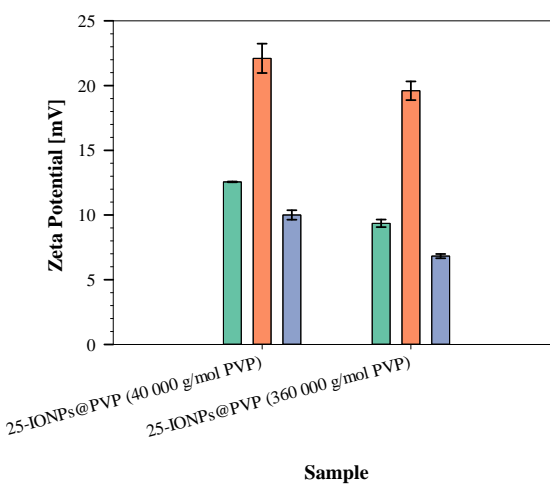
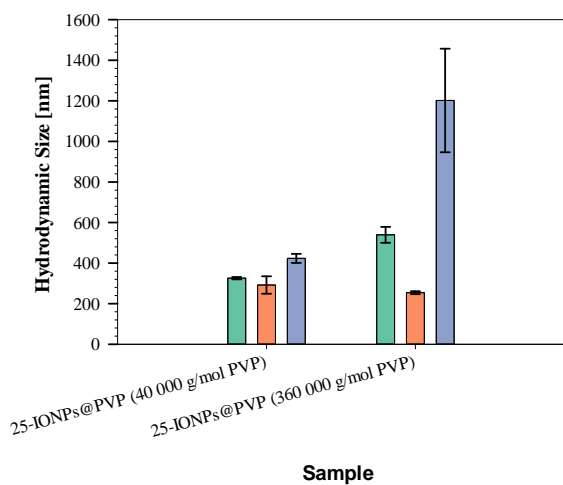
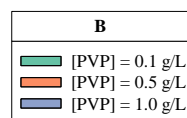
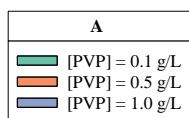
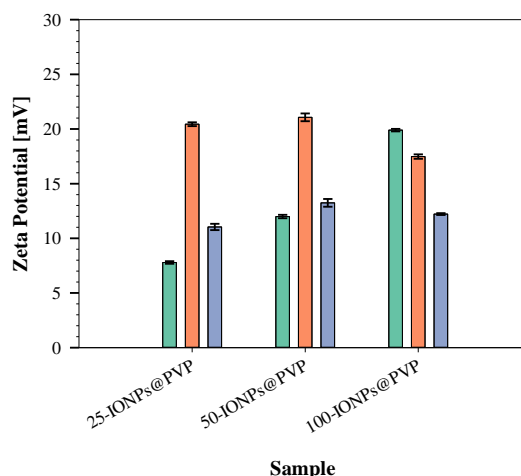
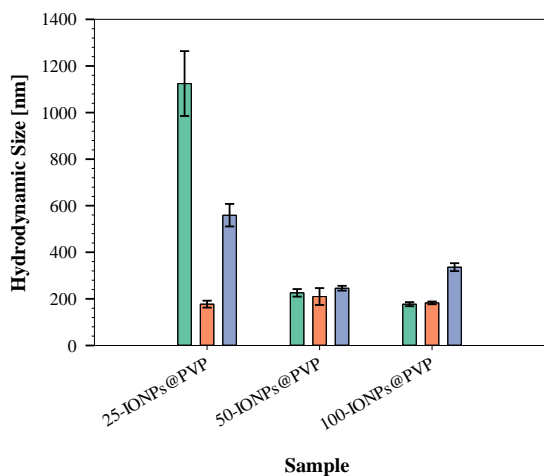
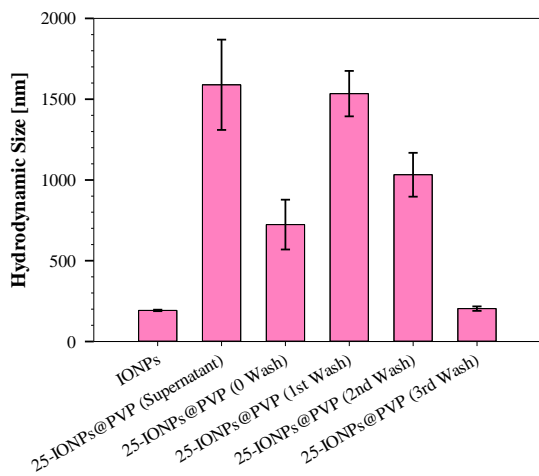


Figure 9. 5: (A) Hydrodynamic size and (B) Zeta potential of *x*-IONPs@PVP for 10 000 g/mol PVP with various concentrations. (C) Hydrodynamic size and (D) zeta potential of 25-IONPs@PVP for 40 000 and 360 000 g/mol PVP with various concentrations. The letter *x* represents the mass of IONPs used for characterization (25, 50, or 100 mg). The error bars indicate the standard deviation from the triplicate measurement of the specific sample.

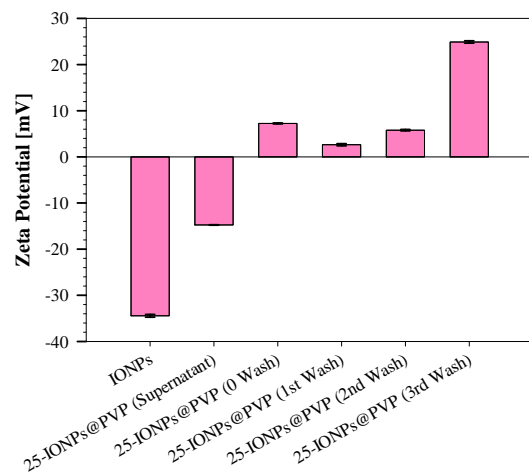
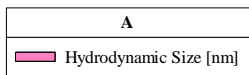
Examination of Various Washing Steps

The effect of various washing steps of 25-IONPs@PVP for 10 000 g/mol and 0.5 g/L PVP on the hydrodynamic size is shown in **Figure 9.6-A**. The sample 25-IONPs@PVP for the 3rd wash was replicated from the experimental design and was also used for the measurement of ZP. The samples with supernatant and 0, 1st, and 2nd washes were also produced to study whether there was an increase or decrease in hydrodynamic size in comparison to 3rd wash. The results indicate that there are no variations in size apart from 0 and 2nd wash. The hydrodynamic size of IONPs and 3rd wash of 25-IONPs@PVP show no difference. This also applies to the hydrodynamic size of the supernatant and the 1st wash of 25-IONPs@PVP, because both samples provide nearly the same results. The findings in overall demonstrate that the hydrodynamic size of IONPs@PVP apart from the 3rd wash is too large. This might be an indication that the particles behave in an aggregative state.

Previously, it was mentioned that the study discussed by Isci *et al.* (58) is not consistent with the DLS results from **Figure 9.4-C** and **D** due to positive surface charge, but **Figure 9.6-B** confirms that the paper discussed by Isci *et al.* in fact is in good agreement with the sample obtained from the supernatant. Since the study performed by Isci *et al.* did not wash the particles, the surface charge is negative due to excess of PVP in the dispersion. Thus, the results of the experiment found clear support for Isci *et al.* The findings on zeta potential after washing, however, at least demonstrate that the surface charge becomes positive due to pH change in the system, which is shown in the respective figure. The negative charge is neutralized, resulting in a positive charge. All washing steps demonstrate poor stability except the 3rd wash of IONPs@PVP. The replication of the 3rd wash shows the highest ZP with a value of 24.90 ± 0.25 mV. But the point where the figure passes through zero ZP is the isoelectric point. This is generally the point where aggregation is most likely to take place, where the colloidal system is least stable.



Sample



Sample

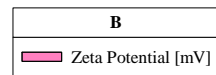


Figure 9. 6: (A) Hydrodynamic size and (B) zeta potential of 25-IONPs@PVP with supernatant and various washing steps for 10 000 g/mol and 0.5 g/L PVP in water dispersion. The sample for non-functionalized IONPs is from the mixed IONPs batch. The error bars indicate the standard deviation from the calculated triplicate measurement of the specific sample.

9.2.2 Structural Identification Analysis

The results characterized by DLS provide a positive surface charge in the presence of PVP. The purpose of this subsection is to determine whether PVP molecules are present in the dispersion or not. The potential selected samples are from the DLS measurement due to smaller hydrodynamic size and higher ZP. These samples are compared to pure PVP and non-functionalized IONPs. The DLS measurements alone are not an indication of whether PVP is coated on the surface or not. Thus, the study of observation of peaks using FT-IR provides information about the existing functional groups of IONPs@PVP.

Examination of Polyvinylpyrrolidone Peaks

The FT-IR spectra of various molecular weights of PVP are shown in **Figure 9.7-A**. For the structural analysis of PVP, a sharp peak at 1659 cm^{-1} attributes to the frequency of carbonyl bond (C=O). This is the sharpest peak that first indicates whether carbonyl bonding appears on the spectrum or not according to literature. This sharp peak is in line with Zare *et al.*, Zulfiqar *et al.*, Heiran *et al.*, Pandey *et al.*, and Arsalani *et al.* (54-57, 66), where the peak provides signal around 1659 cm^{-1} . Another peak to observe is the peak of 1421 cm^{-1} which is attributed to the CH₂ scissoring bending vibration. This peak is consistent with Zulfiqar *et al.* and Arsalani *et al.* with peaks at 1452 and 1460 cm^{-1} , respectively. The peak at 1260 cm^{-1} indicates C-N stretching vibration of N-vinylpyrrolidone. This peak is quite in line with Pandey *et al.* and Arsalani *et al.* with peak of 1289 cm^{-1} . The peak at 2925 cm^{-1} attributes to the asymmetric stretching of the CH₂ chain which is in good agreement with Arsalani *et al.* The comparison between various molecular weights shown in the figure shows the same results. Overall, the FT-IR results validate that there is existence of PVP.

The FT-IR spectra of IONPs@PVP with various mass of IONPs for 10 000 g/mol and 0.5 g/L PVP are shown in **Figure 9.7-B**. The results demonstrate three things. Firstly, the sharp peak at 558 cm^{-1} indicates the presence of Fe-O bond which is in good agreement with non-functionalized IONPs. To confirm the peaks of IONPs synthesized from the co-precipitation method, the sharp peak in this wavelength is attributed to the frequencies of Fe-O binding to IONPs. To compare the FT-IR results from previous studies, the magnetite peak is in line with Zare *et al.*, Zulfiqar *et al.*, Heiran *et al.*, Pandey *et al.*, and Arsalani *et al.* (54-57, 66), where the range of magnetite peak is between 564 and 591 cm^{-1} . It is verified that the Fe-O bond to IONPs and IONPs@PVP produces similar results. Secondly, no peaks are detected at 1659 and 1260 cm^{-1} , which is contrary to the findings of pure PVP and previous studies where IONPs are coated with PVP through carbonyl (C=O) interaction. This demonstrates that this result does not tie well with results obtained for pure PVP because IONPs is not coordinated through the carbonyl group in PVP and that N-vinylpyrrolidone polymer chains are possibly not present. This result highlights that little is known about the PVP peaks of IONPs@PVP with comparison to pure PVP. This suggests that there might be because of depletion effect where free chains of PVP do not interact on the surface of IONPs, but only in the dispersion itself. Lastly, all samples of IONPs@PVP show similar results.

The FT-IR spectra of IONPs@PVP with various mass of IONPs for 40 000 g/mol and 0.1 g/L PVP are shown in **Figure 9.7-C**. Similar to the previous result based on 10 000 g/mol PVP, the sharp peak at 558 cm^{-1} found clear support for the presence of Fe-O bond, and thus it is confirmed that the Fe-O bond to IONPs and IONPs@PVP produces similar results. From the findings, however, there are no signs of PVP peaks in IONPs@PVP. Since no peaks are detected at 1659 and 1260 cm^{-1} for IONPs@PVP, the findings might demonstrate that no PVP molecules are present on the surface of IONPs. The FT-IR spectra of IONPs@PVP with various mass of IONPs for 360 000 g/mol and 0.1 g/L PVP are shown in **Figure 9.7-D**. The results also demonstrate that there is a peak detected at 558 cm^{-1} which is attributed to the Fe-O bond to IONPs. However, no signs of PVP peaks are observed for IONPs@PVP. This also implies that the results might indicate that there are no PVP molecules present on the surface of IONPs since no peaks are detected at 1659 and 1260 cm^{-1} . All samples of IONPs@PVP show similar results for both molecular weights.

From the brief review above, FT-IR alone does not provide a conclusive result based upon whether the polymer material is coated on the surface or not. Other results such as particle size, ZP, and pH must be taken into consideration.

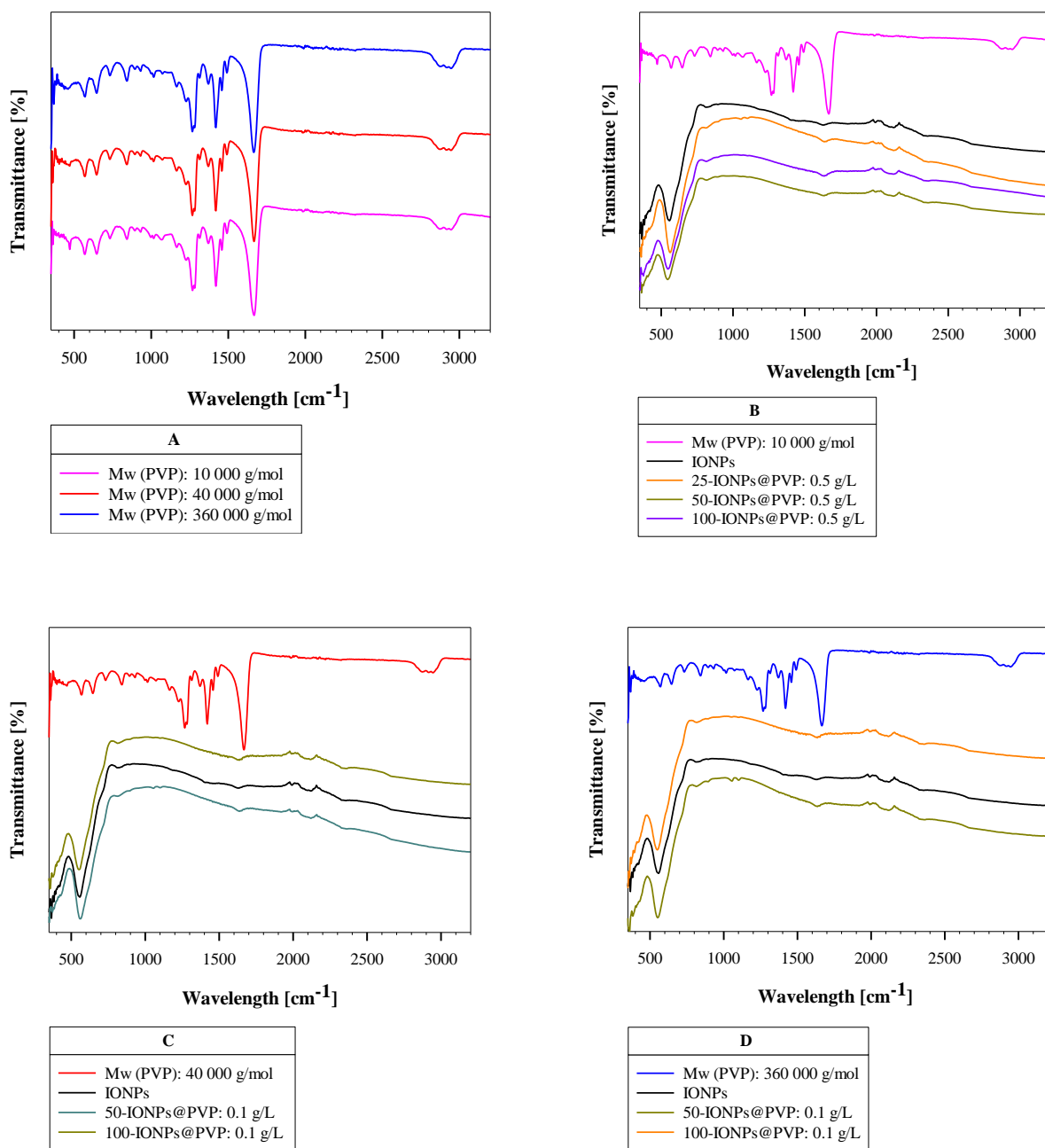


Figure 9. 7: FT-IR spectra of (A) various molecular weights of PVP, (B) *x*-IONPs@PVP for 10 000 g/mol and 0.5 g/L PVP, (C) *x*-IONPs@PVP for 40 000 g/mol and 0.1 g/L PVP, and (D) *x*-IONPs@PVP for 360 000 g/mol and 0.1 g/L PVP. The letter *x* represents the mass of IONPs used for characterization (*x* = 25, 50 or 100 mg). The spectra of pure PVP and non-functionalized IONPs are used to compare with IONPs@PVP.

Examination of Polyvinylpyrrolidone Peaks in Various Washing Steps

The purpose of this subsection is to examine whether PVP peaks are present or not with respect to various washing steps of IONPs@PVP. The selective sample is 25-IONPs@PVP for 10 000 g/mol and 0.5 g/L PVP. This is the replicated sample elucidated from *subsection 9.2.1-Examination of Various Washing Steps*. The samples with supernatant and 0, 1st, and 2nd washes were also used for FT-IR analysis.

The FT-IR spectra of 25-IONPs@PVP with supernatant for 10 000 g/mol and 0.5 g/L PVP is shown in *Figure 9.8-A*. With regards to the ZP of the supernatant given in *Figure 9.6-B*, the results show that the surface charge is negative. With comparison to the FT-IR spectra, the result indicates that there is a peak at 558 cm^{-1} which is attributed to the Fe-O bond to IONPs. There are also signs of PVP peaks observed, implying the presence of PVP molecules since the most important peaks are detected around 1659 and 1260 cm^{-1} . Although the FT-IR spectra reveals the existence of PVP peaks of IONPs@PVP, it remains unclear whether IONPs are coordinated through the carbonyl group or not. It is important to note that the previous results do not show any PVP peaks after washing in *subsection 9.2.2-Examination of Polyvinylpyrrolidone Peaks*. From this standpoint, the surface of IONPs is not coated with the polymer owing to excess of PVP in the supernatant, which means that free PVP chains surround the surface of IONPs without any interactions. Therefore, this can be interpreted as not successfully coated. Also, at this stage of understanding, the signal to the magnetite bond is because of IONPs, whereas the signals to C=O and C-N stretching vibrations are due to free PVP molecules, but not PVP coated IONPs.

The FT-IR spectra of 25-IONPs@PVP with various washing steps in *Figures 9.8 B-E* present no PVP peaks. All spectra provide similar results where the magnetite bond is observed, but no signs of C=O and C-N peaks. This is an indication that PVP molecules are not present after removal of the supernatant. The results show that 0, 1st, 2nd, and 3rd washes do not provide the desired outcome due to the fact that PVP molecules are not present or that PVP molecule chains are potentially not coated on the surface of IONPs. An important question associated with the coating process is whether FT-IR can detect that a molecule has been coated or not. It remains unclear, because the PVP peaks can be observed along with magnetite bonding, but still it does not imply that the polymer is coated using FT-IR. The technique is based on the identification of functional groups within molecules and not just one molecule. Thus, FT-IR does not necessarily confirm whether IONPs are coated with PVP or not.

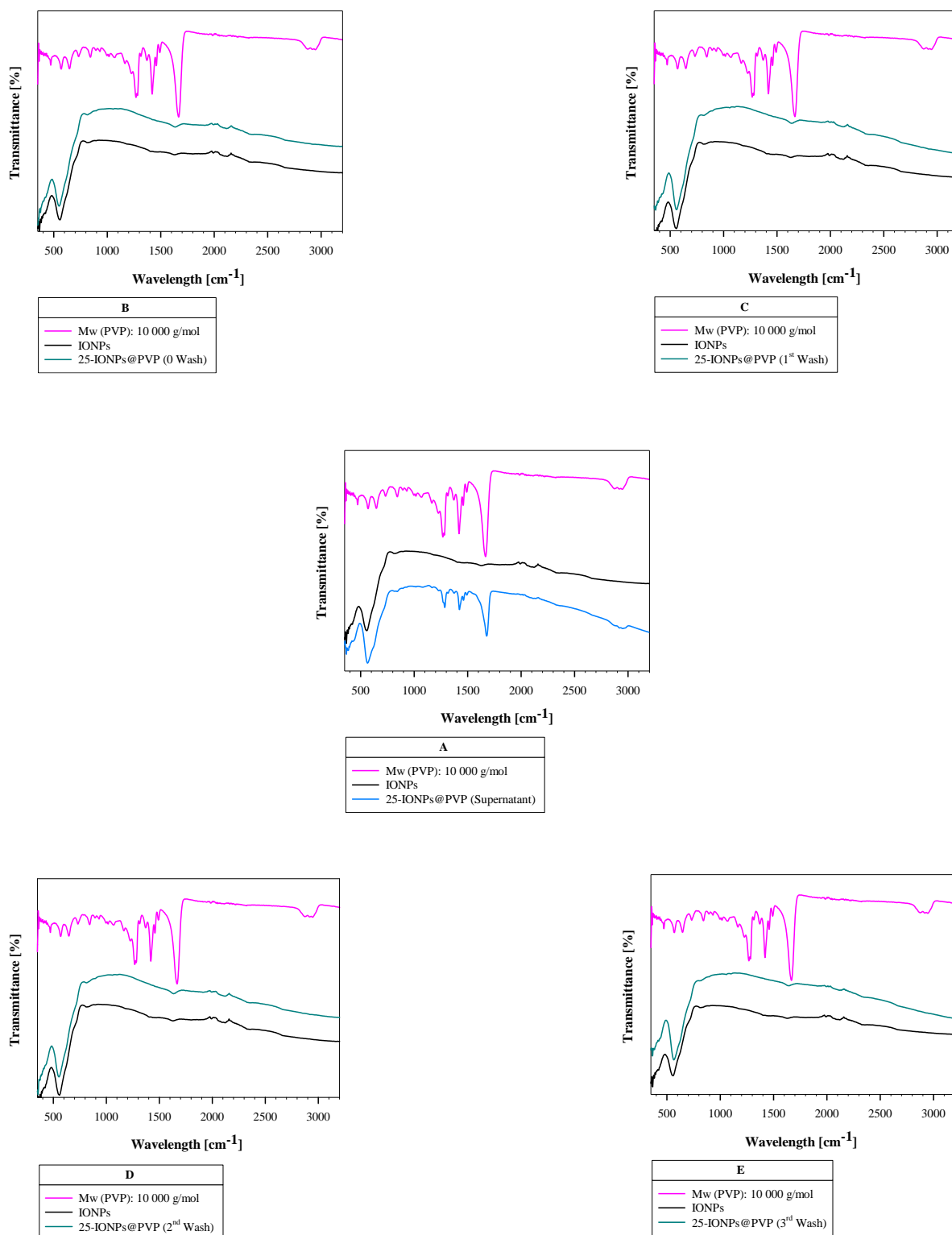


Figure 9. 8: FT-IR spectra of 25-IONPs@PVP for 10 000 g/mol and 0.5 g/L PVP: (A) Supernatant, (B) 0 wash, (C) 1st wash, (D) 2nd wash, and (E) 3rd wash. The FT-IR spectra of pure PVP and non-functionalized IONPs are used to compare with IONPs@PVP.

9.2.3 pH Analysis

According to the results from DLS and FT-IR, the potential samples are studied using pH as a quantity control. The use of pH determines whether the samples are in acidic or basic solution on a logarithmic scale. The scale ranges from 0 to 14, on which 7 is neutral, and values lower than 7 provide an acidic solution, whereas values greater than 7 provide a basic solution. The purpose of this subsection is to examine how IONPs affect the pH in the presence of with and without PVP. The reason for studying pH is to explore why PVP provides a positive surface charge and how to control the stability of the particles.

Study of pH

The selected samples characterized by DLS are used for pH analysis, as shown in **Table 9.4**. The samples were analyzed without pH adjustment by placing the electrode directly into the samples. The pH of non-functionalized IONPs is measured to be 9.2, whereas the samples of IONPs@PVP have a pH in the range between 7.1 and 7.8. The sample 25-IONPs@PVP with supernatant provides a pH value of 8.6, which is higher than IONPs@PVP after washing, but lower than IONPs. The findings show that the addition of PVP to the dispersion decreases the pH, and this might be mainly due to the reaction of IONPs dispersed in water in the presence of PVP. According to the methodology, the *post-situ* functionalization involves overnight shaking between IONPs and PVP molecules in water, and this may lead to the pH approaching neutrality (pH = 7).

It is also speculated that PVP might be acidic according to the study shown by Kurakula *et al.* (49) in **section 5**, where the pH varies from 3 to 7. Adding the polymer to the system might lead to a decrease in pH. As shown in the previous DLS results, the presence of PVP appears to decrease the absolute value of the ZP and leads to positive surface charge. Therefore, it is likely that the low pH causes the surface charge to become positive, while the high pH results in a more negative surface charge. This appears to be true because the absolute value of the ZP for the supernatant shown in **Figure 9.6-B** is lower than non-functionalized IONPs. This is due to IONPs without the presence of PVP being more alkaline with a higher pH value.

A decrease in the absolute value of the ZP may also be due to bridging flocculation, as demonstrated in the study by Isci *et al.* (58). Un-charged PVP molecule chains partially adsorbed on the negative surface charge of the IONPs by steric interactions may decrease the absolute value of the ZP to a certain degree depending on the concentration of the sample. Increasing the concentration of PVP might even result in depletion effect where no PVP molecule chains interact on the surface of the IONPs, and isoelectric point can be reached. A combination of the concentration of the solution and the pH can influence the ZP extensively. Other factors such as the mass of IONPs and the molecular weight of PVP may also influence the final value of the ZP to a certain degree. However, the pH appears to be the main factor in determining the surface charge of the IONPs in the presence of PVP.

When comparing the DLS results from *Figure 9.4-C* and *D*, it must be pointed out that the pH was measured using the main samples from *Table 9.4*, and not the samples diluted by a factor of 1:100 from DLS characterization. The results shown in the table are the pH measurements of PVP coating of IONPs re-dispersed in 3 mL MQ water after washing, which are considered as original samples.

Table 9. 3: pH results based on the original samples.

Sample	Molecular Weight of PVP [g/mol]	Concentration of PVP [g/L]	pH
IONPs	0	0	9.2
100-IONPs@PVP	10 000	0.1	7.7
25-IONPs@PVP	10 000	0.5	7.4
50-IONPs@PVP	10 000	0.5	7.4
100-IONPs@PVP	10 000	0.5	7.8
50-IONPs@PVP	40 000	0.1	7.2
100-IONPs@PVP	40 000	0.1	7.5
50-IONPs@PVP	360 000	0.1	7.1
100-IONPs@PVP	360 000	0.1	7.6
25-IONPs@PVP (Supernatant)	10 000	0.5	8.6

Relationship between Zeta Potential and pH

In aqueous media, the pH of the sample is one of the most essential factors affecting the ZP. It was previously mentioned that the addition of PVP results in a decrease in the pH. If more alkali is added to the system, the particles have the tendency to attain a more negative charge, meanwhile the addition of acids can lead to the charge being neutralized and this can lead to the build-up of positive charge. In order to confirm the speculations, the classification of dispersion is possible to evaluate from *Figure 9.9*. The plot shows zeta potential as a function of pH where 7 points are added to the plot for each sample. These samples are IONPs and IONPs@PVP. The error bars represent the standard deviation of three zeta potential measurements for each sample. The IONPs sample is from the mixed batch, while the selective sample for IONPs@PVP is from the sample 100-IONPs@PVP with 10 000 g/mol and 0.1 g/L PVP.

When ZP is greater than +30 mV or smaller than -30 mV, the dispersion is considered stable. In a such region can be identified when the pH is low or when the pH is high, as illustrated in the figure. For IONPs, the isoelectric point appears to be approximately at pH 5.8, whereas IONPs@PVP appear to have an isoelectric point of approximately pH 7.7. The results demonstrate that the IONPs should be stable at pH less than 4 and greater than 9, while the IONPs@PVP should also be stable at pH less than 4 but greater than 10. The findings show that at low pH adequate positive surface charge is present, meanwhile at high pH adequate negative surface charge is present. The main problem with colloidal stability is when the pH of IONPs and IONPs@PVP is between 4 and 9, and 4 and 10, respectively, as the ZP values are between -30 and +30 mV. In these regions, the particles tend to aggregate, and the system becomes less stable. Thus, controlling the pH shows to be very important. These findings support that the addition of acids cause low pH, while the addition of bases cause high pH. It is by now generally confirmed that the positive surface charge of IONPs in the presence of PVP is due to a decrease in pH.

The relationship between the ZP and the pH seems to cast a new light on whether PVP is coated on the surface of IONPs or not. As shown in *Figure 9.9*, the ZP values of IONPs at pH 3.4 and 5.8 are determined to be 35.57 ± 0.14 and 8.84 ± 0.30 mV, respectively. The ZP values of IONPs@PVP at pH 3.4 and 5.8 appear to be nearly the same with 36.80 ± 0.19 and 9.34 ± 0.06 mV, respectively. However, at pH 4.1 seems to provide different ZP values where IONPs and IONPs@PVP are measured to be 33.00 ± 0.23 mV and 25.85 ± 0.30 mV, respectively. As the ZP reaches the negative charge region, the values between IONPs and IONPs@PVP do not match with each other. It is important to note that the pH of both samples in the negative region was not selected at the same points because the pH level of IONPs@PVP was very sensitive to pH change when the base was added dropwise, so the pH level increased significantly. However, the negative region provides a useful information about the differences in the ZP. The ZP values at pH 8.3 for IONPs and 8.8 for IONPs@PVP are measured to be -24.87 ± 0.21 and -14.50 ± 0.73 mV, respectively. The results show that IONPs are more stable at this pH level because this is an indication that the particles tend to be more stable at pH 8-9 without the presence of PVP.

As the results demonstrate, there is clearly a slight difference between the samples. The 1st reason suggests that PVP is partially adsorbed on the surface of IONPs due to bridging flocculation. The 2nd reason might be because PVP molecule chains are weakly adsorbed on the surface of IONPs due to inefficient coating on the surface of IONPs. The 3rd reason might be because of depletion stabilization where PVP molecules are in the dispersion but do not interact on the surface of IONPs. This might be an indication that all of these reasons can change the pH system, which results in a positive surface charge, and likely to result in a slight difference in isoelectric point between non-functionalized IONPs and IONPs@PVP. Although the findings are consistent with the DLS results, it appears that the findings are not consistent with the structural identifications because no PVP peaks are observed for IONPs@PVP. Alternatively, it could mean that the third reason is in line with the FT-IR results because no PVP peaks are detected due to depletion stabilization, but the presence of PVP in the dispersion without interaction on the surface of IONPs can change the pH system. However, the FT-IR results are not decisive in the coating process. Therefore, the conclusion is that the change from negative to positive surface charge and the small change in isoelectric point are mainly due to partial or weak adsorption of PVP, or insignificant owing to depletion stabilization. The study of pH appears to be the key to understanding the coating process.

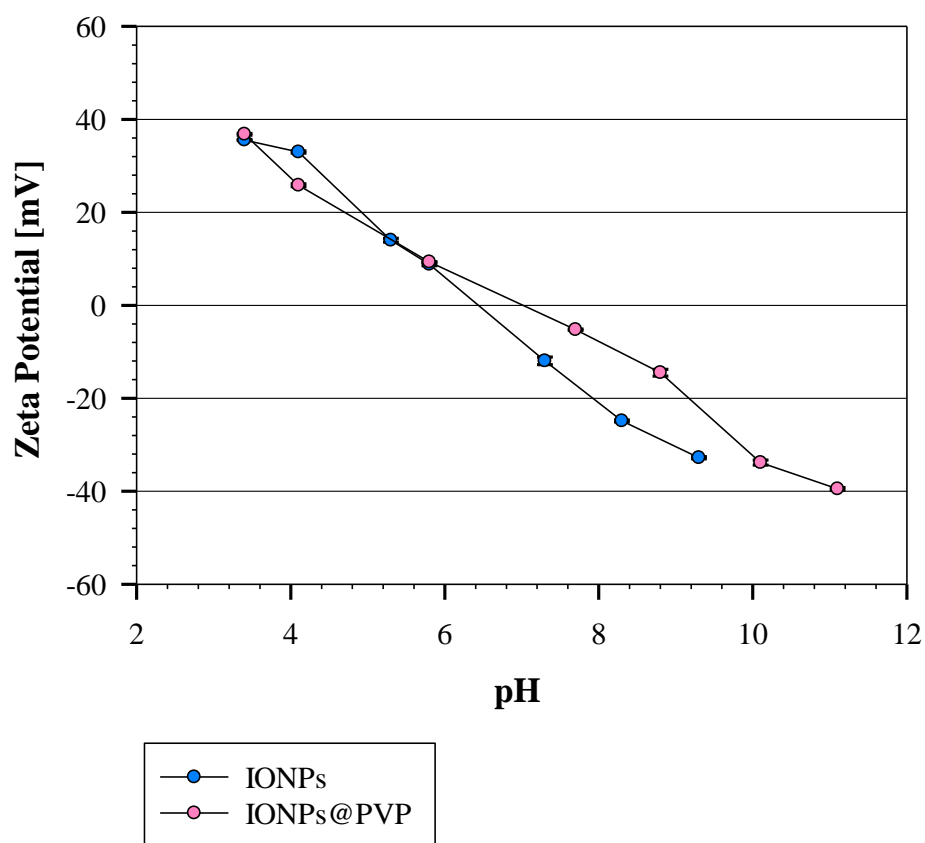


Figure 9. 9: Zeta potential as a function of pH for IONPs and IONPs@PVP. The sample for non-functionalized IONPs is from the mixed IONPs batch, whereas the sample for PVP coating of IONPs is from the sample 100-IONPs@PVP for 10 000 and 0.1 g/L PVP. The error bars represent the standard deviation from the calculated triplicate measurements of the specific sample.

Dilution

The impact on volume can also change the pH if more water is added. If the samples are in acidic or basic solution, the concentration of that decreases as the volume of solution increases, and this may result in the pH approaching neutrality. Since IONPs are in basic solution, dilution may reduce the pH. The addition of water has the tendency to reduce the concentration of ions in the dispersion. When alkali is diluted with water the concentration of OH⁻ decreases, resulting the pH to decrease.

It is important to note that the comparison with the DLS results from **Figure 9.4-C**, the ZP of 100-IONPs@PVP for 10 000 and 0.1 g/L PVP appears to have a value of 19.90 ± 0.11 mV, while the ZP shown in **Figure 9.9** appears to have a value of -5.21 ± 0.14 mV. These values are from the same sample, but with different dilutions. Using the dilution with a factor of 1:20 appears to reach close to the isoelectric point at pH 7.7 but using a factor of 1:100 also provides nearly the same results with a pH value of 7.9, but with a more stable ZP, as shown in **Table 9.5**. The results indicate that the pH remains the same when more water is added to the sample, but the ZP appears to be different at various dilutions. After the measurement of ZP for 1:20, the particles settle down, whereas for 1:100 the particles do not settle down. It appears that the ZP is also affected by the concentration because the particles have the tendency to get close to each other due to the attractive force when increasing the concentration. However, the concentration does not appear to affect the pH, and this might be due to the sample becoming nearly like pure water.

Table 9. 4: pH results on 100-IONPs@PVP for 10 000 g/mol and 0.1 g/L PVP based on original sample in comparison to various dilutions. The ZP value for the dilution at 1:20 is from **Figure 9.4-C**, while the ZP value for the dilution at 1:100 is from **Figure 9.9**. No ZP is measured for the original sample.

Sample	Molecular Weight of PVP [g/mol]	Concentration of PVP [g/L]	Dilution [mL]	pH	Zeta Potential [mV]
100-IONPs@PVP	10 000	0.1	Original Sample	7.7	None
100-IONPs@PVP	10 000	0.1	1:20	7.7	-5.21 ± 0.14
100-IONPs@PVP	10 000	0.1	1:100	7.9	19.90 ± 0.11

9.3 Silica Coating of Iron Oxide Nanoparticles with Polyvinylpyrrolidone

The coating process of IONPs@PVP appears not to provide desirable properties associated with particle size and stability because IONPs without the presence of PVP demonstrate to have a better colloidal stability. In this subsection, the purpose is to understand how PVP affects the silanization process by studying the particle size, particle size distribution, and morphology. The intention is to analyze if there are any differences in size, size distribution and morphology in the presence of with and without PVP. From previous subsection, the findings demonstrate that PVP is either partially or weakly adsorbed on the surface of IONPs, or negligibly not coated. Therefore, it is also interesting to examine whether PVP is coated on the surface of IONPs or not after silanization. According to the experimental design shown in **Table 8.4**, the inner parameters of IONPs@PVP were selected because of small H_d and high ZP compared to the other samples from **Figure 9.4**. The selected inner parameters of IONPs@SiO₂ were selected because of the work performed by Ali and Nissen-Sollie (62, 63), in which the catalyst NH₄OH, the precursor TEOS, and the solvent IPA were used as reaction parameters. The amounts of the corresponding catalyst, precursor and solvent were determined to be 6, 2, and 20 mL.

9.3.1 Morphology Analysis

The obtained SEM images show the findings in terms of the morphology of IONPs@SiO₂ in the presence of with and without PVP. All SEM images include scale bars to annotate image size. Scale bars provide important information about the size of the materials, in which orients readers to bridge the gap between the image and reality. Scale bars were added to all images using the ImageJ software program.

Figure 9.10-A shows the SEM image of 25- IONPs@SiO₂ in the presence without PVP. With the lowest amount of IONPs, the particles do not aggregate to a large extent. In some areas of the SEM sample, the size or number of aggregates can be found, but mostly spherical shapes are observed. The presence of silica as an outer layer appears to shield the repulsive electrostatic interaction, where it involves good dispersion, high chemical stability, and simple surface modification. **Figure 9.10-B** shows the SEM image of 25-IONPs@SiO₂ in the presence of PVP for 10 000 g/mol and 0.5 g/L PVP. The image shows that mostly spherical particles are found, and few agglomerates are observed. **Figure 9.10-C** also shows a similar result for the highest molecular weight with 360 000 g/mol and 0.1 g/L PVP, in which mostly spherical shapes are found, whereas few agglomerates are detected.

The overall results from the figure show that there is nearly no difference between silica coating of IONPs in the presence of with and without PVP with the lowest mass of IONPs and different molecular weights of PVP in terms of spherical shapes. The addition of PVP does not produce shapes such as cubes, rods, or hexagons. Other undesirable morphologies such as irregular shapes and incompletely fused particles can be observed to a very small extent, but these are considered negligible or insignificant.

In terms of agglomerations or aggregates, most of the aggregates produced are only observed in a few areas of the SEM samples. From the previous subsection related to the PVP coating of IONPs, all samples provide positive surface charge with low stability compared to non-functionalized IONPs. Thus, it is speculated that the presence of PVP might result in more aggregates in the system for silica coated IONPs. *Figure 9.11* shows the SEM images of the corresponding SEM images shown in *Figure 9.10*, but in the form of aggregates. The purpose is to analyze the size of the aggregates for each sample. *Figure 9.11-B-1* and *B-2* show aggregates of 25-IONPs@PVP@SiO₂ for 10 000 g/mol and 0.5 g/L PVP, in which the aggregate size seems to be small. The aggregation size is also small for 25-IONPs@SiO₂ without PVP, which are not included in the figure. It appears that both samples provide less aggregates, but it is a challenge to analyze whether the presence of PVP provides nearly the same results as the one without PVP when using SEM. Because of this potential limitation, both samples are treated as somehow similar in terms of aggregation size. However, when comparing with 25-IONPs@PVP@SiO₂ for 360 000 g/mol and 0.1 g/L PVP, the aggregate size increases slightly, as shown in *Figure 9.11-C-1*. It appears that higher molecular weight of PVP increases more aggregates to some extent compared to the lower molecular weight of PVP.

As in overall results, few aggregates are observed for the lowest mass of IONPs even though the highest molecular weight appears to produce slightly more aggregates. The silica coating appears to strengthen the electrostatic repulsion that helps keeping the particles apart and provide colloidal stability. The presence of PVP, however, does not impact the final morphology to a large extent, and it is nearly negligible.

Spherical shapes can also be observed when the mass of IONPs increases. **Figure 9.12-A** shows the SEM image of 50-IONPs@SiO₂ in the presence without PVP. A closer observation confirms the spherical shapes of the silica coated IONPs. **Figure 9.12-B** also confirms spherical particles for 50-IONPs@PVP@SiO₂ with 10 000 g/mol and 0.5 g/L PVP. As revealed by SEM, the particles seem to be separated from each other due to the repulsive interaction. The spherical particles can also be observed for 50-IONPs@PVP@SiO₂ with 360 000 g/mol and 0.1 g/L PVP, as shown in **Figure 9.12-C**. The Stöber process highlighted in **section 6** involves the mixture of catalyst, solvent, and precursor to produce silica coated IONPs, where the addition of silica precursor protects the particles from getting closer to each other. The spherical shapes, however, seem to be the same for all samples when 50 mg of the IONPs are used for the *post-situ* surface modification. It is also worth remarking that SEM is a quantitative technique for analyzing the number of particles presented in the sample, which makes it possible to count the particles and analyze the variations in the sizes.

However, the drawback of adding more particles to the dispersion may result in an increase in aggregation size even though most of the particles demonstrate to have spherical shapes in SEM. **Figure 9.13-A-1** shows the SEM image of 50-IONPs@SiO₂ in the presence without PVP, in which the size of the aggregates increases to a large extent compared to 25 mg of the IONPs. Most likely, this reflects the formation of clusters of aggregates due to higher concentrations, although the inner parameters such as catalyst, precursor and solvent of the silica coated IONPs are under the same reaction condition. This can be explained considering that the stabilization is limited to a certain degree. Thus, the size of the aggregates remains high, which appears to indicate that these aggregates do not provide desirable properties for the applications in diagnostics. On the other hand, **Figure 9.13-B-1** shows the SEM image of 50-IONPs@PVP@SiO₂ for 10 000 g/mol and 0.5 g/L PVP, in which the stabilization is also limited to some extent due to increased aggregation size. This is an indication that the addition of PVP might result in poor colloidal stability. This also applies to 50-IONPs@PVP@SiO₂ for 360 000 g/mol and 0.1 g/L PVP, which is shown in **Figure 9.13-C-1**. During the analysis, the aggregation sizes in **Figure 9.13** do not show significant differences between the samples. Thus, it is speculated that the presence of PVP does not considerably affect the silanization process in terms of aggregation size. However, the study of morphology is not enough to conclude whether the polymer is coated on the surface of IONPs or not.

As the mass of the IONPs increases to 100 mg, more aggregates are observed than spherical particles, as shown in **Figure 9.14**. This is likely due to the concentration of the sample. Therefore, the silica coated IONPs are considered as an aggregation state, and this results in poor stabilization of the particles. **Figure 9.14-A** shows the SEM image of 100-IONPs@SiO₂ in the presence without PVP. Very few spherical particles can be observed because the aggregate size increases extensively. **Figure 9.14-B** shows the SEM image of 100-IONPs@PVP@SiO₂ for 10 000 g/mol and 0.5 g/L PVP. The results also demonstrate that the aggregation size increases. **Figure 9.14-C** shows the SEM image of 100-IONPs@PVP@SiO₂ for 360 000 g/mol and 0.1 g/L PVP. Increasing the molecular weight of PVP does not appear to decrease the aggregation size. This is an indication that all these samples from this particular figure demonstrate poor colloidal stability. In comparison to the DLS characterization shown in **Figure 9.4-C**, the ZP value of 100-IONPs@PVP for 360 000 g/mol and 0.1 g/L PVP is lower than 25 and 50 mg of the IONPs, and this might be an indication that the SEM image shows more aggregates. In **Figure 9.4-D**, the ZP value of 100-IONPs@PVP for 10 000 g/mol and 0.5 g/L PVP is also lower than 25 and 50 mg of the IONPs, resulting in more aggregates.

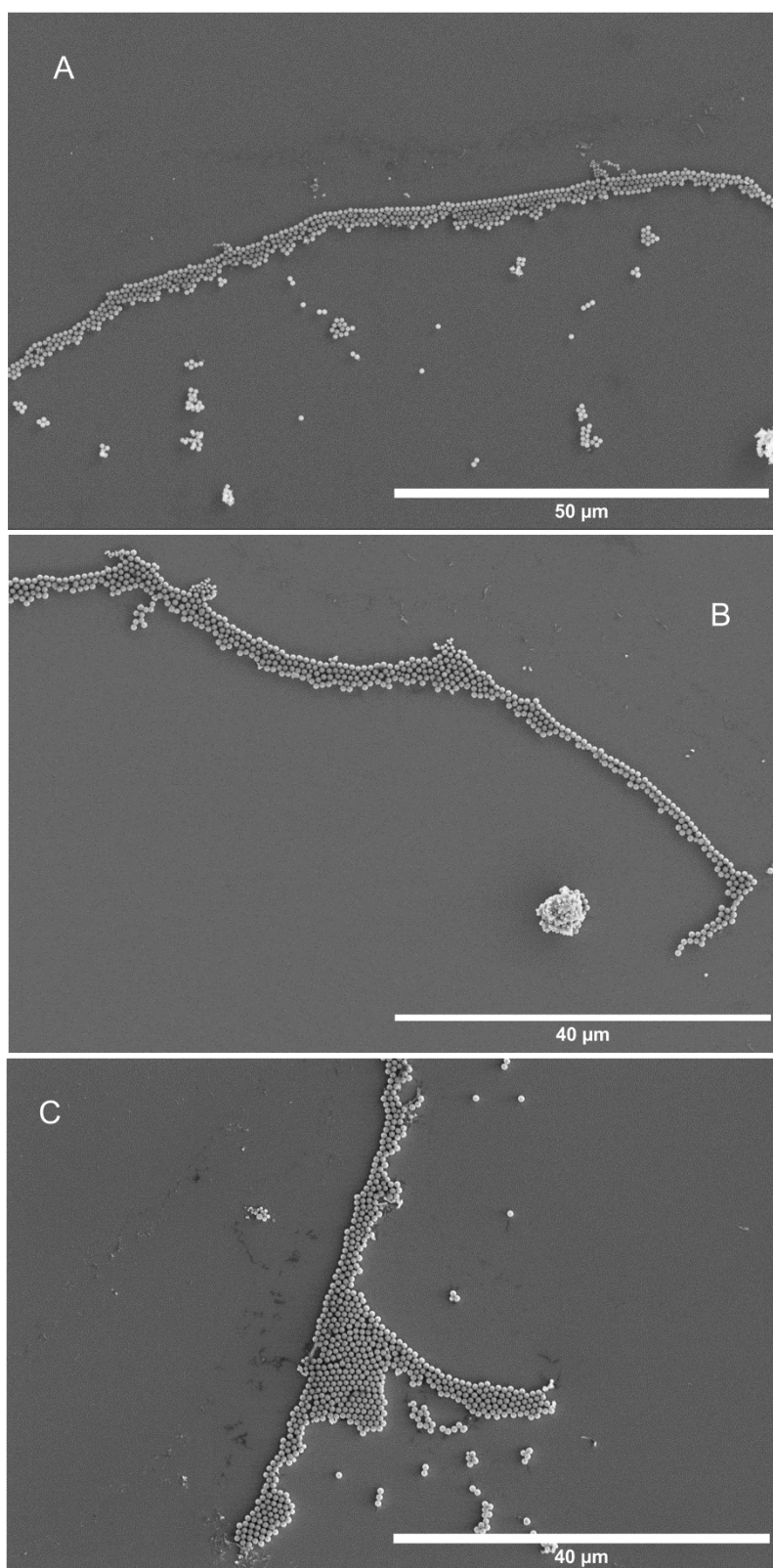


Figure 9. 10: SEM images of (A) 25-IONPs@SiO₂, (B) 25-IONPs@PVP@SiO₂ for 10 000 g/mol and 0.5 g/L PVP, and (C) 25-IONPs@PVP@SiO₂ for 360 000 g/mol and 0.1 g/L PVP.

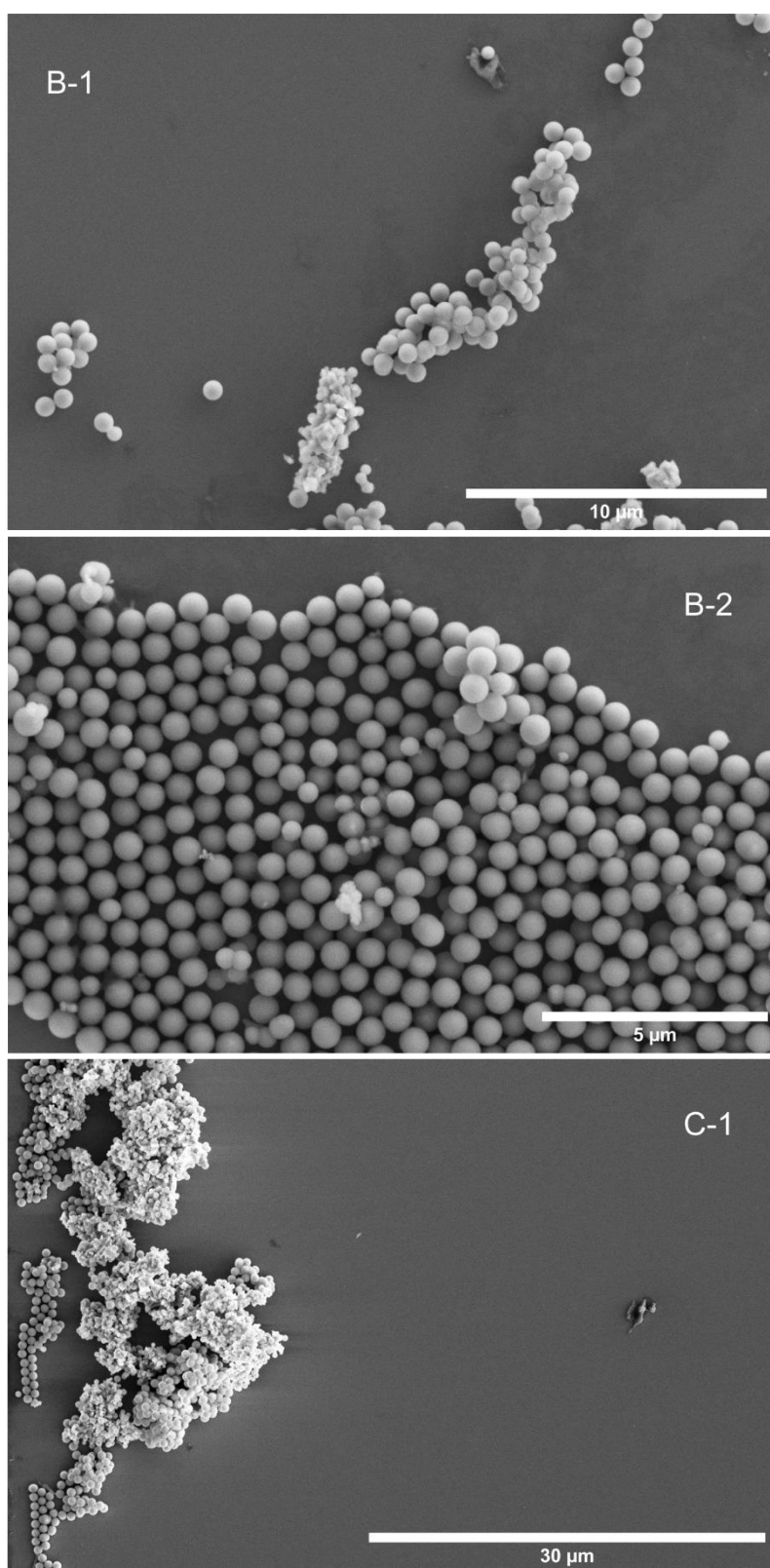


Figure 9. 11: SEM images of (B-1, B-2) 25-IONPs@PVP@SiO₂ for 10 000 g/mol and 0.5 g/L PVP, and (C-1) 25-IONPs@PVP@SiO₂ for 360 000 g/mol and 0.1 g/L PVP in terms of aggregation.

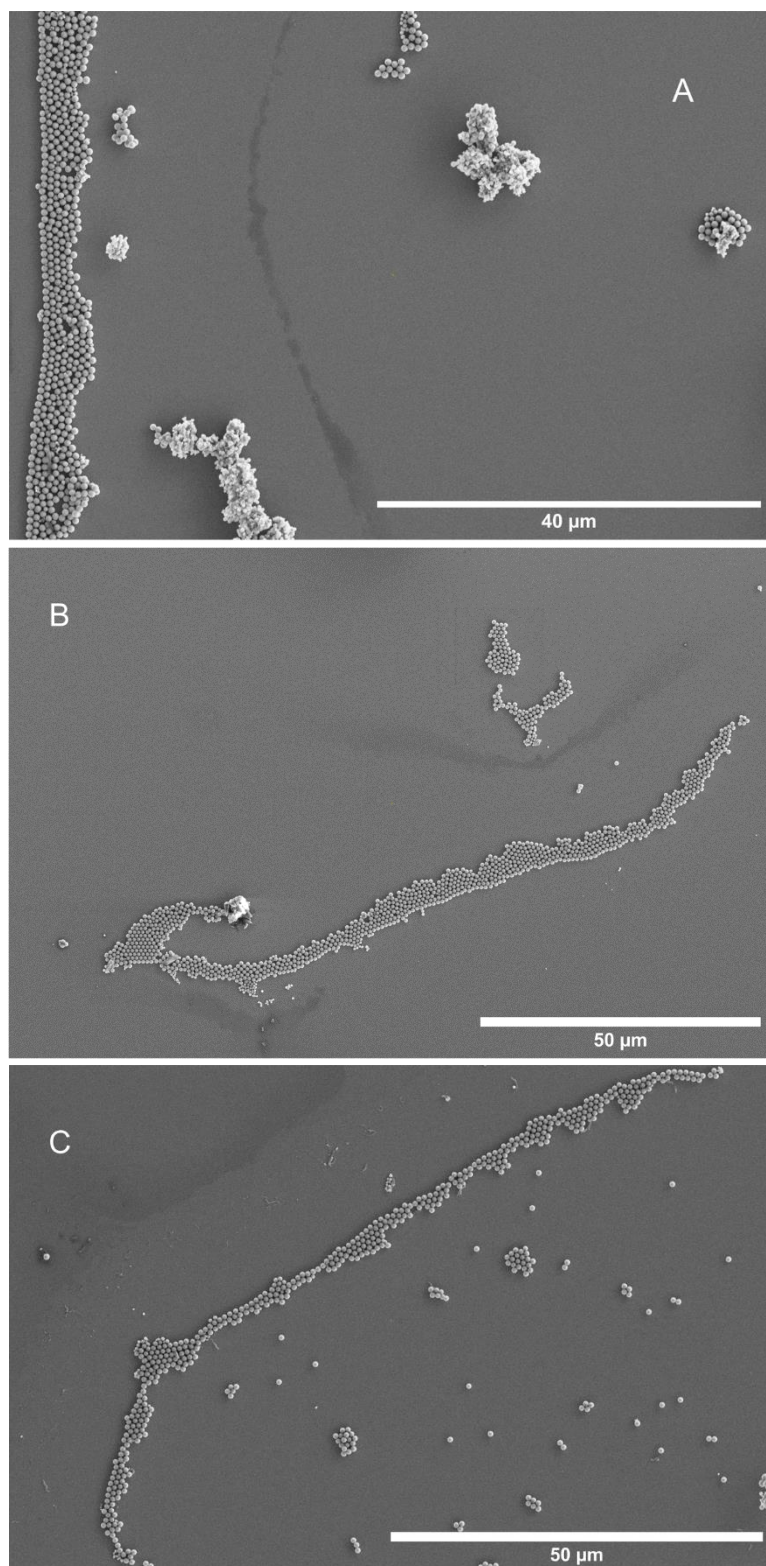


Figure 9. 12: SEM images of (A) 50-IONPs@SiO₂, (B) 50-IONPs@PVP@SiO₂ for 10 000 g/mol and 0.5 g/L PVP, and (C) 50-IONPs@PVP@SiO₂ for 360 000 g/mol and 0.1 g/L PVP.

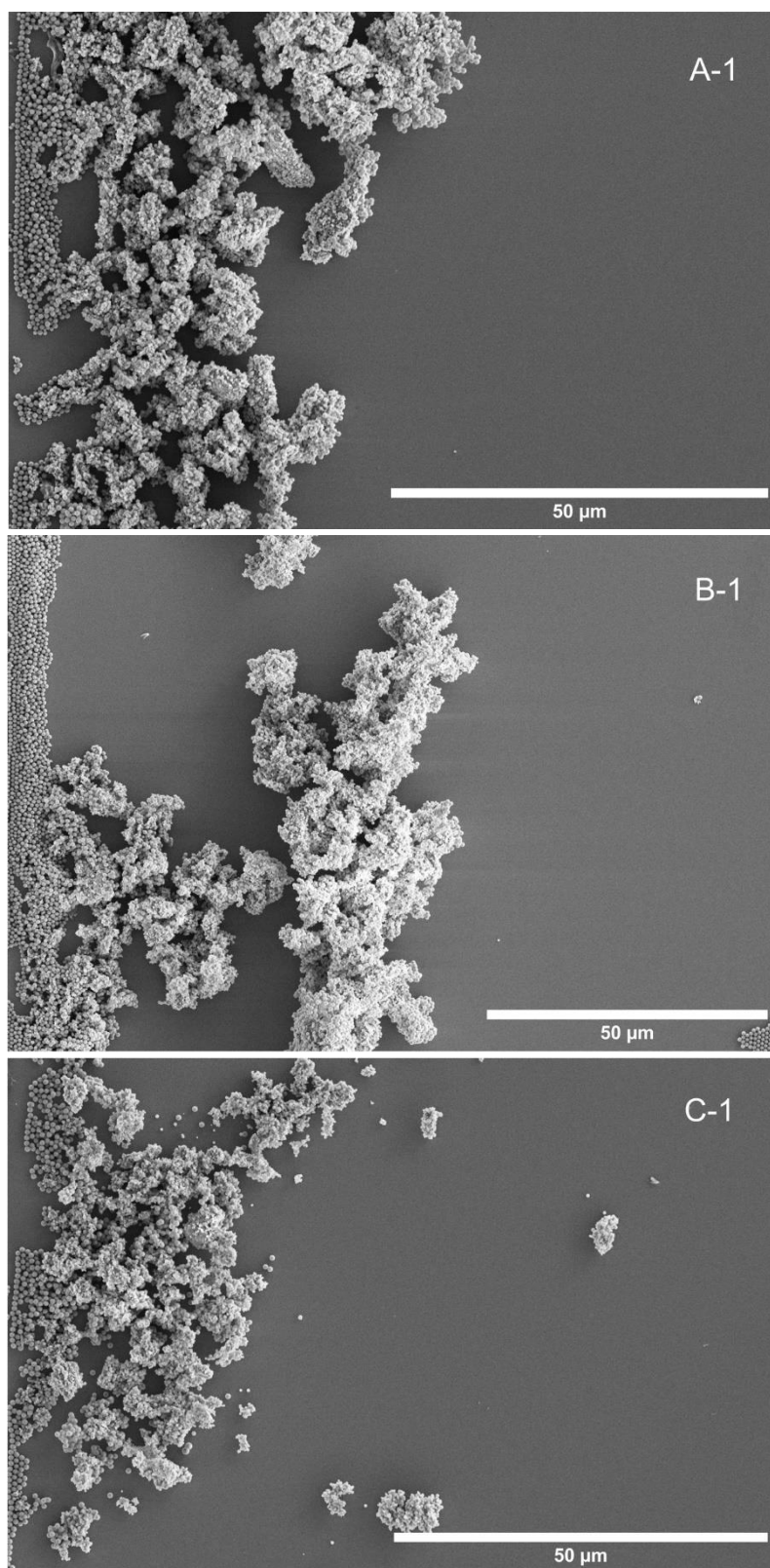


Figure 9. 13: SEM images of (A-1) 50-IONPs@SiO₂, (B-1) 50-IONPs@PVP@SiO₂ for 10 000 g/mol and 0.5 g/L PVP, and (C-1) 50-IONPs@PVP@SiO₂ for 360 000 g/mol and 0.1 g/L PVP in terms of aggregation.

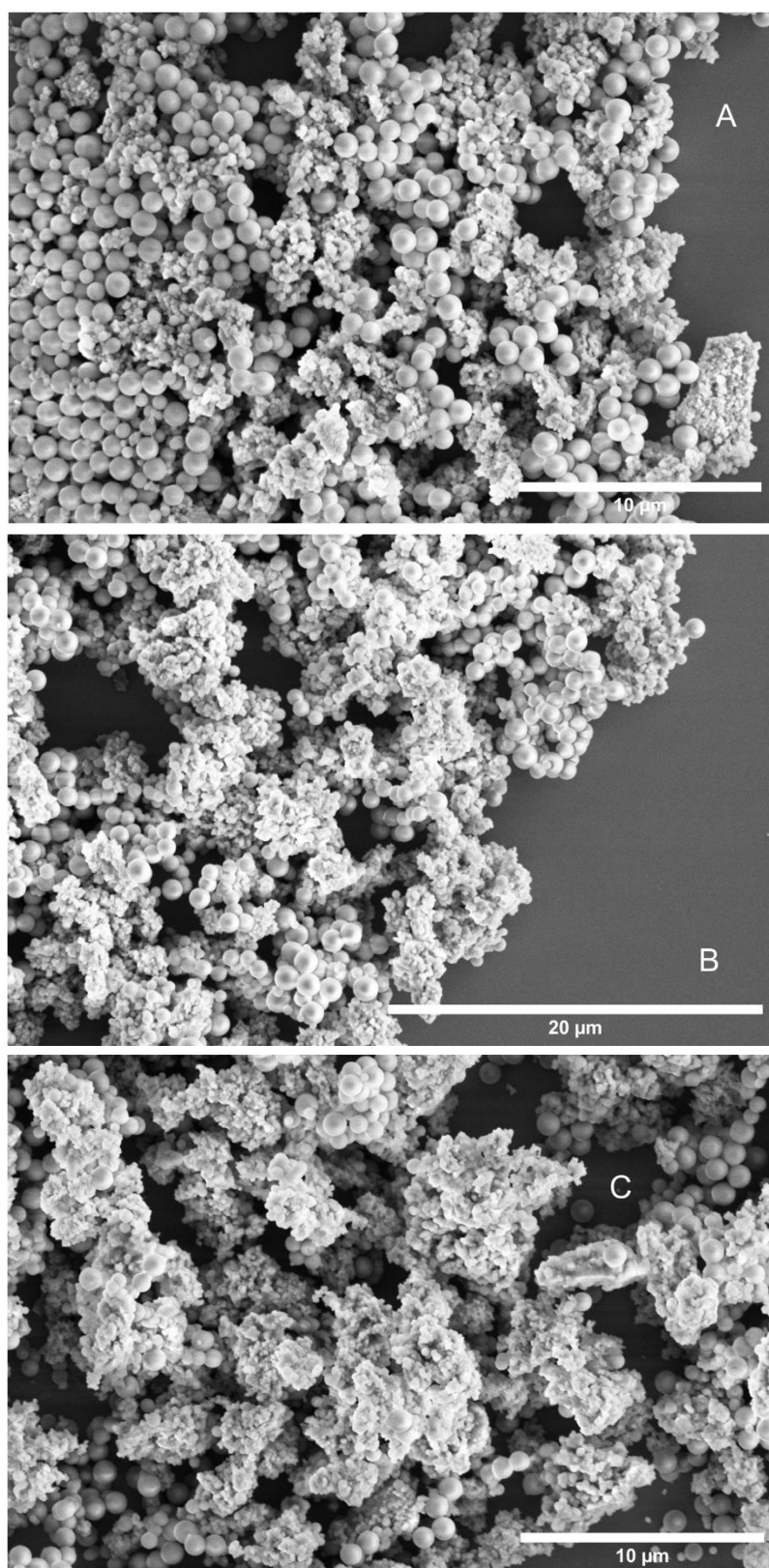


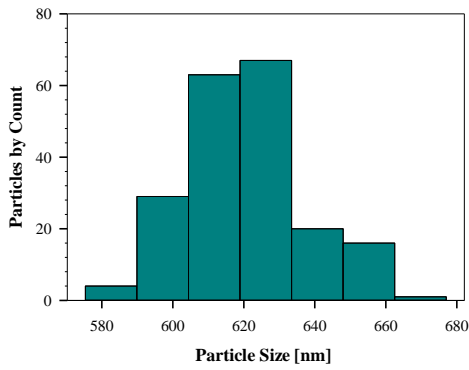
Figure 9. 14: SEM images of (A) 100-IONPs@SiO₂, (B) 100-IONPs@PVP@SiO₂ for 10 000 g/mol and 0.5 g/L PVP, and (C) 100-IONPs@PVP@SiO₂ for 360 000 g/mol and 0.1 g/L PVP.

9.3.2 Particle Size Distribution Analysis

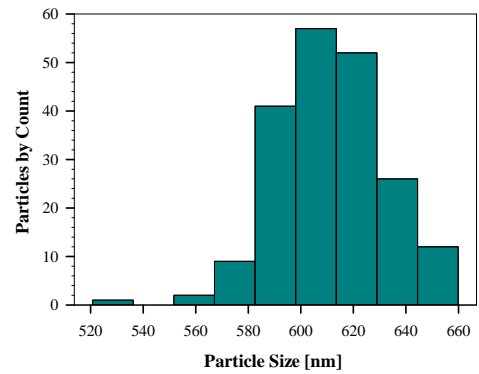
One of the most important outer parameters apart from the morphology is the examination of the particle size distribution. The masses of the IONPs such as 25 and 50 mg show spherical shapes and thus 200 particles are counted to measure the size distribution using the ImageJ software program. **Figure 9.15-A** shows the particle size distribution of 25-IONPs@SiO₂ without the presence of PVP. The particle size range is approximately between 575 and 675 nm. The findings show that the size distribution is to a certain extent narrow. This is an indication that the presence of silica has the capability to enhance the repulsive interaction between the particles, resulting in less aggregates and small polydispersity of the particles. However, when comparing the particle size distribution with 25-IONPs@PVP@SiO₂ for 10 000 g/mol and 0.5 g/L PVP shown in **Figure 9.15-B**, the size range is approximately between 525 and 660 nm. The addition of PVP provides to a small extent a broader size distribution than without PVP. With a higher molecular weight such as 360 000 g/mol, the size range is found to be approximately between 552 and 647 nm, as shown in **Figure 9.15-C**. The size distribution shows to be narrower than the silica coating of IONPs without PVP and with PVP from the lowest molecular weight. This might be an indication that the effect of molecular weight on particle size distribution provides a slight difference.

The particle size distribution of 50-IONPs@SiO₂ without the presence of PVP has a size range between 598 and 726 nm, which is shown in **Figure 9.15-D**. The size distribution is to some extent narrow, but the size appears to be higher than 25 mg of the IONPs to a certain extent. In the presence of PVP, the lowest molecular weight has a size range between 630 and 720 nm, which is shown in **Figure 9.15-E**. It appears that the presence of PVP appears to provide smaller distribution than without PVP. However, in comparison to the highest molecular weight of PVP, the size range is found to be approximately between 627 and 744 nm, as shown in **Figure 9.15-F**. The size distribution appears to be slightly higher than the lowest molecular weight of PVP.

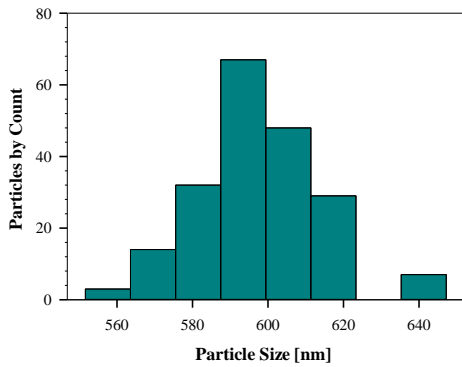
The overall findings from **Figure 9.15** demonstrate that the presence of PVP does not impact the final particle size distribution to a large extent, and this might be due to the fact that the presence of PVP does not affect the silanization process or that the polymer is not successfully coated on the surface of IONPs. Thus, the differences in morphology, particle size distribution, and average diameter were found to be somehow similar.



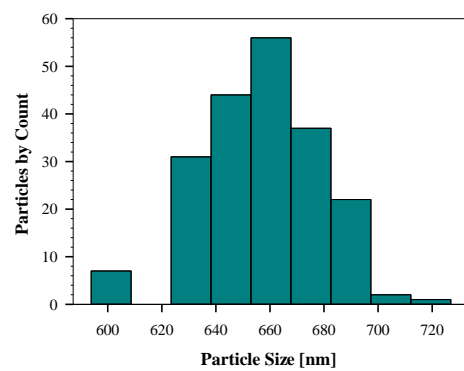
A
25-IONPs@SiO₂



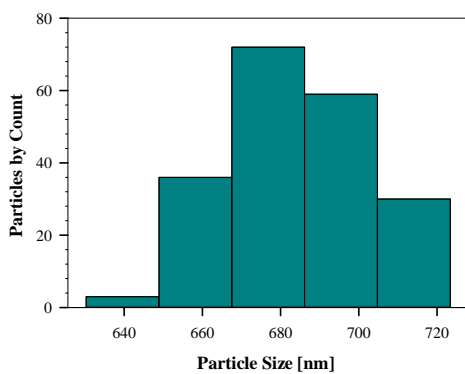
B
25-IONPs@PVP@SiO₂ for 10 000 g/mol PVP



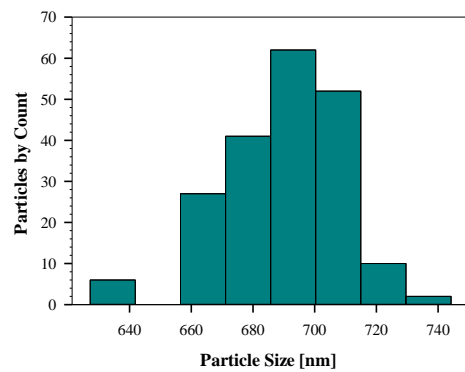
C
25-IONPs@PVP@SiO₂ for 360 000 g/mol PVP



D
50-IONPs@SiO₂



E
50-IONPs@PVP@SiO₂ for 10 000 g/mol PVP



F
50-IONPs@PVP@SiO₂ for 360 000 g/mol PVP

Figure 9. 15: Particle size distribution of 25-IONPs@SiO₂ (A) without PVP, (B) 10 000 g/mol and 0.5 g/L PVP, and (C) 360 000 g/mol and 0.1 g/L PVP. Particle size distribution of 50-IONPs@SiO₂ (D) without PVP, (E) 10 000 g/mol and 0.5 g/L PVP, and (F) 360 000 g/mol and 0.1 g/L PVP. Particle size distribution characterized by SEM and particles counted using the ImageJ software program.

9.3.3 Particle Size Analysis

In order to examine the differences in size between the samples, **Figure 9.16** shows the particle size (average diameter) of each sample characterized by SEM, in which the error bars indicate a measure of the polydispersity of the particle size distribution. The average diameter is measured by taking the average of 200 particles. The results clearly show that there are nearly no differences between 25-IONPs@SiO₂ in the presence of without PVP and 25-IONPs@PVP@SiO₂ for 10 000 g/mol and 0.5 g/L PVP, because the average diameters appear to be 619.20 ± 19.60 and 614.70 ± 22.10 nm, respectively. However, the sample 25-IONPs@PVP@SiO₂ for 360 000 g/mol and 0.1 g/L PVP appears to provide an average diameter of 599.00 ± 17.40 nm. Although the highest molecular weight shows a slight decrease in size, the overall findings demonstrate that there are no significant differences between the samples when 25 mg of the IONPs are used.

Increasing the mass of the IONPs to 50 mg also shows no significant differences between the samples for the corresponding 10 000 and 360 000 g/mol PVP with 685.50 ± 21.60 and 689.50 ± 21.53 nm. Without the presence of PVP, however, the average diameter is found to be 655.40 ± 23.80 nm. There is a slight difference when PVP is used, but as an overall result, 50 mg of IONPs also show no significant differences. The highest mass of IONPs, which is 100 mg, is excluded due to the fact that the SEM images mostly show aggregates, and there are not enough particles to count.

The findings are somehow in good agreement with the SEM images and particle size distribution from **subsection 9.3.1** and **9.3.2**, respectively, because the lowest mass of IONPs turns out to be lower in size compared to 50 mg. This is an indication that higher mass of IONPs results in more aggregates, and this leads to an increase in size. Increased in size might be due to the polydispersity of the particle size distribution. The results also show that PVP does not significantly affect the final average diameter, and this is line with the SEM images and particle size distributions because the morphology and size distribution do not appear to be significantly affected by the presence of PVP. Therefore, there is a possibility that the presence of PVP has no effect on the silanization process or the coating process of IONPs@PVP is not efficient owing to the bridging flocculation or weak adsorption on the surface of IONPs. Another reason might be due to the fact that PVP is not coated on the surface of IONPs due to depletion effect and thereby it is recommended that the methodology should be changed.

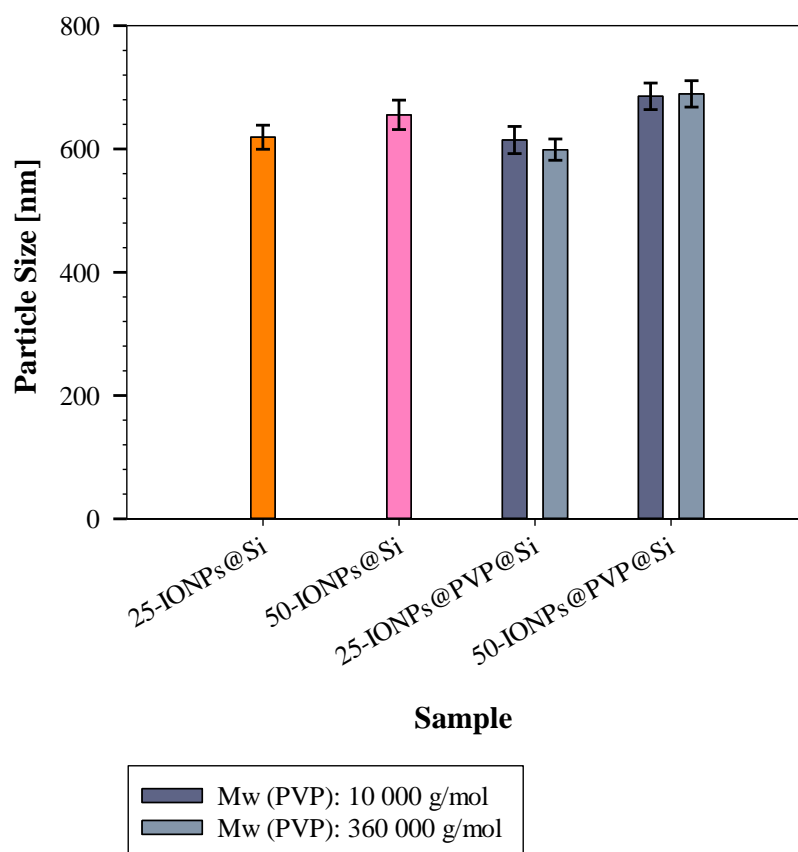


Figure 9. 16: Particle Size (average diameter) of IONPs@SiO₂ in the presence of with and without PVP characterized by SEM, where the error bars represent a measure of the polydispersity of the particle size distribution. The letter x represents the mass of IONPs used for the characterization (x = 25, 50, or 100 mg). The abbreviation of SiO₂ stands for Si.

10 Conclusion

The aim of the work was to control the particle size involving the interplay between mass, molecular weight, concentration, pH, and zeta potential to achieve monodispersed IONPs and reduce their aggregation with the use of PVP as a coating agent followed by silanization. It was hypothesized that the presence of PVP increases stability, reduces aggregation, and provides narrow size distribution of IONPs. The findings indicate that the presence of PVP on the surface of IONPs synthesized by the co-precipitation method provides hydrodynamic size and zeta potential values ranging from 177 to 1915 nm and 6 to 20 mV, respectively, depending on the mass of IONPs, and molecular weight and concentration of PVP. The discovery of PVP does not significantly affect the particle size, particle size distribution, and morphology after silanization. The results on structural identification suggest that PVP is potentially not coated on the surface of IONPs. However, a discovery associated with the surface charge of PVP coating of IONPs demonstrates to be positive and appears to be consistent with the relationship between zeta potential and pH. The isoelectric point between IONPs and PVP coating of IONPs appears to be slightly different. This is an important finding in the understanding of the coating process, and the results may validate that PVP is either partially or weakly adsorbed on the surface of IONPs, or alternatively no adsorbed PVP molecule chains on the surface of IONPs but may result in pH change. The results of the experiment do not support the hypothesis that the presence of PVP increases stability, reduces aggregation, and provides monodispersed particles due to poor colloidal stability.

10.1 Recommendations

One possible method of improving the colloidal stability of IONPs synthesized by the co-precipitation method in the presence of PVP is to control the pH. Since this work aimed to control the size of IONPs by the *post-situ* surface modification, it is of interest to explore the synthesis by the *in-situ* surface modification due to the fact that the pH can be controlled in the presence of PVP. The presence of PVP results in a decrease in pH and thus it is important to obtain the final product with a pH between 10 and 11, and not pH between 7 and 8 since isoelectric point is attained according to the methodology in this thesis. When the pH is above 10, it is likely that bridging flocculation, weakly adsorption, or depletion stabilization can be prevented to a large degree, which results in better stabilization. Another method is to make PVP a charged molecule because the combination of repulsive and electrostatic interaction increases the stability of the system. If the latter does not work, replacing PVP with another polymer might be another option to increase the stability of IONPs. The overall work shows that the surface modification needs to be improved in such a way that PVP is adsorbed efficiently.

Bibliography

1. Abo-zeid Y, Ismail NSM, McLean GR, Hamdy NM. A molecular docking study repurposes FDA approved iron oxide nanoparticles to treat and control COVID-19 infection. *European Journal of Pharmaceutical Sciences*. 2020;153.
2. Kouhpayeh S, Shariati L, Boshtam M, Rahimmanesh I, Mirian M, Esmaeili Y, et al. The Molecular Basis of COVID-19 Pathogenesis, Conventional and Nanomedicine Therapy. *International Journal of Molecular Sciences*. 2021;22(11).
3. Srivastava M, Srivastava N, Mishra PK, Malhotra BD. Prospects of nanomaterials-enabled biosensors for COVID-19 detection. *Science of the Total Environment*. 2021;754.
4. NTNU. NTNU COVID-19 test [Available from: <https://www.ntnu.edu/ntnu-covid-19-test>].
5. Gemini. Samfunnets viktigste beredskapslager 2020 [Available from: <https://gemini.no/2020/07/samfunnets-viktigste-beredskapslager/>].
6. Gemini. From thousands of tiny magnetic balls to 150,000 COVID-19 tests per week 2020 [Available from: <https://norwegianscitechnews.com/2020/04/from-thousands-of-tiny-magnetic-balls-to-150000-covid-19-tests-per-week/>].
7. Souza DM, Andrade AL, Fabris JD, Valerio P, Goes AM, Leite MF, et al. Synthesis and in vitro evaluation of toxicity of silica-coated magnetite nanoparticles. *Journal of Non-Crystalline Solids*. 2008;354(42-44):4894-7.
8. Zhu W, Wei ZQ, Han C, Weng XS. Nanomaterials as Promising Theranostic Tools in Nanomedicine and Their Applications in Clinical Disease Diagnosis and Treatment. *Nanomaterials*. 2021;11(12).
9. Khan AU, Chen L, Ge GL. Recent development for biomedical applications of magnetic nanoparticles. *Inorganic Chemistry Communications*. 2021;134.
10. Sosa-Acosta JR, Silva JA, Fernandez-Izquierdo L, Diaz-Castanon S, Ortiz M, Zuaznabar-Gardona JC, et al. Iron Oxide Nanoparticles (IONPs) with potential applications in plasmid DNA isolation. *Colloids and Surfaces a-Physicochemical and Engineering Aspects*. 2018;545:167-78.
11. Smerkova K, Dostalova S, Vaculovicova M, Kynicky J, Trnkova L, Kralik M, et al. Investigation of interaction between magnetic silica particles and lambda phage DNA fragment. *Journal of Pharmaceutical and Biomedical Analysis*. 2013;86:65-72.
12. Mahmoudi M. Superparamagnetic iron oxide nanoparticles : synthesis, surface engineering, cytotoxicity and biomedical applications. New York: Nova Science Publishers; 2011.
13. Ling WH, Wang MY, Xiong CX, Xie DF, Chen QY, Chu XY, et al. Synthesis, surface modification, and applications of magnetic iron oxide nanoparticles. *Journal of Materials Research*. 2019;34(11):1828-44.
14. Zhu N, Ji HN, Yu P, Niu JQ, Farooq MU, Akram MW, et al. Surface Modification of Magnetic Iron Oxide Nanoparticles. *Nanomaterials*. 2018;8(10).
15. Mahmed N, Heczko O, Lancok A, Hannula SP. The magnetic and oxidation behavior of bare and silica-coated iron oxide nanoparticles synthesized by reverse co-precipitation of ferrous ion (Fe²⁺) in ambient atmosphere. *Journal of Magnetism and Magnetic Materials*. 2014;353:15-22.
16. Pershina AG, Sazonov AE, Filimonov VD. Magnetic nanoparticles - DNA interactions: design and applications of nanobiohybrid systems. *Russian Chemical Reviews*. 2014;83(4):299-322.

17. Nosrati H, Salehiabar M, Davaran S, Ramazani A, Manjili HK, Danafar H. New advances strategies for surface functionalization of iron oxide magnetic nano particles (IONPs). *Research on Chemical Intermediates*. 2017;43(12):7423-42.
18. Tiwari AP, Satvekar RK, Rohiwal SS, Karande VA, Raut AV, Patil PG, et al. Magneto-separation of genomic deoxyribose nucleic acid using pH responsive Fe₃O₄@silica@chitosan nanoparticles in biological samples. *Rsc Advances*. 2015;5(11):8463-70.
19. Abu Noqta O, Aziz AA, Usman IA, Bououdina M. Recent Advances in Iron Oxide Nanoparticles (IONPs): Synthesis and Surface Modification for Biomedical Applications. *Journal of Superconductivity and Novel Magnetism*. 2019;32(4):779-95.
20. Tran HV. *Synthesis and Characterization of Functionalization of Iron Oxide Nanoparticles for Biomedical Applications*. Trondheim: Norwegian University of Science and Technology; 2021.
21. Jadhav SV, Nikam DS, Khot VM, Thorat ND, Phadatare MR, Ningthoujam RS, et al. Studies on colloidal stability of PVP-coated LSMO nanoparticles for magnetic fluid hyperthermia. *New Journal of Chemistry*. 2013;37(10):3121-30.
22. Bui TQ, Ngo HTM, Tran HT. Surface-protective assistance of ultrasound in synthesis of superparamagnetic magnetite nanoparticles and in preparation of mono-core magnetite-silica nanocomposites. *Journal of Science-Advanced Materials and Devices*. 2018;3(3):323-30.
23. Maneepprakorn W, Dharakul T, Maurizi L, Ieee, editors. *Silica-Coated Superparamagnetic Nanoparticles as Contrast Agent for Magnetic Resonance Imaging: Synthesis and physicochemical characterizations*. IEEE NANO 2015 15th INTERNATIONAL CONFERENCE ON NANOTECHNOLOGY; 2015 Jul 27-30; Rome, Italy 2015.
24. Vallabani NVS, Singh S. Recent advances and future prospects of iron oxide nanoparticles in biomedicine and diagnostics. *3 Biotech*. 2018;8(6).
25. Zhang L, Dong WF, Sun HB. Multifunctional superparamagnetic iron oxide nanoparticles: design, synthesis and biomedical photonic applications. *Nanoscale*. 2013;5(17):7664-84.
26. Wollschläger J. *Reactive Molecular Beam Epitaxy of Iron Oxide Films: Strain, Order, and Interface Properties*. In: Wandelt K, editor. *Encyclopedia of Interfacial Chemistry*. Oxford: Elsevier; 2018. p. 284-96.
27. Marghussian V. 4 - *Magnetic Properties of Nano-Glass Ceramics*. In: Marghussian V, editor. *Nano-Glass Ceramics*. Oxford: William Andrew Publishing; 2015. p. 181-223.
28. Enriquez-Navas PM, Garcia-Martin ML. Chapter 9 - *Application of Inorganic Nanoparticles for Diagnosis Based on MRI*. In: de la Fuente JM, Grazu V, editors. *Frontiers of Nanoscience*. 4: Elsevier; 2012. p. 233-45.
29. Hernández-Hernández AA, Aguirre-Álvarez G, Cariño-Cortés R, Mendoza-Huizar LH, Jiménez-Alvarado R. Iron oxide nanoparticles: synthesis, functionalization, and applications in diagnosis and treatment of cancer. *Chemical Papers*. 2020;74(11):3809-24.
30. Wu W, Wu ZH, Yu T, Jiang CZ, Kim WS. Recent progress on magnetic iron oxide nanoparticles: synthesis, surface functional strategies and biomedical applications. *Science and Technology of Advanced Materials*. 2015;16(2).
31. Dadfar SM, Roemhild K, Drude NI, von Stillfried S, Knuchel R, Kiessling F, et al. Iron oxide nanoparticles: Diagnostic, therapeutic and theranostic applications. *Advanced Drug Delivery Reviews*. 2019;138:302-25.

32. Mørk PC. Surface and Colloid Chemistry - Basic Principles and Theories. Trondheim; 2004.
33. Kontogeorgis GM, Kiil S. Introduction to applied colloid and surface chemistry. Chichester: Wiley; 2016.
34. Pashley RM, Karaman ME. Applied colloid and surface chemistry. Chichester, West Sussex, England ;,Hoboken, N.J.: J. Wiley; 2004.
35. Espallargas N, Armada S. Future development of thermal spray coatings : types, designs, manufacture and applications. Amsterdam, Netherlands: Woodhead Publishing; 2015.
36. Mohd Omar F, Aziz H, Stoll S. Nanoparticle Properties, Behavior, Fate in Aquatic Systems and Characterization Methods. Journal of Colloid Science and Biotechnology. 2014;3:1-30.
37. Ramírez-García G, Trapiella-Alfonso L, d'Orlyé F, Varenne A. Chapter 17 - Electrophoretic Methods for Characterizing Nanoparticles and Evaluating Their Bio-interactions for Their Further Use as Diagnostic, Imaging, or Therapeutic Tools. In: Poole CF, editor. Capillary Electromigration Separation Methods: Elsevier; 2018. p. 397-421.
38. Barhoum A, García-Betancourt ML, Rahier H, Van Assche G. Chapter 9 - Physicochemical characterization of nanomaterials: polymorph, composition, wettability, and thermal stability. In: Barhoum A, Makhoulf ASH, editors. Emerging Applications of Nanoparticles and Architecture Nanostructures: Elsevier; 2018. p. 255-78.
39. Moore J, Cerasoli E. Particle Light Scattering Methods and Applications. In: Lindon JC, Tranter GE, Koppenaal DW, editors. Encyclopedia of Spectroscopy and Spectrometry (Third Edition). Oxford: Academic Press; 2017. p. 543-53.
40. Hiremath PG, S R, Binnal P, Theodore T. Chapter 9 - Fluoride Contamination in Underground Water and Its Treatment. In: Singh P, Hussain CM, Rajkhowa S, editors. Management of Contaminants of Emerging Concern (CEC) in Environment: Elsevier; 2021. p. 249-80.
41. Liz-Marzán LM, Correa-Duarte MA, Pastoriza-Santos I, Mulvaney P, Ung T, Giersig M, et al. Chapter 5 - CORE-SHELL NANOPARTICLES AND ASSEMBLIES THEREOF. In: Nalwa HS, editor. Handbook of Surfaces and Interfaces of Materials. Burlington: Academic Press; 2001. p. 189-237.
42. Michael FM, Khalid M, Walvekar R, Siddiqui H, Balaji AB. 2 - Surface modification techniques of biodegradable and biocompatible polymers. In: Shimpi NG, editor. Biodegradable and Biocompatible Polymer Composites: Woodhead Publishing; 2018. p. 33-54.
43. Stuart MAC. ADSORBED POLYMERS IN COLLOIDAL SYSTEMS - FROM STATICS TO DYNAMICS. Polymer Journal. 1991;23(5):669-82.
44. González García Á, Nagelkerke MMB, Tuinier R, Vis M. Polymer-mediated colloidal stability: on the transition between adsorption and depletion. Advances in Colloid and Interface Science. 2020;275:102077.
45. Koczur KM, Mourdikoudis S, Polavarapu L, Skrabalak SE. Polyvinylpyrrolidone (PVP) in nanoparticle synthesis. Dalton Transactions. 2015;44(41):17883-905.
46. Oesch F, Fruth D, Hengstler JG, Fabian E, Berger FI, Landsiedel R. Enigmatic mechanism of the N-vinylpyrrolidone hepatocarcinogenicity in the rat. Arch Toxicol. 2021;95(12):3717-44.
47. Protsenko V, Gordiienko V, Butyrina T, Vasil'eva E, Danilov F. Hard chromium electrodeposition from a trivalent chromium bath containing water-soluble polymer. Turkish journal of chemistry. 2014;38(1):50-5.
48. Li J, Inukai K, Takahashi Y, Tsuruta A, Shin W. Effect of PVP on the synthesis of high-dispersion core-shell barium-titanate-polyvinylpyrrolidone nanoparticles. Journal of Asian Ceramic Societies. 2017;5(2):216-25.

49. Kurakula M, Rao GSNK. Pharmaceutical assessment of polyvinylpyrrolidone (PVP): As excipient from conventional to controlled delivery systems with a spotlight on COVID-19 inhibition. *J Drug Deliv Sci Technol.* 2020;60:102046-.
50. Hernandez-Hernandez AA, Aguirre-alvarez G, Carino-Cortes R, Mendoza-Huizar LH, Jimenez-Alvarado R. Iron oxide nanoparticles: synthesis, functionalization, and applications in diagnosis and treatment of cancer. *Chemical Papers.* 2020;74(11):3809-24.
51. Wu W, He QG, Jiang CZ. Magnetic Iron Oxide Nanoparticles: Synthesis and Surface Functionalization Strategies. *Nanoscale Research Letters.* 2008;3(11):397-415.
52. Han YD, Lu ZY, Teng ZG, Liang JL, Guo ZL, Wang DY, et al. Unraveling the Growth Mechanism of Silica Particles in the Stober Method: In Situ Seeded Growth Model. *Langmuir.* 2017;33(23):5879-90.
53. abu noqta O, Abdul Aziz A, adamu usman I. Synthesis of PVP Coated Superparamagnetic Iron Oxide Nanoparticles with a High Saturation Magnetization. *Solid State Phenomena.* 2019;290:301-6.
54. Zare K, Sadjadi MS, Farhadyar N, Fathi F. Synthesize and Characterization of Multifunctional Silica Coated Magnetic Nanoparticles Using Polyvinylpyrrolidone (PVP) as a Mediator. *Journal of nano research.* 2012;16:43-8.
55. Zulfiqar, Afzal S, Khan R, Zeb T, Rahman Mu, Burhanullah, et al. Structural, optical, dielectric and magnetic properties of PVP coated magnetite (Fe₃O₄) nanoparticles. *Journal of materials science Materials in electronics.* 2018;29(23):20040-50.
56. Heiran A, Hassanajili S, Escrochi M, editors. Synthesis and Characterization of Fe₃O₄ Magnetite Nanoparticles Coated by Polyvinylpyrrolidone. *Eco-friendly and Smart Polymer Systems; 2020 2020//; Cham: Springer International Publishing.*
57. Pandey G, Singh S, Hitkari G. Synthesis and characterization of polyvinyl pyrrolidone (PVP)-coated Fe₃O₄ nanoparticles by chemical co-precipitation method and removal of Congo red dye by adsorption process. *International Nano Letters.* 2018;8(2):111-21.
58. Isci S, Isci Y, Bekaroglu MG. Particle interactions of polyvinylpyrrolidone-coated iron oxide particles as magnetic drug delivery agents. *Applied Physics a-Materials Science & Processing.* 2017;123(8).
59. Abu-Noqta OA, Aziz AA, Usman AI. Colloidal Stability of Iron Oxide Nanoparticles Coated with Different Capping Agents. *Materials Today: Proceedings.* 2019;17:1072-7.
60. Kim KD, Kim HT. Formation of silica nanoparticles by hydrolysis of TEOS using a mixed semi-batch/batch method. *Journal of Sol-Gel Science and Technology.* 2002;25(3):183-9.
61. Nozawa K, Gailhanou H, Raison L, Panizza P, Ushiki H, Sellier E, et al. Smart control of monodisperse Stber silica particles: Effect of reactant addition rate on growth process. *Langmuir.* 2005;21(4):1516-23.
62. Ali Z. Insights into Growth Mechanism, Control of Particle Size and Particle Size Distribution of Silica Coated Iron Oxide Nanoparticles. Trondheim: Norwegian University of Science and Technology; 2020.
63. Nissen-Sollie H. Study of Particle Sizes and Morphologies of Silica Coated Iron Oxide Nanoparticles Synthesized via a Semi-Batch Process. Trondheim: Norwegian University of Science and Technology; 2021.
64. Kermanian M, Sadighian S, Naghibi M, Khoshkam M. PVP Surface-protected silica coated iron oxide nanoparticles for MR imaging application. *Journal of Biomaterials Science-Polymer Edition.* 2021;32(10):1356-69.

65. Gao Z, Ring HL, Sharma A, Namsrai B, Tran N, Finger EB, et al. Preparation of Scalable Silica-Coated Iron Oxide Nanoparticles for Nanowarming. *Adv Sci (Weinh)*. 2020;7(4):1901624-n/a.
66. Arsalani N, Fattahi H, Nazarpour M. Synthesis and characterization of PVP-functionalized superparamagnetic Fe₃O₄ nanoparticles as an MRI contrast agent. *Express Polymer Letters*. 2010;4(6):329-38.

